Laboratory Studies of Heterogeneous Processes Relevant to Mars

by

Raina V. Gough

B.S., Montana State University, 2004

A thesis submitted to the

Faculty of the Graduate School of the

University of Colorado in partial fulfillment

of the requirements for the degree of

Doctor of Philosophy

Department of Chemistry and Biochemistry

2010

This thesis entitled:

Laboratory Studies of Heterogeneous Processes
Relevant to Mars

written by Raina V. Gough

has been approved for the Department of Chemistry and Biochemistry by

_____

Margaret Tolbert

_____

Brian Toon

Date: _____

The final copy of this thesis has been examined by both the signatories, and we find that both the content and the form meet acceptable presentation standards of scholarly work in the above mentioned discipline.

Gough, Raina V. (Ph.D. Chemistry)

Laboratory Studies of Heterogeneous Processes Relevant to Mars

Thesis directed by Professor Margaret A. Tolbert

Heterogeneous (gas-surface) processes may play an important role in both the atmospheric and surface chemistry of Mars. Atmospheric species may be affected by the chemistry and physical properties of the planetary surface and the surface material may be affected by the components and properties of the atmosphere. In this thesis, several laboratory studies are described which experimentally investigate two types of atmosphere-surface systems likely to exist on Mars.

First, experiments were performed to better understand the spatial and temporal variability of atmospheric methane (CH_4) on Mars. Reported CH_4 plumes in the atmosphere of Mars are difficult to explain using known chemical or physical processes. The observations imply a strong, present-day source and also a rapid yet unknown CH_4 sink. We have investigated the potential role of mineral dust in CH_4 variability. First, using a Knudsen cell capable of simulating Martian temperature and pressure conditions, we have studied the adsorption of CH_4 to a Martian mineral analog as a function of temperature. An uptake coefficient was determined and then applied to the Martian surface-atmosphere system. Our results suggest that adsorption to soil grains could possibly affect the CH_4 mixing ratio on a seasonal time scale especially at mid-latitude regions.

Additionally, chemical oxidation of CH_4 by oxidants thought to exist in the Martian regolith was studied. The Viking mission in the 1970's found Martian soil

was able to oxidize complex organic compounds to CO_2. The identity of the oxidant is unknown, but has been proposed to be either hydrogen peroxide or perchlorate salts. We used a gas chromatograph to determine if simulated Mars soil containing these oxidants was able to oxidize CH_4 to CO_2. However, no CH_4 was oxidized within the detection limit of the instrument and only an upper limit reaction coefficient could be reported. Even these upper limit values suggest CH_4 could not be removed from the Martian atmosphere rapidly enough to cause variability.

We have also studied the interactions of another important trace gas on Mars, water vapor, with perchlorate, a highly deliquescent salt recently discovered in polar soil. A Raman microscope equipped with an environmental cell was used to study phase transitions of the salts. The relative humidity (RH) at which deliquescence (absorption of water vapor by the solid to become an aqueous solution) and efflorescence (crystallization of the aqueous solution) occur were determined as a function of temperature, hydration state and associated cation. We show that the deliquescence RH for perchlorate salts can be low (~40% RH for anhydrous sodium perchlorate, for example). Thermodynamics can predict deliquescence; however, the kinetic inhibition of crystallization causes efflorescence to occur at much lower RH values than deliquescence which allows supersaturated salt solutions to exist in a metastable state. Based on the diurnal RH and temperature cycles on Mars, aqueous solutions could be stable or metastable for several hours a day at the Phoenix landing site. The astrobiological implications of potential liquid H_2O on Mars are significant.

Acknowledgements

I am grateful to many people who made graduate school at the University of Colorado such an interesting and fulfilling experience. I would like to thank all members of the Tolbert Group for their advice and friendship over the years. I am very grateful to Courtney Hatch, Melissa Trainer and Melinda Beaver for teaching me so much and to Christa Hasenkopf, my wonderful officemate, for for never being too busy to discuss science or life. All other past and present members of the Tolbert group have also been marvelous to work with, learn from and drink coffee with.

My research advisor Maggie Tolbert has been a wonderful teacher, mentor and role model. One of the best things about working for Maggie is that she rarely says no; rather, she is enthusiastic about most ideas and results and directions. Because of this, I have been able to do a lot of very interesting things that were only tangentially related to my research. I want to thank Maggie for: letting me go on geology field trips to Hawaii, Yellowstone and Utah, allowing (and paying for) me to take mostly unrelated classes in random departments, funding my travel to conferences even when I didn't even present, putting up with the teaching certificate activities, and letting me study the phase transitions of perchlorate salts just for fun.

I am very grateful to Matt Wise and Kelly Baustian for sharing their Raman microscope with me and helping me interpret results. I want to thank John Bognar, one of my undergraduate research advisors at Montana State, for giving me confidence in my ideas and encouraging me to go to grad school at CU. I have had great professors here at CU, especially Jose Jimenez, Brian Toon, Steve Mojzsis and

Alexis Templeton. The electronics, machine, and glass shops here at CIRES have been very helpful in the course of my research.

I was very lucky to be able to get advice and ideas from Chris McKay and Brian Toon, leaders in the field of planetary science. Also, thanks to Vincent Chevrier at the University of Arkansas for very helpful discussions of the thermodynamics of perchlorate phase transitions. I am grateful to Tom McCollom of LASP for allowing me to use his GC and other lab equipment. Also, I would like to thank Hanna Sizemore, Addie Dove, Katherine Wright, and Lisa Mahew for their expertise in various topics and techniques.

Financially, this work was supported by NASA Mars Fundamental Research Grant NNX09AN19G and 05-MFRP05-0066, NASA grant NNX08AG93G, and a CIRES Graduate Student Fellowship.

Table of Contents

List of Tables

List of Figures

Chapter I

Introduction

1.1 Mars and Earth: a comparison

In this thesis, we discuss several studies which experimentally investigate chemical reactions and physical processes that may be occurring on the surface or in the atmosphere of Mars. To set the stage, we will begin with an introduction to Mars and how it compares and contrasts with a more familiar planet: Earth.

Listed in Table 1.1 are several physical parameters and atmospheric properties of both Earth and Mars. At first glance, Mars is very different than the Earth. On average, Mars is 78 million miles further from the sun and is therefore thought to be outside of the "habitable zone". The temperature on the surface of Mars rarely rises above 0°C and sometimes drops as low as 148 K (-125°C). The planet is significantly smaller than Earth: 1/2 the diameter and $1/10^{th}$ the mass. As a result, the gravity is only 38% that of Earth.

Despite these differences, Mars is similar to Earth in many ways. The Martian landscape contains volcanoes and canyons, valleys and craters, rock outcrops and sand dunes. Although dry today, there is evidence for river deltas, hot springs and perhaps even the shoreline of an ancient ocean. These features and others suggest that Mars experienced a warm, wet period during which liquid water flowed across the surface carving channels, eroding crater walls and creating sedimentary rocks and evaporite minerals.

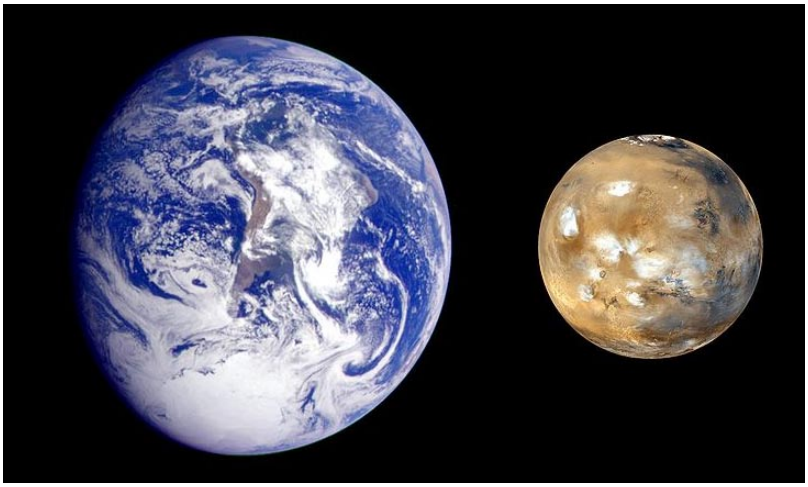

Figure 1.1 A composite image of Earth and Mars which depicts the relative sizes of the two planets. The image of Earth was acquired by the Galileo orbiter in 1990 when it was flying by Earth on its way to Jupiter. The image of Mars was acquired by the Mars Global Surveyor orbiter in 1999.

	Earth	**Mars**
diameter	12,756 km	6,794 km
mass	5.97×10^{24} kg	0.642×10^{24} kg
average distance from the sun	1 AU	1.524 AU
solar irradiance	1380 W/m^2	595 W/m^2
rotation period (length of day)	23.93 hr	24.62 hr
revolution period (length of year)	1 year	1.88 year
obliquity (axial tilt)	23.44°	25.19°
average temperature	286 K	210 K
minimum/maximum temperature	208 K / 328 K	148 K / 293 K
surface pressure	1 bar	6 - 9 mbar
atmospheric scale height	7.6 km	11 km
topographic range	20 km	30 km
gravity	9.8 m/s^2	3.7 m/s^2
major atmospheric components	78.1% N_2 20.9% O_2 0.93% Ar	95.3% CO_2 2.7% N_2 1.6% Ar
mean molecular weight	28.97 g/mol	43.34 g/mol

Table 1.1 Comparison of some key physical, orbital and atmospheric parameters for Earth and Mars.

Although thought to be largely volcanically and geologically dead, current-day Mars is still active in many ways. The Martian atmosphere experiences weather somewhat similar to that found on Earth: the formation and movement of ice clouds, massive dust storms, and even snow in the upper atmosphere. The Viking lander in 1970's photographed frost on the Martian surface in the early morning; the thin layer disappeared quickly when the sun rose. Like Earth, the polar regions of Mars have ice caps that grow and shrink seasonally as well as permanent polar ice caps.

There are other similarities: a day on Mars is similar in duration to a day on Earth (24.65 hours instead of nearly 24); however, it is typically called a sol. The obliquity of the two planets (the degree of axial tilt) is also very similar: Earth is tilted at 23.5°, Mars is currently at 25.2°. As the orbit of Mars is much more eccentric than Earth's, the duration and intensity of seasons on Mars are affected not just by axial tilt but also by the variation in distance from the Sun.

The work in this thesis is laboratory based; however, it was performed in order to better understand interactions that could be occurring between the atmosphere and the surface of Mars. Therefore, it is important to understand the properties and composition of these two related systems in more detail.

1.2 The atmosphere of Mars

The atmospheric compositions of Earth and Mars are very different, with the Martian atmosphere containing mainly CO_2 (95.3%) with small amounts of N_2 (2.7%) and argon (1.6%) in contrast to the oxygen-rich terrestrial atmosphere which is so important for life. There are also small amounts of O_2 (0.13%), CO (0.08%) and NO

(100 ppmv) in the atmosphere of Mars. The air is much thinner on Mars; on average, the pressure at the surface is about 7 mbar (about 0.7% that of Earth). This mean surface pressure is equal to the pressure found 35 km above the Earth's surface.

There are large topographic differences on Mars which cause the pressure to vary dramatically depending on geographic location. On the top of the highest mountain on Mars (Olympus Mons), the pressure is only 0.3 mbar, although 30 km lower at the bottom of the Hellas Impact Basin, a large impact feature in the southern hemisphere, the pressure is 11.5 mbar. Additionally, the atmospheric pressure at a given location on Mars varies seasonally by as much as 30% due to condensation of some of the CO_2 atmosphere during the winter months. Nowhere on of Earth are such dramatic pressure fluctuations found.

Due to the combination of low temperatures and low pressures on the surface of Mars today, liquid water is not predicted to be stable. Although water does exist in the other two states of matter, ice is expected to sublimate rather than melt and water vapor will condense directly into the solid phase. These phase transitions of water are actively occurring on Mars and result in a H_2O mixing ratio that varies widely with location and time of day or year. The variable water is due to local processes which affect mixing ratio (adsorption of water to soil grains, nucleation of ice onto mineral aerosol in the atmosphere, deposition of water vapor onto the polar caps) as well as atmospheric dynamics occurring on a global scale.

Another important component of the Martian atmosphere is mineral dust. The atmosphere is quite dusty even during periods of relatively low dust activity. As a result, the Martian sky appears to be orange or light brown when viewed from the

planet's surface. The optical depths measured by the two Viking landers range from 0.4 to greater than 2.0 over the course of a Martian year (Colburn et al., 1989). These particles are most likely 1.5-2.0 μm in diameter (Chassefiere et al., 1995) and well mixed up to 20-30 km (Lemmon et al., 2004). The composition of this dust, unsurprisingly, is similar to the bulk surface material (Hamilton et al., 2005) as the aeolian activity constantly recycles these small mineral particles between the surface and atmosphere.

1.3 The surface of Mars

The surface area of Mars (1.448×10^8 km^2) is quite similar to the area of dry land on Earth (1.489×10^8 km^2). Figure 1.2 shows an approximately true color image taken in 1997 by a camera onboard the Mars Pathfinder Lander. This image is representative of much of the Martian landscape: it shows gently rolling hills, small rocks, large boulders, and a fine reddish dust covering everything. The surface resembles certain dry, desolate regions of earth such as the slopes of Mauna Kea in Hawaii or the deserts of southern Utah. Unlike Earth, which has active weathering processes to erode landforms and plate tectonics to recycle crustal material, the Martian surface has remained mostly unchanged for billions of years. As a result, most of the surface is very old and heavily cratered.

Determination of the chemical and mineralogical composition of different regions of the Martian surface is still an active area of research, but significant information does currently exist due to spectrometers on orbiting spacecraft as well as instruments onboard Mars landers and rovers. The chemical composition of the

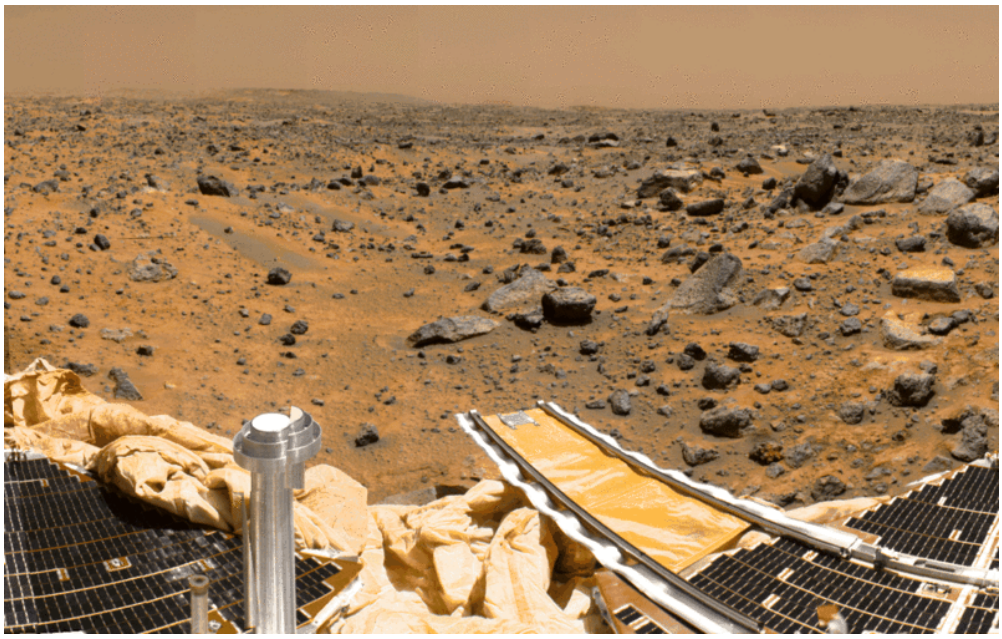

Figure 1.2 An approximately true color image taken by a camera onboard the Mars Pathfinder Lander several days after landing on Mars at 19.13°N, 33.22°W in July 1997.

SiO_2	48.6 ± 2.5
Fe_2O_3	17.5 ± 1.8
Al_2O_3	8.3 ± 0.8
MgO	7.5 ± 1.2
CaO	6.3 ± 1.0
SO_3	5.4 ± 1.1
Na_2O	2.2 ± 0.9
TiO_2	1.1 ± 0.2
Cl	0.6 ± 0.2
K_2O	0.3 ± 0.1

Table 1.2 Chemical composition (in %) of Martian soil measured by the alpha proton X-ray spectrometer on the Mars Pathfinder Sojourner Rover (Bell et al., 2000).

Martian soil (often termed “regolith” in the case of Mars) near the Pathfinder landing site is listed in Table 1.2. The major oxides are SiO_2 and Fe_2O_3.

Mineralogically, the Martian surface is basaltic in composition. Common volcanic silicate species such as feldspars and pyroxene are abundant (Bandfield et al., 2000). Other minerals are present in smaller amounts: sheet silicates such as phyllosilicate clays, hematite (Fe_2O_3), and sulfate minerals such as gypsum ($CaSO_4 \bullet H_2O$) (Christensen et al., 2004). These species are interesting to planetary geologists as the formation or deposition most likely required liquid water.

In addition to characterizing the mineralogy of the surface, the chemical reactivity of the upper regolith has also been studied. In the 1970’s as part of the Viking program, NASA sent two landers to different locations on the surface of Mars to perform what were at the time considered “life detection experiments”. The Labeled Release (LR) experiment onboard each lander investigated the ability of the soil to oxidize a solution of ^{13}C-labeled organic molecules into $^{13}CO_2$ (Levin and Straat, 1976). Prior to launch, oxidation of the organic solution was a criteria for the discovery of life. However, it is now widely believed that an oxidant associated with the mineral grains, or perhaps the soil itself, was chemically reactive. Perhaps confirming this hypothesis, the gas chromatograph-mass spectrometer onboard Viking Lander 2 failed to detect any organic compounds in the upper 10 cm of soil (Biemann, 1979). As organics are continuously reaching the surface exogenously (through meteoritic or cometary influx), this negative result suggests the presence of an oxidizing pathway actively destroying organics. It is thought that this oxidant is H_2O_2 (Huguenin et al., 1979; Bullock et al., 1994) which is photochemically

produced in the atmosphere and then diffuses into the soil, although perchlorate salts have also been suggested. This reactive soil could be important for understanding atmosphere-surface interactions on Mars.

1.4 Methane on Mars

1.4.1 Observations

In 2004, several groups reported observations of methane (CH_4) in the atmosphere of Mars (Formisano et al., 2004; Krasnopolsky et al., 2004; Mumma et al., 2004). These observations from both ground-based and orbiter-based instruments all suggested a mixing ratio around 10 ppb. This is a difficult measurement to make due to the small amount of CH_4 on the planet. In the case of ground-based observations, the possibility of telluric CH_4 contamination could add further uncertainty (Zahnle et al., 2010). However, the consistency in reported mixing ratios between measurements taken with different instruments and using different absorbance features has inspired confidence in the reported CH_4 observations.

These reports have excited the planetary science community by presenting several mysteries. The presence of CH_4 alone is intriguing, as it should only exist for a few hundred years in the Martian atmosphere. It has been calculated that the CH_4 lifetime due to destruction by photochemistry and gas phase oxidation by OH• and $O(^1D)$ is about 340 years (Krasnopolsky et al., 2004). Therefore it is clear that, either chemically or biologically, the CH_4 is being replaced on a regular basis and cannot merely be a remnant of past volcanism.

Even more fascinating is the recently observed spatial and temporal variability of the atmospheric CH_4 (Geminale et al., 2008; Mumma et al., 2009). Ground-based observations suggest the CH_4 is not evenly distributed as would be expected for a gas with a several hundred year lifetime; rather, it is concentrated over a few "hotspots" and the activity appears to be seasonal. These plumes, depicted in Fig. 1.2, contain large amounts of CH_4 (~19,000 metric tons) yet disappear within a few years (Mumma et al., 2009). Figure 1.3 shows a series of latitudinal profiles of CH_4 mixing ratios measured by Mumma et al. (2009) using three different ground-based telescopes. Both the geographic and temporal variability of Martian CH_4 are illustrated here. Measurements were taken in early northern spring in 2006 (a: 17°), early northern summer in 2003 (b and c: 122°) and late northern summer in 2003 (d: 155°). When present, the CH_4 is clearly concentrated over the equatorial and northern mid-latitude regions. Comparing profiles (b) and (c), taken at the same time of year, the CH_4 mixing ratio appears to vary longitudinally as well. When the profiles are integrated, the 2003 measurements represent a global mean mixing ratio of ~6 ppb. However, 3 Earth years (1.5 Martian years) later, the globally averaged mixing ratio is only ~2 ppb.

1.4.2 Implications for CH_4 lifetime

The observed decrease in mixing ratio between 2003 and 2006 shown in Fig. 1.3 implies a destruction lifetime of at least ~4 Earth years. The lifetime could potentially be shorter than 1 Earth year if the CH_4 release and subsequent destruction cycle repeats every Martian year, but the data lack the temporal resolution to determine this. Regardless, the destruction lifetime for CH_4 appears to be an order of

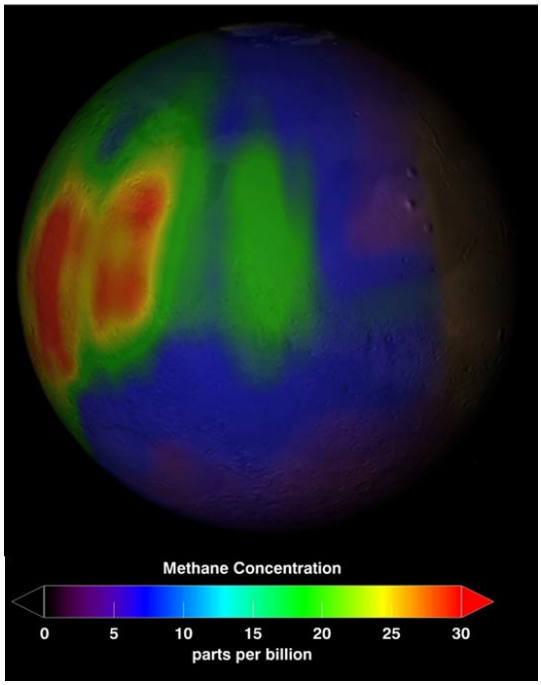

Figure 1.3 Visualization of a CH_4 plume observed in the Martian atmosphere in 2003 during the northern summer season (Mumma et al., 2009). (Image credit: Trent Schindler/NASA)

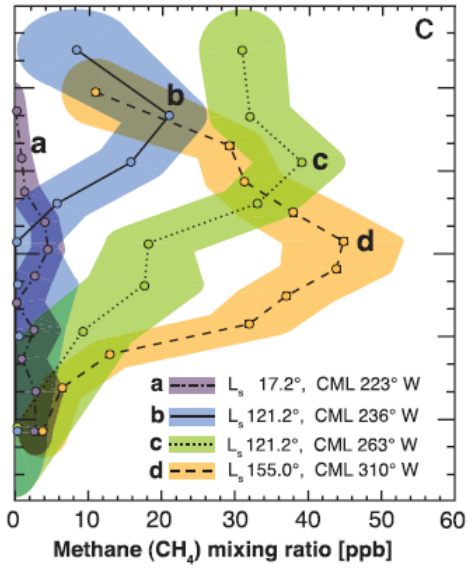

Figure 1.4 Latitudinal profiles of CH_4 mixing ratios at different longitudes and seasons depict the geographic and temporal variability of Martian CH_4 (Mumma et al., 2009). Profile (a) was taken in 2006 and implies a global mean mixing ratio of ~2 ppb, and profiles (b), (c) and (d) were taken in 2003 and, when combined, represent a global mean mixing ratio of ~6 ppb.

magnitude shorter than the time scale of the known loss pathways.

Theoretical models have attempted to recreate these short-lived CH_4 plumes using a general circulation model (GCM), and have confirmed that some unknown process must be rapidly destroying the atmospheric CH_4. Levevre and Forget (2009) examined CH_4 chemistry using the Laboratoire de Météorologie Dynamique (LMD) GCM and found the lifetime could be even shorter than originally suggested. They report that a CH_4 lifetime of less than 200 days is necessary to explain the observations, which would require an unidentified CH_4 loss process 600 times faster than photochemical destruction. The implications of this mysterious sink are great: if CH_4 is being destroyed rapidly, it also must be created at far higher rates than previously believed. For example, the annual CH_4 source needed to maintain a 10 ppb mixing ratio if the lifetime is 340 years is 270 tons/year (Krasnopolsky et al., 2004). However, Lefevre and Forget (2009) suggest that the very short CH_4 lifetime suggested by the high variability would require a CH_4 source of ~150,000 tons/year.

1.4.3 Methane source: biotic or abiotic?

The excitement over this discovery stems partially from the fact that on Earth nearly all CH_4 is produced by life, either past or present. The main terrestrial CH_4 source is methanogenic bacteria living in anaerobic conditions such as the digestive systems of cows, termites and marine zooplankton or in environments such as wetlands or rice paddies (Atreya et al., 2007). It is exciting to ponder the possibilities of colonies of methanogenic (CH_4 producing) bacteria living on present-day Mars. Although the environment on Mars is not conducive to life due to the extreme cold

and intense UV radiation, the possibility of life existing in subsurface habitats cannot be ruled out.

However, it is likely that abiotic CH_4 production mechanisms could exist on Mars today. It has been suggested that geochemical processes such as serpentinization could reduce CO_2 to CH_4 (Oze and Sharma, 2005). However, liquid H_2O is required for this reaction. The CH_4 could be being released from clathrate structures buried deep under the regolith or the polar caps (Chastain and Chevrier, 2007). Although clathrates would not be expected to form on Mars today due to the low partial pressures of the required components (H_2O and CH_4), they could have formed in the past and are currently degassing or dissociating due to obliquity-driven changes in temperature (Prieto-Ballesteros et al., 2006) or variations in subsurface salinity (Madden et al., 2007).

1.4.4 The mysterious methane sink

As we concluded above, it appears some unknown process is removing CH_4 from the atmosphere over a time scale of years (Mumma et al., 2009) or perhaps even as quickly as 200 days (Lefevre and Forget, 2009). It is not known what chemical or physical mechanism is responsible for the rapid CH_4 loss. Several possible CH_4 sinks have been proposed, but the work described in this thesis was the first to experimentally study potential removal pathways of Martian CH_4. It had been frequently suggested in the literature that heterogeneous processes are destroying CH_4 on Mars (Formisano et al., 2004; Krasnopolsky et al., 2004; Geminale et al., 2008;

Mumma et al., 2009); however, neither the type of surface responsible nor the feasibility or rate of such a process was known.

In this thesis, we describe laboratory studies which explore two different types of CH_4 loss pathways. First, in Chapter 2, we study the possibility of CH_4 adsorption to Martian soil as a temporary, seasonal CH_4 sink. We experimentally determine the kinetics and temperature dependence of CH_4 physisorption onto a common Martian soil analog using a high vacuum chamber capable of simulating Martian conditions. Then, in Chapter 3, we study the potential chemical destruction of CH_4 by oxidants thought to exist on the surface and in the shallow subsurface of Mars. In this study, we used gas chromatography to analyze the headspace of the reaction environment to determine if oxidation of CH_4 had occurred. In both cases, we apply our experimental data to the Martian surface-atmosphere system and comment on the ability of a given process to affect the CH_4 on Mars.

1.5 Perchlorate on Mars

After the observations of atmospheric CH_4, the discovery of perchlorate salts in the Martian soil was one of the most interesting discoveries of the Mars exploration program in the past few years. Small amounts of perchlorate salts were recently discovered at the Phoenix landing site at high northern latitudes (68°N, 234°E). The Wet Chemistry Laboratory (WCL) instrument onboard the Phoenix Lander detected ~0.5% perchlorate (ClO_4^-) by mass in the soil nearby the lander (Hecht et al., 2009).

Perchlorate has unique physical, chemical and biochemical properties, thus scientists from many areas are interested in this discovery. One potentially important

characteristic of perchlorates is that they are highly deliquescent. Deliquescence is the process of absorbing water vapor from the atmosphere to produce a saturated aqueous solution. Previous work has suggested that perchlorate has a very low deliquescence relative humidity (43% RH) (Zhang et al., 2005; Zhao et al., 2005). However, these studies were performed at room temperature. In order to understand the role of perchlorate salts on Mars and their interaction with atmospheric water vapor, phase transition experiments must be performed at low temperatures more relevant to Mars. Therefore in Chapter 4 we study the deliquescence (solid $\rightarrow$ aqueous solution) and the reverse process, efflorescence (aqueous solution $\rightarrow$ solid), of the particular perchlorate salts found on Mars. We use a Raman microscope to determine the relative humidity at which these transitions occur.

Previous discussions of perchlorate solution stability on Mars have only considered thermodynamics. In Chapter 4, we demonstrate and discuss the role that kinetics could play in inhibiting salt crystallization and therefore allowing supersaturated salt solutions to exist. We also discuss some related properties such as the eutectic temperatures (T_E) of perchlorate solutions and propose that the eutectic temperature of sodium perchlorate is actually much lower than previously suggested. Then, we estimate the periods of time during a diurnal cycle on Mars during which either stable or metastable solutions could exist in the shallow subsurface.

Chapter II

Methane adsorption on a Martian soil analog

2.1 Introduction

As briefly discussed in the introduction, trace amounts of methane (CH_4) have recently been discovered in the Martian atmosphere. Ground-based measurements as well as orbiter-based observations by Mars Express have indicated the average global mixing ratio of CH_4 is about 10 ppbv (Formisano et al., 2004; Krasnopolsky et al., 2004). This discovery has created interest and excitement in the Mars science community, mainly because the source of the CH_4 is unknown. Possible sources include volcanic activity (Wong et al., 2003), meteoritic influx (Formisano et al., 2004), hydrothermal alteration of minerals (Lyons et al., 2005; Oze and Sharma, 2005; Atreya et al., 2007), or the release of CH_4 stored in subsurface clathrate structures (Max and Clifford, 2000; Prieto-Ballesteros et al., 2006; Chastain and Chevrier, 2007; Madden et al., 2007). As the dominant source of CH_4 on Earth is biogenic activity, the presence of methanogens on or under the Martian surface is also an exciting possibility (Boston et al., 1992; Weiss et al., 2000; Jakosky et al., 2003; Varnes et al., 2003; Krasnopolsky et al., 2004).

In addition to the detection of CH_4 in the Martian atmosphere, several studies have also reported significant variability in the atmospheric CH_4 concentration (Formisano et al., 2004; Geminale et al., 2008; Mumma et al., 2009). It is unclear if the variation is temporal or spatial, latitudinal or longitudinal, or correlated with any

other trace atmospheric species. Regardless, the cause of the variability of CH_4 is unknown. Currently, the only known pathways by which CH_4 is destroyed are direct photolysis by solar UV radiation and homogeneous oxidation by OH and O (^1D). The lifetime of CH_4 with respect to these loss pathways is around 340 years, significantly longer than the vertical mixing time (~10 days) and the horizontal mixing time (~0.5 years) on Mars (Krasnopolsky et al., 2004). Consequently, one would expect the CH_4 in the Martian atmosphere to be well mixed, but observations suggest otherwise. It seems likely that there is another process removing CH_4 from the atmosphere. In order to explain the observations, this unknown loss pathway, whether it is a temporary or permanent CH_4 sink, probably has a lifetime shorter than one Martian year (Lefevre and Forget, 2009).

One CH_4 loss pathway which has been proposed is the dissociation of CH_4 by large-scale electric fields that result from convective dust activity (Farrell et al., 2006). However, it has recently been suggested that electric discharges may not occur during Martian dust saltation and therefore CH_4 dissociation is perhaps less significant than previously thought (Kok and Renno, 2009).

Another CH_4 sink that has been proposed but is poorly understood is heterogeneous reaction with the dusty Martian surface (Formisano et al., 2004; Krasnopolsky et al., 2004). Krasnopolsky et al., (2006) ruled out oxidation of Martian CH_4 by metal oxides, as the low surface temperatures on Mars result in slow reaction kinetics. However, simple adsorption, a process likely facilitated by cold temperatures, has not been experimentally or theoretically investigated. Specifically,

both the rate of adsorption and the equilibrium surface coverage are higher at lower temperatures for many systems (Adamson, 1973).

Although the regolith is probably a poorly sorted mixture containing small pebbles, rock fragments and clods (Moore et al., 1999), it is believed that a large portion consists of fine mineral dust particles, the majority of which are probably in the range of 5 to 10 μm in diameter and possibly smaller (Cooper and Mustard, 1999). The large specific surface area of these mineral particles (SSA_{soil}), which is estimated to be 1.7×10^4 m^2 kg^{-1} (Ballou et al., 1978) but is possibly higher, in combination with the large soil depths which may be available to diffusing atmospheric species over short time scales, could allow CH_4 to access and adsorb to a very large total surface area of mineral dust. It is not yet known, however, if any interaction occurs between the CH_4 and mineral dust, causing CH_4 to be either temporarily or permanently removed from the atmosphere. There have been no quantitative studies of the kinetics of CH_4 adsorption onto any surface under Martian conditions and no studies of CH_4 adsorption onto JSC-Mars-1, the standard soil used to simulate the Martian regolith.

A parameter that is useful in quantifying the heterogeneous loss of a gas phase species onto a given surface is the uptake coefficient, γ. This is defined as the fraction of collisions with the surface that lead to loss from the gas phase as a result of chemical reaction, chemisorption or physisorption. In this paper, we experimentally determine γ for the adsorption of CH_4 onto JSC-Mars-1 using a Knudsen cell able to mimic the low temperature and pressure conditions found on Mars. We have measured values of γ for CH_4 adsorption on JSC-Mars-1 from 115 to 135 K and

extrapolated the values to higher temperatures with more relevance to the Martian surface. Finally, we apply these γ values to the Martian atmosphere/surface system and discuss the likely time scales of CH_4 removal by heterogeneous adsorption to the regolith at typical Martian temperatures, CH_4 mixing ratios and diffusion depths. We show that the adsorptive loss of CH_4 to soil at equatorial and mid-latitudes is a possible explanation for the observed atmospheric variability.

2.2 Experimental Methods

2.2.1 Sample

The material located in the top layers of the Martian regolith is thought to be largely the product of mechanical weathering of basaltic rock, with minor chemical alteration (Christensen et al., 2004; Hamilton et al., 2005). Specifically, it has been suggested that palagonitization of basalt more readily explains the bulk Martian surface dust composition than does any other process (McSween and Keil, 2000). The structure of palagonite is heterogeneous in nature and mineralogically amorphous, although possibly microcrystalline (Murakami et al., 1989). JSC-Mars-1 is a weathered basalt from Mauna Kea, HI that is spectrally and chemically similar to mineral dust on Mars (Morris et al., 2003).

The major elemental composition of JSC-Mars-1 as determined by X-ray fluorescence is as follows: 43.5% SiO_2, 23.3% Al_2O_3, 15.6% Fe_2O_3, 6.2% CaO, 3.4% MgO, 3.8% TiO_2 and 2.4% Na_2O (Allen et al., 1998). The exact mineralogies present, along with the nature of the active mineral surface that may be adsorbing CH_4, is not known.. However, we chose to use JSC-Mars-1 for CH_4 adsorption studies as it is the

terrestrial analog most commonly used in laboratory studies of the Martian surface (Singer, 1982; Orenberg and Handy, 1992; Quinn and Orenberg, 1993).

JSC-Mars-1 was obtained from Dr. Carlton Allen of Lockheed Martin Space Mission Systems & Services (Houston, TX). The sample was the sub-mm size fraction of a palagonite tephra collected from a cinder cone located in the saddle between Mauna Loa and Mauna Kea volcanoes on the island of Hawaii (Allen et al., 1998). The material was ground with a mortar and pestle in order to increase the homogeneity of the sample and decrease the average particle size to be more representative of the fine-grained, mechanically-weathered dust on the Martian surface. Using scanning electron microscopy, particle sizes were found to range from ~1-10 μm. In order to determine the total surface area available to adsorbing gas molecules for a given JSC-Mars-1 sample, the Brunauer-Emmett-Teller (BET) specific surface area (SSA_{BET}) was measured and found to be 1.00×10^{5} m^2 kg^{-1} (measurement performed by Material Synergy, Oxnard, CA).

We analyzed the potential biological activity of the JSC-Mars-1 samples using fluorescence microscopy and DNA-specific fluorescent dyes able to detect the presence of single cells. We did not definitively identify any cells in the JSC-Mars-1 sample studied, leading us to believe the analog is relatively biologically clean.

2.2.2 Knudsen Cell

Samples of JSC-Mars-1 were weighed and then placed on a silicon wafer which was attached to a gold-coated copper mount using stainless steel clips. Thermal contact was improved by placing indium foil between the silicon wafer and mount and also between other junctions in the system. The entire sample mount assembly

was attached to a liquid nitrogen (N_2)-cooled cryostat. The desired sample temperature was attained by resistively heating against the liquid N_2. Heating occurred within a vacuum jacket separate from the main chamber to ensure the temperatures of the sample, mount and silicon wafer were uniform. The temperature was controlled with a Eurotherm temperature controller that could maintain temperatures from 100 to 300 K. A type-T thermocouple directly monitored the sample temperature. The sample could be isolated from the reactant gas flow by covering it with a retractable Teflon cup which seals against the chamber walls with an o-ring. Methane gas (Airgas, research grade) was introduced to the chamber through a leak valve.

All CH_4 uptake experiments were performed in a stainless steel, high vacuum chamber described in detail previously (Frinak et al., 2004) and shown schematically in Fig. 2.1. The main chamber houses a UTI 100C electron impact ionization quadrupole mass spectrometer (QMS) to monitor the partial pressures of gas phase species, as well as an ionization gauge and an MKS Baratron capacitance monometer to measure total pressure. The pressure in the chamber was always low enough so that the system was in the Knudsen regime. The chamber was evacuated through a calibrated escape orifice by a 210 L s^{-1} turbomolecular pump (Pfeiffer). The effective area of this escape orifice (A_{eff}), a value used when converting CH_4 pressure to flow, was found to be 0.00833 ($\pm 6.7\times10^{-4}$) cm^2 when calibrated with N_2.

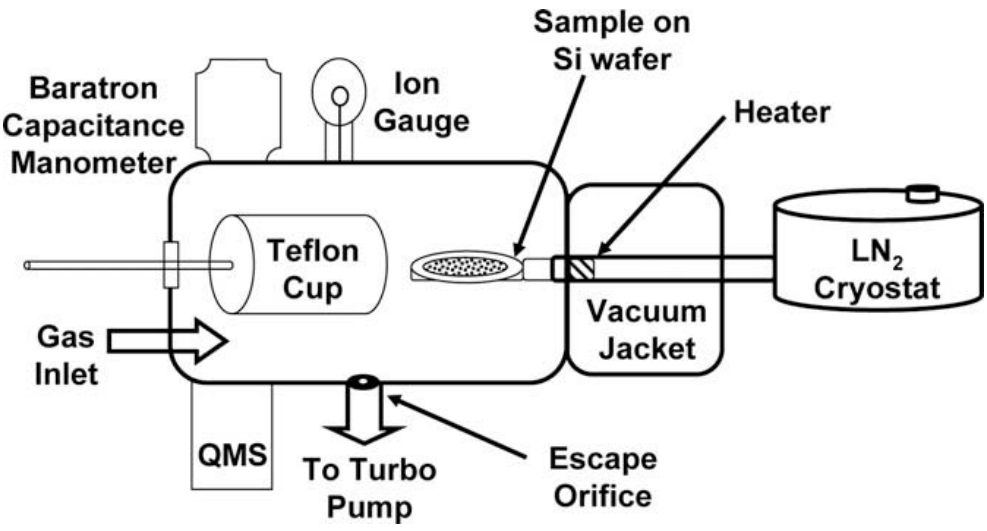

Figure 2.1 Experimental schematic of Knudsen cell reaction chamber.

2.2.3 Experimental Procedure

After addition of a sample, the Knudsen cell was evacuated for 48 hrs or until a background pressure of 2×10^{-7} Torr was achieved. A typical experiment began by cooling the JSC-Mars-1 sample to the desired temperature between 115 and 135 K. The sample was isolated by closing the Teflon cup. Then, a CH_4 calibration was performed to correlate the QMS signal intensity at *m/z* = 15 amu to the CH_4 pressure as measured by the capacitance manometer. Following the calibration, a given partial pressure of CH_4 (P_{CH4}) was added to the chamber through a leak valve. The CH_4 signal was allowed to stabilize for approximately 30 min before exposure to the sample.

Once a constant CH_4 flow was established, the Teflon cup was retracted and the sample was exposed to the gas phase CH_4 for the desired period of time, t_{exp}. After exposing the cooled sample to the desired partial pressure of CH_4, the leak valve was closed and all unbound, gas phase CH_4 was pumped out of the vacuum chamber for 8 minutes. Then, temperature programmed desorption (TPD) was performed to desorb any adsorbed CH_4. The temperature of the sample was increased at a linear rate which varied from 5 to 50 K min^{-1}. The CH_4 thermally evolved from the sample was detected by monitoring *m/z* = 15 amu with the QMS.

2.2.4 Data Analysis

The QMS signal at *m/z* = 15 amu collected throughout the experiment was converted to P_{CH4} using calibration data. This pressure was then converted to flow (CH_4 molecules s^{-1}) using Eq. 2.1:

$$F_{CH_4} = \frac{P_{CH_4} A_{eff}}{(2\pi M_w k_B T)^{1/2}} \quad (2.1)$$

where M_w is the molecular weight of CH_4, k_B is the Boltzmann constant and all other values have been defined previously. A graph of flow (molecules s^{-1}, left axis) and T (K, right axis) vs. time (s) for a typical experiment is shown in Fig. 2.2a with the important events labeled. The TPD portion of the experiment is enlarged in Fig. 2b. This particular experiment was performed at T = 115 K, t_{exp} = 440 s, P_{CH4} = 5×10^{-4} Torr, and JSC-Mars-1 sample mass (m_{sample}) = 1.00 g. The desorbed CH_4 was quantified by integrating the area underneath the desorption peak which yields the number of CH_4 molecules desorbed, N_{des}.

As some bound CH_4 molecules may desorb from the JSC-Mars-1 surface after the CH_4 exposure ends and be pumped out of the chamber before TPD begins, the amount of desorbed CH_4 measured during TPD is probably a lower limit of what was originally bound to the surface, i.e. $N_{des} \leq N_{ads}$. As this difference would be very difficult to quantify, for subsequent data analysis and interpretation we assume that the total number of CH_4 molecules that were adsorbed to the surface following exposure, N_{ads}, is equal to N_{des}.

As seen in Fig. 2.2b, experiments performed on a blank Si wafer resulted in significantly less CH_4 adsorption than when a sample was present. This was typical of all experimental conditions studied and confirmed that nearly all of the CH_4 adsorption occurred on the JSC-Mars-1 particles and not the Si wafer or some other component of the experimental system. Specifically, blank experiments always yielded N_{ads} values less than 10% of the N_{ads} value determined from similar experiments performed on a JSC-Mars-1 sample. All values of N_{ads} that appear in this

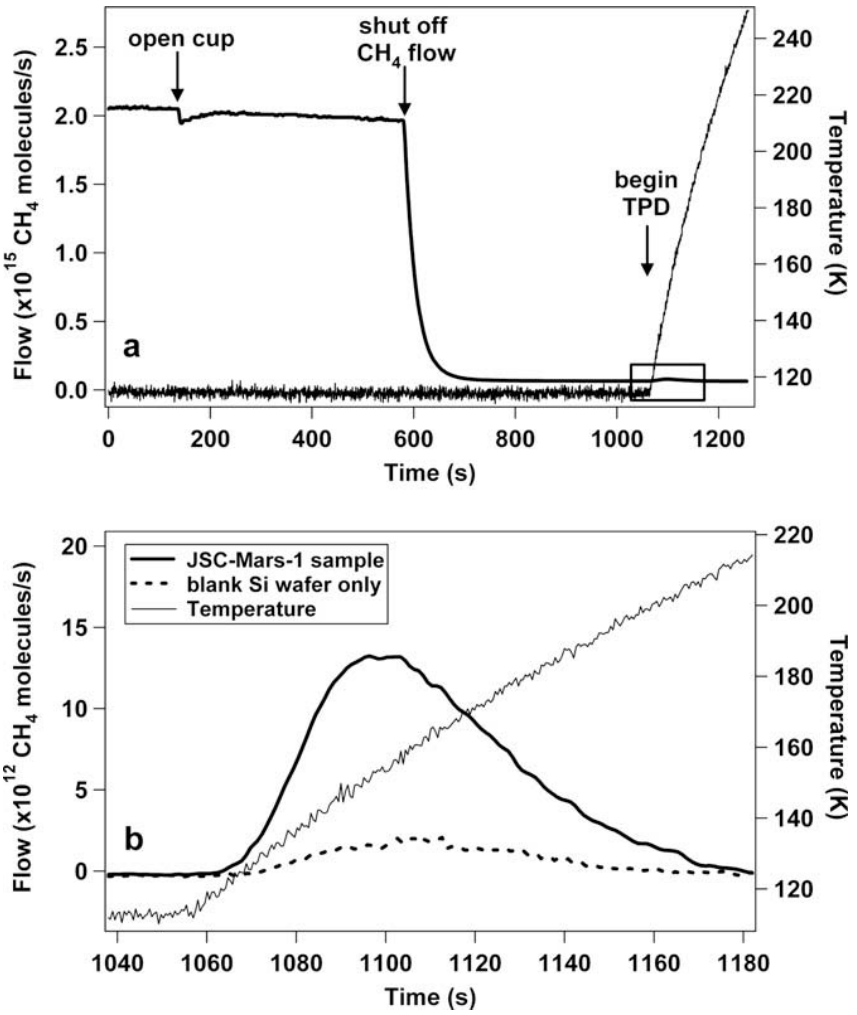

Figure 2.2 (a.) Plot of CH_4 flow (left axis, thick line) and temperature (right axis, thin line) vs. time for a typical experiment performed at $P_{CH4} = 5\times10^{-4}$ Torr, $m_{sample} = 1.0$ g, $T = 115$ K and $t_{exp} = 440$ s. The three significant events during an experiment which contribute to changes in flow are labeled. The shaded area is enlarged in (b.) which shows a typical TPD profile. The flow axis is expanded to clearly show the CH_4 desorption peak. An experiment performed on a blank Si wafer under the same conditions is also shown (dashed line).

paper's results were corrected for the small amount of uptake that did occur on the blank by subtracting the N_{ads} of the corresponding blank. Methane adsorption is occurring at very low temperatures (T ≤ 145 K) during experiments and desorption is usually complete by T = 200 K, temperatures too low for any microbiological metabolization involving CH_4. As we also failed to positively detect any biological contamination in the JSC-Mars-1 sample, we are confident that the CH_4 adsorption/desorption occurring is purely abiotic.

2.2.5 Experiments Performed

To understand the factors that affect the adsorption process and to more accurately apply the results to Mars, CH_4 desorption experiments were performed as a function of m_{sample}, T, P_{CH4}, and t_{exp}. Values of m_{sample} ranged from 0.1 to 1.0 g, and values of t_{exp} ranged from 100 to 3000 s. Due to the limits of detection of the QMS, we could not detect any CH_4 desorption at sample temperatures above 135 K. Thus studies were performed over the temperature range 115 to 135 K. Methane uptake studies were performed at P_{CH4} values of 5×10^{-5} to 1×10^{-3} Torr. These values are higher than the actual partial pressure of CH_4 in the Martian atmosphere by 3 – 4 orders of magnitude, as a 10 ppbv mixing ratio on Mars corresponds to ~5×10^{-8} Torr. However, instrumental limits of detection prevented us from performing experiments at such low CH_4 partial pressures.

2.3. Results of methane adsorption experiments

2.3.1 Sample mass dependence

To determine if the entire BET surface area of our samples was available for CH_4 adsorption, we studied the amount of CH_4 adsorbed as a function of m_{sample}. JSC-Mars-1 sample masses of 0.10 g, 0.50 g, and 1.00 g, as well as a blank Si wafer (0.00 g sample) were studied and the resulting plot is shown in Fig. 2.3. Experiments shown here were performed at $P_{CH4} = 5\times10^{-4}$ Torr, $T = 115$ K, and $t_{exp} = 440$ s. It can be seen that the size of N_{ads} increases linearly with m_{sample}, confirming that the experiments were performed in the mass-dependent regime. In studies of more reactive gases, it has been found that uptake no longer increases linearly with sample mass for very large samples (Carlos-Cuellar et al., 2003; Hatch et al., 2007). This regime, which is termed the plateau regime, occurs when incident gas molecules are adsorbed only in the upper layers of the sample on the time scale of the measurement, resulting in mass-independent gas uptake. Due to the linear relationship found between N_{ads} and m_{sample} under all experimental conditions, we assume that diffusion through the sample is not a limiting factor and the entire surface area of the sample is available for CH_4 adsorption over the time scale of an experiment.

2.*3.2 Temperature dependence*

Figure 2.4 shows the amount of CH_4 desorbed as a function of sample temperature. It can be seen that N_{ads} decreases exponentially with increasing temperature. All experiments shown here were performed at $P_{CH4} = 5\times10^{-4}$ Torr, $m_{sample} = 0.5$ g, and $t_{exp} = 440$ s. This general relationship between N_{ads} and T was the

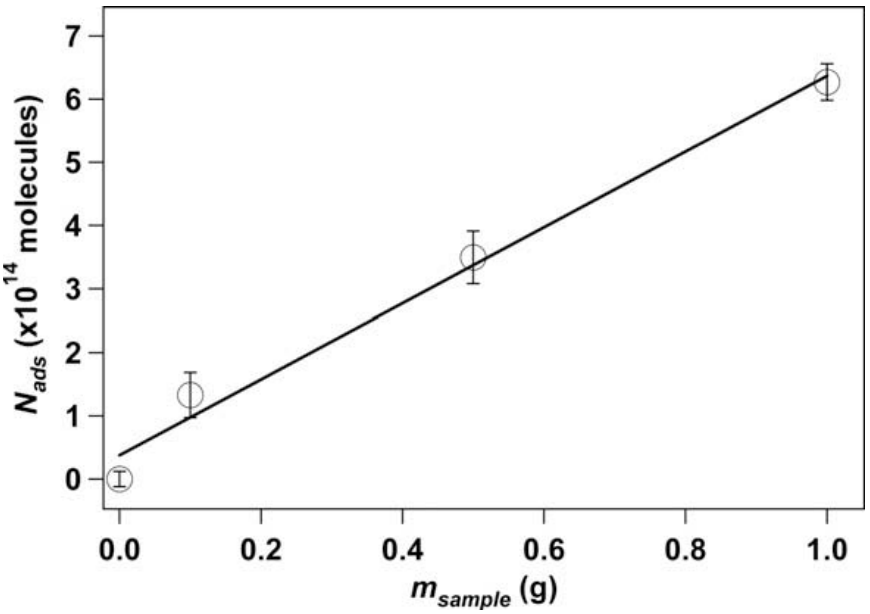

Figure 2.3 Amount of CH_4 adsorbed as a function of JSC-Mars-1 sample mass. All experiments were performed at $P_{CH4} = 5\times10^{-4}$ Torr, $T = 115$ K and $t_{exp} = 440$ s.

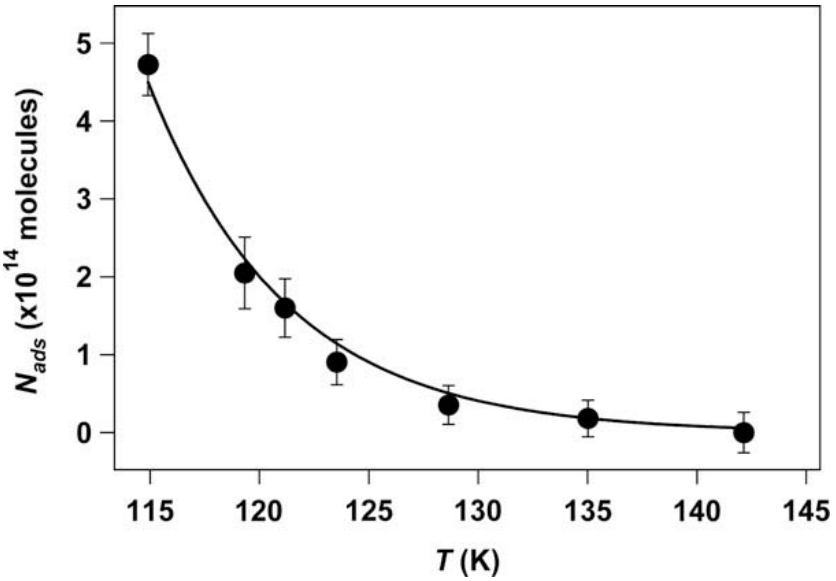

Figure 2.4 Amount of CH_4 adsorbed as a function of sample temperature. All experiments were performed at $P_{CH4} = 5\times10^{-4}$ Torr, $m_{sample} = 0.5$ g, and $t_{exp} = 440$ s. An exponential fit through the data is shown.

same at other values of P_{CH4}, m_{sample} and t_{exp} (not shown). Although different than the temperature dependence of the kinetics of most chemical reactions, this relationship is expected for adsorption for most molecules (Pick, 1981).

2.3.3 Dose dependence

Experiments were performed to determine if the total amount of adsorbed CH_4 depends on both P_{CH4} and t_{exp}. The dose (Torr·s) of CH_4 is defined to be the product of P_{CH4} and t_{exp}, i.e. dose = $P_{CH4} \cdot t_{exp}$. Figure 2.5 shows N_{ads} as a function of dose over the temperature range studied, and it can be seen that N_{ads} is proportional to dose for all temperatures. Note also that we found N_{ads} to be linearly proportional to t_{exp} when P_{CH4} was held constant and linearly proportional to P_{CH4} when t_{exp} was held constant (not shown).

2.3.4 Determination of γ

We use the relationship between CH_4 dose and N_{ads} to determine γ, the uptake coefficient for CH_4 on JSC-Mars-1. For each experiment performed, N_{ads} is converted to a unitless, fractional monolayer coverage (θ) via Eq. 2.2

$$\theta = \frac{N_{ads}}{SSA_{BET} m_{sample} ML_{CH_4}} \tag{2.2}$$

where ML_{CH4} is the monolayer coverage of CH_4 (5.21×10^{14} molecules cm^{-2}) as determined from the size of an adsorbed CH_4 molecule (19.18Å^2) (Chaix and Domine, 1997).

In the Knudsen regime, a dose of 1.0×10^{-6} Torr·s of a gas at room temperature results in monolayer coverage ($\theta = 1$) if $\gamma = 1$. This relationship between dose, γ and θ is shown in Eq. 2.3:

$$\gamma = \frac{\theta}{\text{dose}} \times 10^{-6}\ \text{Torr·sec} \tag{2.3}$$

Therefore, γ is graphically determined by plotting the experimentally determined θ values as a function of dose and applying a linear fit through zero. The data in Fig. 2.5 were analyzed in this manner to determine γ between 115 and 135 K. These values of γ for CH_4 on JSC-Mars-1 are $3.0(\pm0.3) \times 10^{-12}$ at 115 K, $1.6(\pm0.2) \times 10^{-12}$ at 120 K, $6.6(\pm0.7) \times 10^{-13}$ at 125 K, $2.6(\pm0.3) \times 10^{-13}$ at 130 K, and $2.2(\pm0.3) \times 10^{-13}$ at 135 K.

2.3.5 Modeling the uptake coefficient

The uptake coefficient can be modeled for a general system of gases adsorbing onto a solid (Boudart and Djega-Mariadassou, 1984). We assume adsorption is occurring on a clean surface ($\theta = 0$), a valid assumption as the coverage values found in our experiments were very small, with $\theta < 1\times10^{-5}$. We also assume adsorption is not an elementary process: the gaseous molecule (M_g) first forms a weakly bound precursor state (M_p) before adsorption of the molecule occurs (M_a).

$$M_g \underset{k_0}{\overset{\omega k_{coll}}{\rightleftarrows}} M_p \xrightarrow{k_b} M_a \tag{2.4}$$

The rate constants for the formation of the adsorbed precursor state, desorption, and formation of the bound final product are ωk_{coll}, k_0, and k_b, respectively, where ω is the mass accommodation coefficient which we assume is unity, and k_{coll} is the rate.

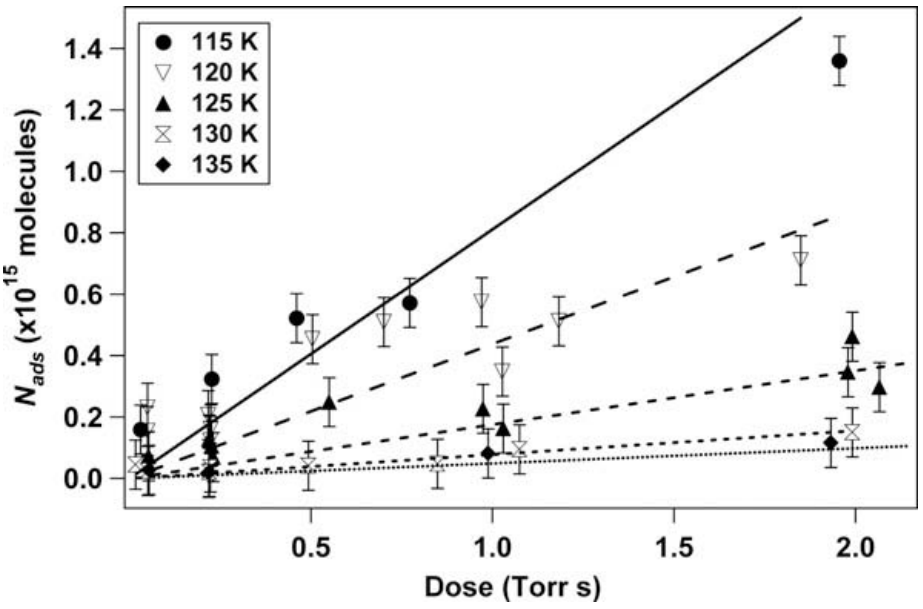

Figure 2.5 Amount of CH_4 adsorbed as a function of dose at a series of temperatures. All experiments shown were performed on a 0.5 g JSC-Mars-1 sample.

constant for collision obtained from the kinetic theory of gases. The uptake coefficient, γ, is therefore equal to

$$\gamma = \frac{adsorption rate}{collision rate} = \frac{k_{bp}[M]}{k_{collg}[M]} \quad (2.5)$$

For the system in Eq. 2.4, a steady state approximation for M_p results in

$$\gamma = \frac{1}{1 + k_0/k_b} \quad (2.6)$$

As described by Warsnop et al. (1989), simple Arrhenius rate expressions can be written to represent both possible fates of an intermediate precursor state: formation of the bound product or evaporation from the surface. These steps would involve overcoming the energetic barriers $\Delta E_{a,bind}$ and $\Delta E_{a,evap}$, respectively. The expression for the ratio of these rate constants, k_b/k_0, can be written in terms of the observed energy barrier of the transition state to adsorbed CH_4 relative to the gas phase, ΔH_{obs}.

$$\frac{k_b}{k_0} = \frac{A\exp\left(\frac{-\Delta H_{obs}}{RT}\right)}{} \quad (2.7)$$

where A is the ratio of preexponential factors for the Arrhenius expressions and contains information regarding the entropy change in the system. Combining Eqs. 6 and 7 yields

$$\ln\left(\frac{\gamma}{1-\gamma}\right) = \ln A + \frac{-\Delta H_{obs}}{RT} \quad (2.8)$$

Figure 2.6 shows a plot of $\ln(\gamma/(1-\gamma))$ vs. T^{-1}. It can be seen that the data is well modeled by this uptake theory that has been used in the past for a wide range of systems (Jayne et al., 1991; Hudson et al., 2002; Shilling et al., 2006). From the slope of Fig. 2.6, we find that the observed energy change, ΔH_{obs}, for CH_4 adsorption onto

JSC-Mars-1 is -4.3 (±0.4) kcal mol^{-1}. This measured value, ΔH_{obs}, is not identical to the overall adsorption enthalpy, ΔH_{tot}; rather, it is a lower limit. However, the value of ΔH_{obs} is similar in size to overall adsorption enthalpies reported by others for similar systems (CH_4 adsorption on mineral surfaces). For example, Golden and Sircar (1994) found ΔH_{tot} = -4.46 kcal mol^{-1} for CH_4 adsorption on a microporous silicate, Pereira et al. (2001) measured ΔH_{tot} = -3.82 kcal mol^{-1} on a pillared clay, and Zhang et al. (1991) found ΔH_{tot} = -4.80 kcal mol^{-1} on a sodium zeolite.

Due to instrument sensitivity, the highest T at which we were able to detect CH_4 adsorption is lower than the minimum surface temperature on Mars. With some possible exceptions (Weiss and Ingersoll, 2000), the temperature of the Martian surface is thought to never drop below about 148 K, the condensation point of CO_2. Therefore, extrapolation out of the range of experimental temperatures is necessary. The linear fit through the data seen in Fig. 2.6 (y = -45.41 (± 1.58) + 2173.4 (± 197) x) was used to extrapolate values of γ to higher temperatures with more relevance to Mars.

The extrapolation that must be performed from our experimental conditions (T and P_{CH4}) to actual Martian surface conditions results in added uncertainty. However, the linear relationship between CH_4 dose and amount of methane adsorbed implies that the extrapolation to much lower CH_4 pressure (but much longer exposure times) is valid. Also, the linear relationship and small error in the data shown in Fig. 2.6 suggest that extrapolation to higher temperatures is also justifiable.

Another possible source of error in the application of our experimental results to Mars is the likelihood of CH_4 co-adsorbing with water and/or CO_2 (depending on

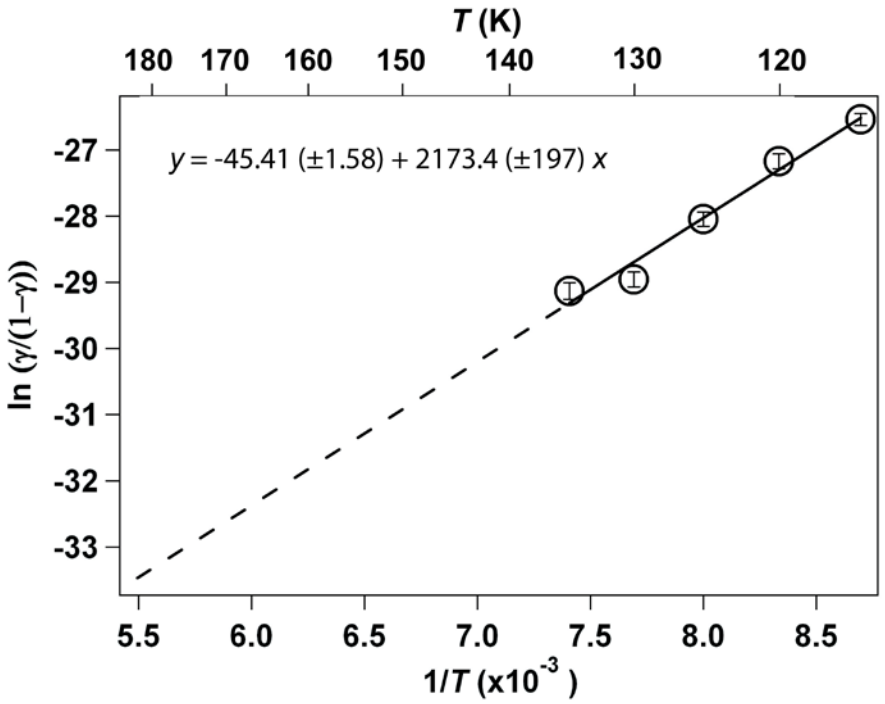

Figure 2.6 Plot to determine ΔH_{obs} for CH_4 adsorption on JSC-Mars-1 using experimentally determined values of the uptake coefficient. The linear fit and function used to extrapolate to warmer temperatures is shown.

the time of day or season on Mars). The condensation of other species could affect methane adsorption by mineral surfaces on Mars. However, work by Trainer et al. (2009) found no uptake of CH_4 by condensed-phase CO_2 or water. Therefore, if minerals were completely ice or dry-ice coated, CH_4 would most likely not be adsorbed. However, we find that CH_4 is occupying very few sites on these minerals, so complete coverage by CO_2 or H_2O may be needed to prevent CH_4 from adsorbing. Future work should explore the effects of co-adsorption of these two species and CH_4.

2.4 Discussion

With information about the total number of collisions between CH_4 and a mineral surface per unit time that occur on Mars and an experimentally determined or extrapolated value of γ at a given surface T, we can estimate a time scale over which a column of CH_4 could be removed from the atmosphere.

In addition to determining the time needed for the Martian regolith to adsorb CH_4, we need to also consider the time needed for the CH_4 molecules in a given atmospheric column to reach the planet's surface. However, as the vertical mixing time of Mars is ~10 days, atmospheric transport is not a limiting factor in the adsorptive loss of CH_4 to soil over the season or year.

To quantify CH_4 loss, first we approximate the CH_4 flux, Φ_{CH4}, (molecules m^{-2} s^{-1}) to any surface on Mars:

$$\Phi_{CH_4} = \frac{1}{4} \nu n_{CH_4} \quad (2.9)$$

where ν is the mean molecular speed (m s^{-1}) of CH_4 at a temperature T given by the Maxwell-Boltzmann distribution of gas velocities, $\nu = (8RT/\pi M_w)^{1/2}$, and n_{CH4} is the

number density of CH_4 on Mars (molecules m^{-3}). On the surface of Mars, a CH_4 mixing ratio of 10 ppbv corresponds to $n_{CH4} = 2.2\times10^{15}$ molecules m^{-3}.

The flux to a mineral surface that is adsorbed, Φ_{ads}, is equal to $\gamma \times \Phi$ and can be used to estimate the time required to remove an atmospheric column of CH_4 by adsorption to soil, τ_{ads}

$$\tau_{ads} = \frac{N_{CH_4}}{\Phi_{ads} \cdot SSA_{soil} \cdot \rho_{soil} \cdot d_{soil}} \tag{2.10}$$

where N_{CH4} is the CH_4 column abundance above 1 m^2 of regolith (molecules m^{-2}), SSA_{soil} and ρ_{soil} are the specific surface area (m^2 kg^{-1}) and density (kg m^{-3}) of the Martian soil, respectively, and d_{soil} is the depth (m) of the regolith column that the CH_4 is able to access. A mixing ratio of 10 ppbv at Martian surface gravity and pressure conditions corresponds to about $N_{CH4} = 2.2\times10^{19}$ CH_4 molecules m^{-2}. We use a value for ρ_{soil} of 1650 kg m^{-3} (Feldman et al., 2004). SSA_{soil} on Mars is usually taken to be 1.7×10^4 m^2 kg^{-1} (Ballou et al., 1978), which is the only value ever reported. However, the accuracy and global applicability of this measurement are unknown and it has been suggested that this value could be an underestimate (Clifford and Hillel, 1983; Mohlmann, 2004). The SSA_{soil} of terrestrial minerals, especially clay minerals, is often 100× higher (Zent et al., 2001; Mohlmann, 2003; Frinak et al., 2005). It is possible that phyllosilicate minerals, known to exist on Mars, may result in a larger SSA_{soil} in localized regions. Therefore, we will study two cases: a "low" SSA_{soil} case (1.7×10^4 m^2 kg^{-1}) and a "high" SSA_{soil} case, where we will take SSA_{soil} to be an order of magnitude higher (1.7×10^5 m^2 kg^{-1}). In each case we assume that this entire surface area is available for CH_4 adsorption.

Diffusion coefficients can be calculated to constrain the depth into the regolith which CH_4 can diffuse, d_{soil}. Gaseous transport through a porous solid can occur via ordinary molecular diffusion and/or Knudsen diffusion. The radius of the pores in the solid, r_{pore}, and the mean free path of the diffusing species, λ, influence which of these diffusive processes will dominate. If the ratio of r_{pore} to λ is large ($r_{pore}/\lambda > 10$), ordinary molecular diffusion, fueled by molecular collisions, will be the dominant mode of transport. However, when diffusion occurs in smaller pores or when gas concentrations are more dilute ($r_{pore}/\lambda < 0.1$), collisions between diffusing molecules and the pore walls is the dominant transport mechanism. This is the region of Knudsen diffusion. For intermediate ratios of r_{pore}/λ, diffusion occurs via both mechanisms, and this is called the transition region (Clifford and Hillel, 1983).

On Mars, λ is about 10 μm at surface pressure. The pore size distribution in the regolith is probably very broad, but typical r_{pore} values of 1-10 μm have been suggested (Fanale et al., 1986; Mellon and Jakosky, 1993; Skorov et al., 2001), resulting in $r_{pore}/\lambda = 0.1 – 1.0$. As CH_4 diffusion through the Martian surface could occur in both the Knudsen and transition regimes, both types of diffusion processes should be considered.

We can determine values for the diffusion coefficient, D_{CH4}, valid for the specific case of atmospheric CH_4 diffusing into the soil pores under Martian T and P_{CH4} conditions. To find D_{CH4} as a function of T and r_{pore}, we employ the general method used by Mellon and Jakosky (1993), specifically equations 10-17 from that paper, to model diffusion of water (H_2O) into the Martian regolith. The Knudsen and molecular diffusion coefficients were separately calculated using CH_4-specific mass,

size, and number density when calculating reduced mass, collision diameter, and mixing ratio. The coefficient components of the collision integral at each temperature (Hirschfelder, 1954) and energies of attraction (Satterfield, 1970) were also specifically for the CH_4/carbon dioxide (CO_2) system, as the primary molecule with which CH_4 will interact during diffusive transport is CO_2. The soil pores are assumed to contain atmospheric concentrations of CO_2. The molecular and Knudsen diffusion coefficients were combined via the Bosanquet interpolation formula to give D_{CH4} for the full range of diffusion types.

Figure 2.7 shows the dependence of D_{CH4} on T and r_{pore}. The smaller box (thick line) represents the range of typical Martian pore radii often reported in the literature (1-10 μm). The larger box (thin line) represents the slightly wider range of r_{pore} values used in this study to determine D_{CH4} values and calculate approximate diffusion times. As expected, the value of D_{CH4} depends only weakly on T and varies mainly as a function of r_{pore}. For r_{pore} values < 1 μm, Knudsen diffusion dominates and D_{CH4} is thus strongly dependent on r_{pore}. For r_{pore} values > 50 μm, molecular diffusion dominates and D_{CH4} is independent of r_{pore}. The transition region of diffusion occurs in the range of r_{pore} values typical of Martian soil, r_{pore} = 1 – 10 μm. The values of the diffusion coefficient we calculate for this r_{pore} size range at 150 K, D_{CH4} = 2.3-7.5 cm^2 s^{-1}, are very similar to values found both theoretically and experimentally for the diffusion of other gas phase species into the Martian regolith (Mellon and Jakosky, 1993; Hudson et al., 2007).

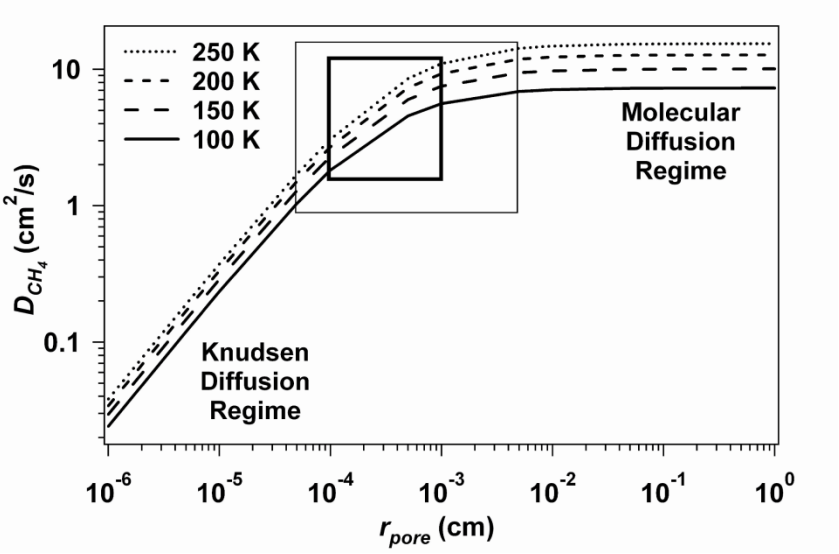

Figure 2.7 Calculation of typical diffusion coefficient values for CH_4 through Martian soil (D_{CH4}) as a function of T and r_{pore}. The black box represents typical Martian pore radii sizes as reported in the literature. The grey box represents the range of r_{pore} values used in this study to calculate characteristic diffusion times.

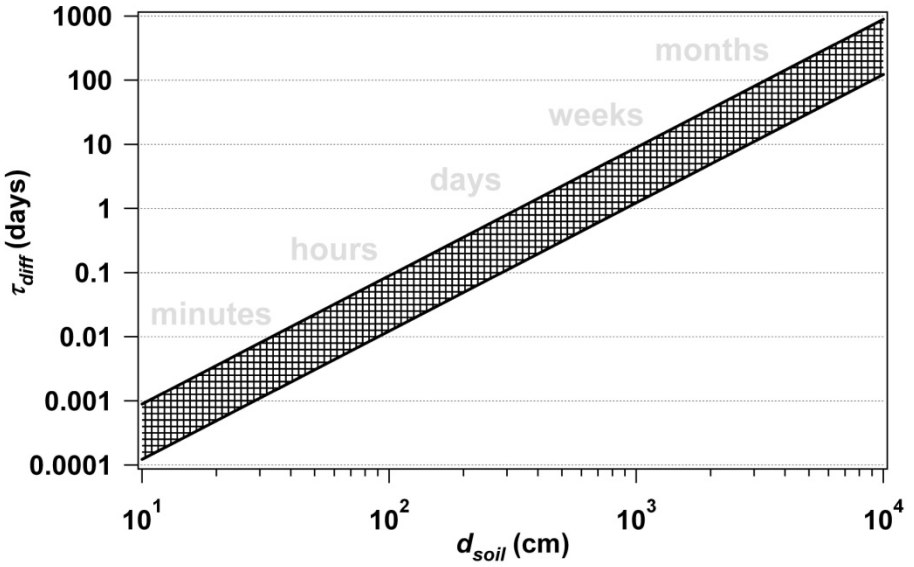

Figure 2.8 The approximate time in earth days, τ_{diff}, needed for CH_4 to diffuse into the Martian surface to depth d_{soil}. The upper limit of the patterned line represents the lifetime that corresponds to diffusion through fine-grained or highly packed/consolidated material (r_{pore} = 0.5 µm). The lower limit of the patterned line represents the lifetime that corresponds to diffusion through material with larger pore sizes (r_{pore} = 50 µm).

The equation of diffusion can be approximated in one dimension in the presence of a constant surface flux to yield the time, τ_{diff}, required for a species to diffusely propagate a given distance, or in this case a vertical depth into the regolith. We will use this approximation, $\tau_{diff} = d_{soil}^2/D_{CH4}$, to estimate the time required for CH_4 to access a given depth of soil. As the pore size range on Mars is not known and likely to be both broad and highly variable, we solve for τ_{diff} as a function of d_{soil} using both r_{pore} of 0.5 μm (D_{CH4} = 1.29 cm^2 s^{-1}) and r_{pore} of 50 μm (D_{CH4} = 9.42 cm^2 s^{-1}) as lower and upper limits, respectively, for the likely range of pore sizes in the Martian regolith. It can be seen in Fig. 2.8 that while CH_4 can access the top meter of regolith in a few hours and the top 10 m in less than a month, time scales longer than a Martian year are needed for CH_4 to diffuse 100 m. These values are similar in magnitude to other CH_4 diffusion times that have been reported (Krasnopolsky et al., 2004).

As we are studying CH_4 adsorption and not CH_4 diffusion, we only consider cases where the CH_4 uptake process is adsorption limited and not diffusion limited. As diffusion into the top 10 m of soil will be relatively rapid compared to a Martian season or year, we consider d_{soil} values of 1 and 10 m when solving for τ_{ads} as a function of T (Eq. 2.10). The results of this calculation are shown in Fig. 2.9. The upper and lower limits of τ_{ads} for each diffusion depth correspond to the low SSA_{soil} (1.7×10^4 m^2 kg^{-1}) and high SSA_{soil} (1.7×10^5 m^2 kg^{-1}) estimates, respectively, for Martian soil. The shaded portion of Fig. 2.9 indicates temperatures below the frost point of CO_2 (148 K). The dashed black line represents one Martian year. In order for a process to explain the reported atmospheric CH_4 variability, it likely occurs on a

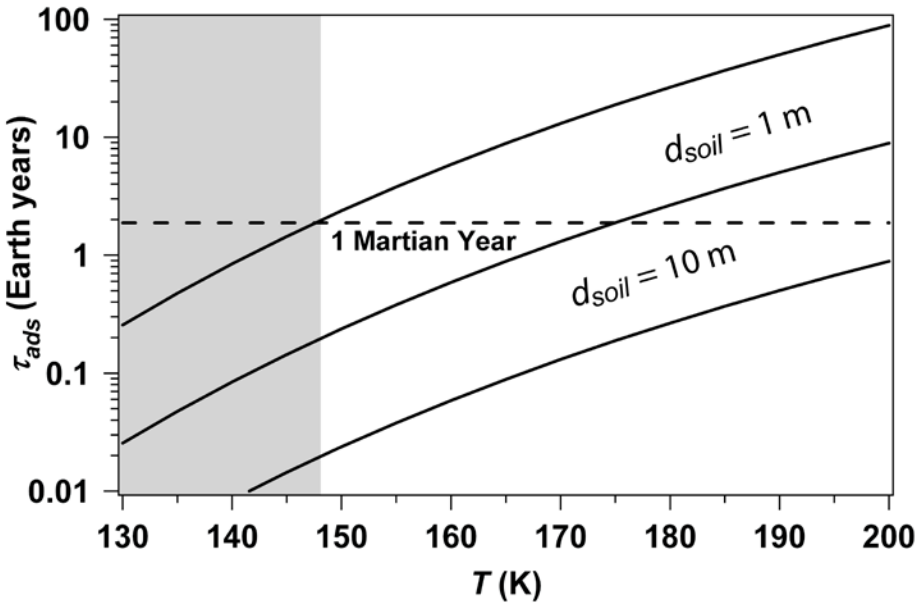

Figure 2.9 Lifetime of CH_4 due to adsorption to soil grains, τ_{ads}, as a function of subsurface soil temperature if CH_4 can diffuse to d_{soil} = 1 m or 10 m. The shaded area at low *T* indicates conditions not likely to occur on or in the Martian regolith under typical conditions.

time scale less than ~1 yr.

It can be seen in Fig. 2.9 that colder surface temperatures, deeper diffusion depths, and higher surface area minerals such as clays or zeolites will result in shorter CH_4 lifetimes. This process could potentially be an important CH_4 sink on Mars if certain soil depth and subsurface temperature scenarios occurred. It is also important to note that all calculated adsorption lifetimes, τ_{ads}, at temperatures higher than 148 K are longer than the values of τ_{diff} at the 1 and 10 m depths studied, confirming that these depths would indeed be accessible to diffusing CH_4 molecules.

Thus far, we have only addressed the kinetics of adsorption. Our experiment can only measure kinetic parameters and equilibrium is not approached, judging from the linear relationship between N_{CH4} and CH_4 dose. Although it is unlikely that a steady state with respect to CH_4 adsorption would exist on Mars either, based on the high temporal variability of atmospheric CH_4 that has been observed, it is important to quantify the possible equilibrium coverage, θ_{eq}, present on Martian mineral surfaces. For adsorption to be an important CH_4 sink, not only must the uptake and release be sufficiently rapid, but θ_{eq} must be large enough under typical Martian T and P_{CH4} conditions to explain the loss of an atmospheric CH_4 column into the top layers of soil. We can calculate the fractional coverage that would exist if an entire atmospheric CH_4 column adsorbed to soil depths of 1 or 10 m using Eq. 2.11.

$$\theta = \frac{N_{CH_4}}{ML_{CH_4} \cdot SSA_{soil} \cdot \rho_{soil} \cdot d_{soil}} \tag{2.11}$$

The highest calculated θ would occur when the atmospheric CH_4 column adsorbs to a shallow depth (d_{soil} = 1 m) of "low" surface area soil (SSA_{soil} = 1.7×10^4 m^2 kg^{-1}). This coverage is small ($\theta = 1.47\times10^{-7}$), and deeper accessible soil depths and larger SSA_{soil} values would result in an even smaller coverage being required to remove significant atmospheric CH_4.

Although equilibrium was not reached on the time scale of our experiments, kinetics can be used to estimate the surface coverage present at equilibrium, θ_{eq}, for given temperature and pressure conditions. The equilibrium constant, K_{eq}, for a simple, one-step adsorption process is approximately equal to k_a/k_d. The rate constant for adsorption, k_a, can simply be approximated as $\gamma\, k_{coll}$, or ¼ $\gamma\, \nu\, (ML_{CH4})^{-1}$. The rate constant for desorption, k_d, can be estimated from transition state theory

$$k_{des} = \frac{k_B T}{h} \exp(\quad / \quad) \qquad (2.12)$$

where η is the evaporation coefficient, h is Planck's constant, and $E_{a,des}$ is the activation energy for desorption. It has been shown that the uptake and evaporation coefficients for a reversible adsorption/desorption process are approximately equal (Haynes et al., 1992 and references therein) so we assume $\eta \approx \gamma$. Also, for weak adsorption processes, such as physisorption, there is no or a very small energetic barrier to adsorption, and $E_{a,des}$ is approximately equal to -(ΔE_{obs}), the adsorption energy we determined experimentally. Therefore, the ratio of rate constants results in the following expression for K_{eq}:

$$K_{eq} = \frac{\nu h}{4 k_B T} \exp(/) \qquad (2.13)$$

It has been shown that the adsorption of CH_4 can be modeled satisfactorily by the Langmuir isotherm, given in Eq. 2.14 (Golden and Sircar, 1994; Himeno et al., 2007); thus, one can use K_{eq} to approximate θ_{eq} for CH_4 at a given P_{CH4} and T:

$$\theta_{eq} = \frac{KP_{eqCH_4}}{1 + KP_{eqCH_4}} \tag{2.14}$$

Figure 2.10 shows the calculated θ_{eq} values at P_{CH4} = 4.5×10^{-8} Torr (corresponding to 10 ppbv CH_4 on Mars) as a function of T (dashed line). Also shown are values of θ_{eq} for other studies of CH_4 adsorption on similar surfaces, including clay and zeolite minerals (open symbols) (Zhang et al., 1991; Golden and Sircar, 1994; Prasetyo and Do, 1999; Pereira et al., 2001; Himeno et al., 2007). These other studies directly measured θ_{eq} experimentally, rather than indirectly determining it from kinetics as we have done. However, as these experiments were not performed at Martian temperatures and pressures, reported K_{eq} values were extrapolated to appropriate conditions prior to determination of these θ_{eq}. Our calculated θ_{eq} values are consistent with these literature values, confirming that the approximations used in the transition from kinetics to thermodynamics were likely valid.

To interpret the θ_{eq} results in a Martian context, the coverage present if all the CH_4 in a 10 ppbv atmospheric CH_4 column adsorbed to a regolith column of d_{soil} = 1 or 10 m is also plotted in Fig. 2.10. The range of values for each depth has the same meaning as in Fig. 2.9. The shaded region represents T < 148 K. At T < 170 K for d_{soil} = 1 m and at T < 200 K for d_{soil} = 10 m, the calculated θ_{eq} values are on the same order or larger than the coverage values required to explain the loss of an atmospheric CH_4 column on Mars. Although CH_4 coverage on Martian minerals undergoing

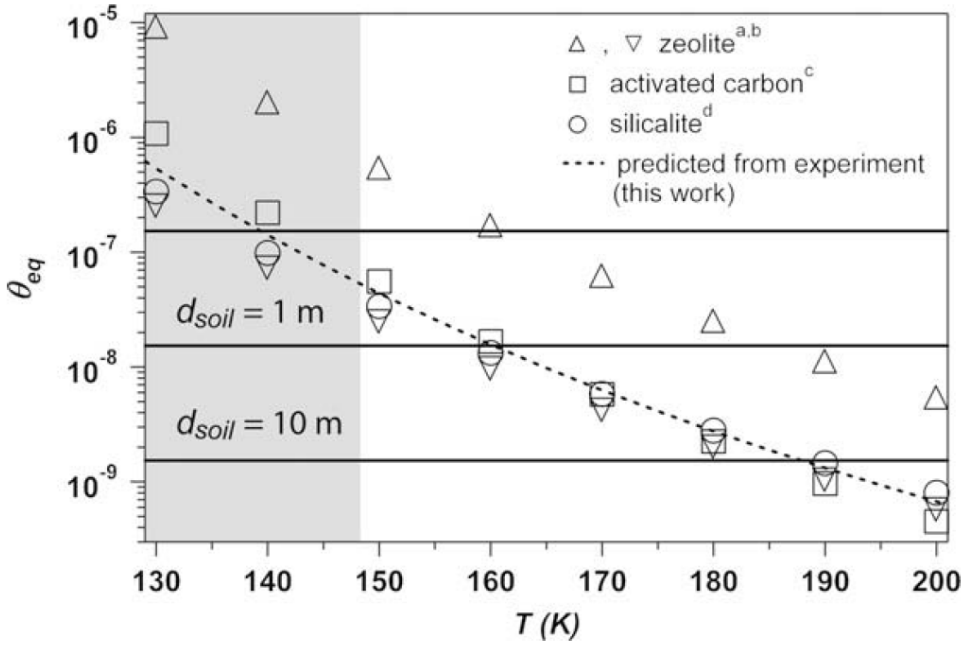

Figure 2.10 Equilibrium surface coverage as function of *T*. Values predicted by the Langmuir isotherm for CH_4 adsorption on JSC-Mars-1 at $P_{CH4} = 4.5 \times 10^{-8}$ Torr, corresponding to 10 ppbv CH_4 on Mars (dashed line) correlate well with experimental θ_{eq} values determined by others for a variety of surface types (symbols: a (Zhang et al., 1991), b (Himeno et al., 2007), c (Prasetyo and Do, 1999), d (Golden and Sircar, 1994). Solid lines represent minimum θ values required for a soil column to adsorb the atmospheric CH_4 column, as described in the text.

seasonal temperature changes is not likely to reach equilibrium, the regolith at depths below the annual thermal wave depth may contain equilibrium adsorbed CH_4 and act as a large reservoir. Our derived θ_{eq} values indicate that our proposed CH_4 recycling mechanism is thermodynamically as well as kinetically feasible.

Below, we discuss the possibility of conditions arising which could lead to non-negligible CH_4 adsorption by the Martian regolith; namely when and where significant atmospheric CH_4 loss could occur in less than a Martian year. We also discuss this proposed adsorption process in the context of recent observations of Martian CH_4.

2.5 Implications for methane on Mars

The Martian surface and subsurface are characterized by large diurnal and annual temperature oscillations. The exact magnitude of the thermal skin depth depends on factors such as the thermal inertia of the local material, but it is thought the diurnal skin depth is on the order of a meter (Jakosky, 1983; Hudson et al., 2007). Simulations by Tokano (2003) suggest the amplitude of seasonal temperature variation becomes zero only below a depth of 10 m. This large seasonal variation in the temperature of the top layer of soil is known to play a significant role in the Martian hydrological cycle, and we suggest it could be important for the Martian CH_4 cycle as well.

As seen in Fig. 2.9, significant CH_4 loss due to adsorption will occur only where 1 m or more of soil is cold for several months, conditions only likely to exist during the winter. We can estimate where the regolith could be a seasonal CH_4 reservoir by determining a typical wintertime temperature profile at each latitude.

Temperature variations in the Martian subsurface have been modeled both for homogeneous dry soil and a layered subsurface (dry soil above an ice table) (Mellon et al., 2004). The depth of the ice table, the sharp boundary between dry soil and the impermeable, icy layer that it covers, remains constant over the year but increases with decreasing latitude (Mellon and Jakosky, 1993), varying from a few mm at the poles to a few m at ±50° latitude (Mellon et al., 2004). As studies suggest gas diffusion through ice could take 10^6 times longer than through a porous soil (Tomoko et al., 2002), the ice table will probably significantly hinder diffusive transport.

For the case of homogeneous, dry soil with a thermal inertia (I) of 250 J m^{-2} K^{-1} $s^{-1/2}$, a value representative of much of the Martian regolith (Putzig et al., 2005), the minimum temperature experienced by the subsurface depends on depth, and increases from the annual minimum surface temperature (T_{min}) at d_{soil} = 0 m to the annual mean surface temperature (T_{mean}) at d_{soil} = 3 m (Mellon et al., 2004). Below 3 m, annual temperature oscillations are small. If subsurface ice is present, however, the wintertime subsurface temperatures increase more rapidly with depth, reaching T_{mean} at the ice table depth (d_{ice}) instead of at d_{soil} = 3 m. We assume similar soil properties such that, for each 10° latitudinal bin, the wintertime subsurface temperatures increase linearly from T_{min} at the surface (d_{soil} = 0 m) to T_{mean} at either d_{soil} = 3 m if d_{ice} > 3 m or $d_{soil} = d_{ice}$ if d_{ice} < 3 m. Values of T_{min} and T_{mean} as a function of latitude were obtained from Tokano et al. (2003) and values of d_{ice} from Mellon et al. (2004). We only consider adsorption by the layers of soil which experience significant annual temperature variation (i.e.: the top 3 m, or the depth of the ice table at latitudes higher than ±55°).

We assume this subsurface temperature profile is valid throughout the Martian winter (200 sols) and calculate the mass of CH_4 (m_{CH4}) in tons that could be lost from the atmosphere during the winter due to adsorption into the regolith. In Fig. 2.11, m_{CH4} lost per 10° latitudinal bin is plotted as a function of latitude for the low and high SSA_{soil} values discussed previously. Poleward of ±55°, the insufficient depth of dry, ice-free soil above the ice table, as well as the small land area per latitudinal bin, results in negligible CH_4 loss. However, the equatorial regions and mid-latitudes have large CH_4 adsorption potential. Also, as this adsorption process is likely to be fully reversible over the year, regions able to adsorb significant CH_4 in the winter will release the CH_4 into the atmosphere when the subsurface warms in the spring and summer.

The dashed line in Fig. 2.11 represents 2111 metric tons of CH_4, which is the average amount of CH_4 that would need to be emitted per 10° latitudinal bin in the northern hemisphere in order to produce the 19,000 ton CH_4 plume observed by Mumma et al. (2009). This plume was observed to be emitted from discrete regions in the northern hemisphere during the northern summer. Our results for the high SSA_{soil} scenario integrated over the entire northern hemisphere yield a possible wintertime CH_4 sink and thus summertime CH_4 source of 30,400 tons. Even if only latitudes between 25 and 45° N are considered, 19,500 tons of CH_4 can be lost and released seasonally. Although it is not likely that this adsorption/desorption process could result in point source CH_4 emission, it is possible that a CH_4 source of the magnitude observed can be explained by this proposed process, particularly if high specific

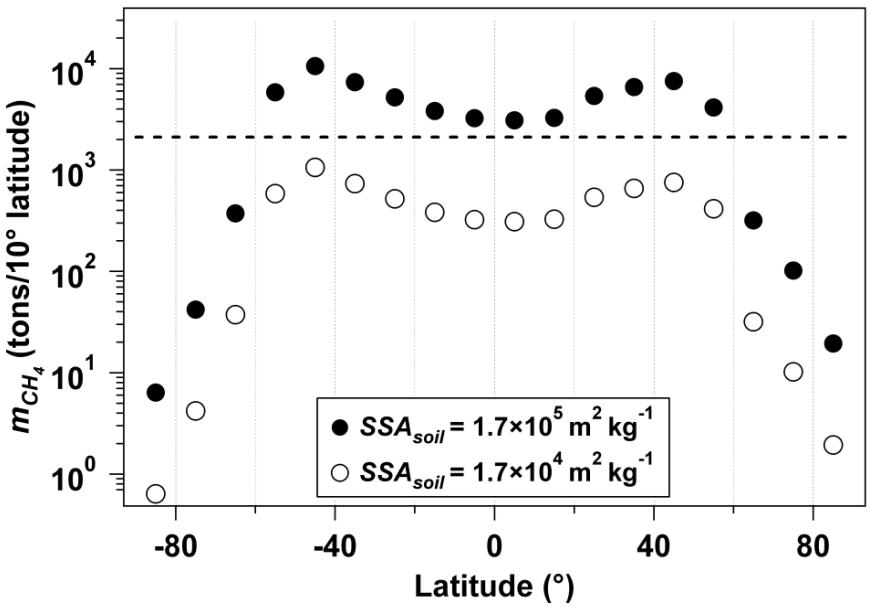

Figure 2.11 The mass of CH_4 that could be removed from the Martian atmosphere by each 10° latitudinal bin during the winter months (200 sols) by adsorption to the regolith, assuming typical wintertime subsurface temperature profiles at each latitude. In the spring and summer, this CH_4 can be released from the regolith.

surface area soil is present in the regolith. Of course, the Martian regolith is not uniform as we have assumed, and our model presented in Fig. 2.11 is meant only to be illustrative. More extensive simulations with global models accounting for the variability of the Martian subsurface and atmospheric transport are warranted. We have also examined only one Mars analog. Mars has a varied surface mineralogy and it is possible some surface materials are even more absorbing than the one we studied, and others less. As a result desorption could be relatively localized to regions with highly absorbing minerals.

Although some details have been reported thus far as to the observed variability of the CH_4 in the Martian atmosphere and its dependence on season, latitude, or longitude, a clear, consistent picture of the behavior of CH_4 on Mars and its probable source and sink locations does not yet exist. Mumma et al. (2008; 2009) find the variability may be seasonal and consistent with episodic release, and suggest that an additional CH_4 destruction pathway is needed, with a lifetime on the order of one year, to explain the existence of the depleted regions. Mumma et al. (2004) and Geminale et al. (2008) both report that the CH_4 may be positively correlated with atmospheric H_2O vapor. These observations would be expected in the case of temperature-dependent CH_4 adsorption, as CH_4 and H_2O would both adsorb to mineral surfaces when temperatures drop in the late fall and winter, and would both desorb as surface and subsurface temperatures rise again in the spring. Indeed, Mumma et al. (2009) hypothesize that the observations are consistent with a CH_4 source that is “activated thermally by warming of a surface zone.”

In order to explain the observed temporal and spatial CH_4 variability, both a relatively rapid source and sink are required. Most other studies of Martian CH_4 have only attempted to explain the currently unknown source, hypothesizing that volcanic activity, clathrate dissociation or biological methanogenesis could be releasing CH_4 into the atmosphere. None of these sources, regardless of magnitude or rate of CH_4 production, could independently explain the observed spatial and temporal variability unless CH_4 is also being rapidly removed from the atmosphere by some other process much more rapid than photolysis. The regolith exchange mechanism discussed in this paper is the only process proposed thus far which intrinsically contains both an atmospheric CH_4 loss and an atmospheric CH_4 production mechanism. Also, as no net CH_4 destruction occurs via this reversible process, there is no required increase, relative to balancing photolysis and gas-phase oxidation, in the magnitude of a potential CH_4 source to account for the observed mixing ratio variations.

2.7 Conclusions

We have studied the adsorption kinetics of CH_4 on JSC-Mars-1 under low pressure and low temperature conditions similar to those found on the Martian surface. We have experimentally determined the value of the uptake coefficient, γ, for this process at T = 115 - 135 K and then extrapolated our temperature-dependent results to Martian surface temperatures. We show that the presence of subsurface conditions such as high surface area soil grains, cold temperatures, and ice table levels on the order of a meter or more can contribute to rapid CH_4 loss. It is both kinetically and thermodynamically possible for the heterogeneous adsorption of CH_4

to mineral surfaces to be a significant, temporary CH_4 sink during the winter on Mars, particularly in the mid-latitude and equatorial regions. These regions could release the CH_4 in the summer months when subsurface temperatures rise. Temperature-dependent surface adsorption is consistent with the reported seasonal and spatial variability in CH_4 concentration.

Chapter III

Constraining the rate of methane oxidation by oxidants in the Martian regolith

3.1 Introduction

As we describe in Chapter 2, weak, temperature-dependent physical adsorption of CH_4 to minerals is a mechanism that could potentially explain the recently observed CH_4 variability in the atmosphere of Mars. However, it is also useful to consider if there might be chemical destruction of methane (and ompensating sources) operating on seasonal time scales. A complete understanding of the Martian CH_4 sinks is important for constraining and quantifying the possible CH_4 sources. In order to understand the CH_4 cycle on Mars, the mechanisms of CH_4 loss, the removal rates, and the geographic location (or spatial homogeneity) of the removal processes are critical data.

Heterogeneous oxidation of CH_4 by the Martian surface is a possible loss pathway that has been proposed (Atreya et al., 2006; Lefevre and Forget, 2009; Mumma et al., 2009), but not yet experimentally investigated. It has been known since the Viking mission in the 1970's that the Martian regolith has the ability to oxidize organic compounds. The Labeled Release (LR) experiment onboard both Viking landers investigated the ability of the soil to oxidize a solution of ^{13}C-labeled organic molecules into $^{13}CO_2$. Prior to launch, oxidation of the organic solution was a criteria for the discovery of life. However, it is now widely believed that a strong

oxidant associated with the mineral grains, or perhaps the soil itself, was chemically reactive.

The species most frequently proposed to be the Martian soil oxidant is hydrogen peroxide (H_2O_2) (Huguenin et al., 1979; Hunten, 1979; Levin and Straat, 1981; Bullock et al., 1994; Zent and McKay, 1994). H_2O_2 could have arrived in the soil via a number of different processes or mechanisms. Following photochemical (Krasnopolsky, 1993) or electrostatic (Atreya et al., 2006; Delory et al., 2006) formation in the atmosphere, the H_2O_2 could diffuse through the subsurface where it could be protected from UV photolysis (Bullock et al., 1994). Alternatively, H_2O_2 could be formed in the soil by interaction of water (H_2O) with pyrite (Davila et al., 2008), olivine (Huguenin et al., 1979) or mechanically ground basaltic minerals (Hurowitz et al., 2007).

Several studies have shown that H_2O_2 is able to closely mimic the Viking LR results, especially when the molecule is complexed with or in the presence of a mineral surface. For example, Levin and Straat (1981) found that a 0.1 M H_2O_2 solution was able to oxidize organic compounds with the approximate kinetics measured by Viking. However, when a γ-Fe_2O_3/silica sand mixture is present, a much lower H_2O_2 concentration (10^{-3} – 10^{-2} M) was able to recreate the LR results. Quinn and Zent (1999) reported that H_2O_2 chemisorbed onto titanium dioxide (TiO_2•H_2O_2) also has the ability to oxidize the organic compounds used in the LR experiment. TiO_2•H_2O_2 was found to possess similar reactivity and thermal stability as the Martian soil studied by Viking.

Although H_2O_2 complexed with Martian soil may be able to rapidly oxidize organic compounds such as sugars and amino acids, it is unclear over what time scale oxidation of gas phase CH_4 could occur. In this work, we have experimentally studied the reaction of CH_4 with several oxidizing analogs. The analog materials studied were peroxide-modified titanium dioxide (TiO_2•H_2O_2), JSC-Mars-1 with H_2O_2, and perchlorate salts (Na^+ and Mg^{2+}).

As mentioned above, Quinn and Zent (1999) discovered that H_2O_2 complexed with the anatase polymorph of TiO_2, was able to oxidize the Viking organic compounds to CO_2. It is also estimated that the regolith contains about 1% TiO_2 (Clark et al., 1977). As it is a suitable chemical analog of the putative soil oxidant on Mars, we chose to study the reactivity of TiO_2• H_2O_2 toward CH_4.

JSC-Mars-1 is a palagonite, or weathered basalt, that is mineralogically amorphous although possibly microcrystalline (Murakami et al., 1989). The major elemental composition of JSC-Mars-1 as determined by X-ray fluorescence is as follows: 43.5% SiO_2, 23.3% Al_2O_3, 15.6% Fe_2O_3, 6.2% CaO, 3.4% MgO, 3.8% TiO_2 and 2.4% Na_2O (Allen et al., 1998). The exact mineralogies present, along with the nature of the active mineral surface, are not known; however, it is a common chemical and spectral analog for the Martian soil (Morris et al., 2003) and frequently used in laboratory studies of the Martian surface (Singer, 1982; Orenberg and Handy, 1992; Quinn and Orenberg, 1993). Therefore, we chose to study the ability of JSC-Mars-1 to oxidize CH_4 both in the presence and absence of H_2O_2.

Perchlorate salts were recently discovered at the Phoenix landing site at a concentration of ~0.5% (Hecht et al., 2009). The salt was detected in three samples

originating from both the surface and shallow subsurface of the north polar landing site. The relevance of this measurement to the general planetary composition is not yet known, but the detection is potentially of interest to the global CH_4 cycle as perchlorate is often reported to be a strong oxidant. Although some have suggested that perchlorate would be fairly unreactive at cold Martian temperatures due to high energetic barriers (Hecht et al., 2009; Catling et al., 2010), the ability of perchlorate salts to oxidize CH_4 has not been investigated. Therefore, we studied the ability of sodium and magnesium perchlorate salts to directly oxidize CH_4. These specific cations (Na^+ and Mg^{2+}) are thought to be the dominant cations at the Phoenix landing site (Hecht et al., 2009).

In addition to the CH_4 studies, a separate series of experiments was performed in which the Viking organic compounds (alanine, glycine, formic acid, glycolic acid and lactic acid) were added to each oxidizing analog. These experiments were done in order to compare to the results of the Viking LR experiment and therefore allow us to compare the reactivity of each analog to the reactivity of the Martian surface.

To detect oxidation of the carbon species (organic solution or CH_4), gas phase CO_2 production was monitored over a 72 hr time period. CO_2 is the complete oxidation product of all organic species, including CH_4, and the quantification of CH_4 oxidation by measurement of evolved CO_2 has commonly been performed (Kiyosu and Krouse, 1989; Kiyosu and Imaizumi, 1996). However, it is possible that other gas-phase oxidation products were formed in the headspace. Therefore, formaldehyde (CH_2O), an intermediate oxidation product of CH_4, was also monitored in select experiments to determine if there was any incomplete oxidation occurring.

3.2 Experimental methods

3.2.1 Sample preparation

TiO_2 (anatase) was synthesized and complexed with H_2O_2 as described in Quinn and Zent (1999). Carefully synthesizing TiO_2, rather than purchasing the material or using natural samples, allowed the chemical state and reactivity of the surface to be carefully controlled and also guaranteed the sample was free of microbial, organic, or other chemical contaminants. It was determined by Quinn and Zent (1999) that calcination for 4 hrs at 250° C results in the removal of molecular H_2O from the sample but leaves the majority of surface hydroxyl groups intact. They found this fully hydroxylated sample was able to mimic the Viking LR results better than a partially dehydroxylated sample (a result of higher temperature calcination).

Peroxide was complexed with the TiO_2 mineral surface by suspending samples of calcined TiO_2 in freshly prepared 1% H_2O_2 solution for 30 min. There was a sudden and dramatic color change from white to yellow, which indicated the formation of the TiO_2•H_2O_2 complex (Munuera et al., 1980). The samples were then rinsed with distilled H_2O and filtered to remove excess, unbound H_2O_2 from the mineral complex (Quinn and Zent, 1999). As we followed the same experimental procedure outlined by Quinn and Zent (1999), we assume the TiO_2•H_2O_2 sample we synthesized has similar properties as they report; namely, the Brunauer-Emmett-Teller (BET) specific surface area (SSA_{BET}) and H_2O_2 coverage of this material are 2.08×10^5 m^2 kg^{-1} and 7.2×10^{17} molecules m^{-2}, respectively. Using scanning electron microscopy (SEM), particle sizes were found to range from ~1-10 μm, with an average particle diameter of ~5 μm. After synthesis, the TiO_2•H_2O_2 was

immediately transferred to a N_2-filled glove bag. After a brief drying period to remove most adsorbed H_2O, 0.1 g portions of the sample were placed into 8.5 cm^3 vials that had been sterilized using an autoclave.

JSC-Mars-1 was obtained from Dr. Carlton Allen of Lockheed Martin Space Mission Systems & Services (Houston, TX). The sample was the sub-mm size fraction of a palagonitic tephra collected from the saddle between Mauna Loa and Mauna Kea volcanoes on the island of Hawaii (Allen et al., 1998). The material was mechanically ground with a mortar and pestle in order to increase the homogeneity of the sample and decrease the average particle size to be more representative of the fine-grained, mechanically-weathered dust on the Martian surface. Using SEM, particle sizes were found to range from ~1-10 μm with an average particle diameter of ~5 μm and the SSA_{BET} was measured to be 1.00×10^5 m^2 kg^{-1} (measurement by Material Synergy, Oxnard, CA). The JSC-Mars-1 sample was weighed into 0.5 g portions and placed into sterilized 8.5 cm^3 vials. Hydrogen peroxide (30% by volume, 0.5 mL) was added to the appropriate vials.

Sodium perchlorate ($NaClO_4$, Sigma Aldrich, >98%) and magnesium perchlorate hexahydrate ($Mg(ClO_4)_2 \bullet 6H_2O$, Sigma Aldrich, 99%) were used without modification. A given perchlorate salt was weighed into 0.5 g portions which were added to 8.5 cm^3 vials.

After the reagents were added, the vials were immediately transferred to a N_2-filled glove bag. The vials were sealed with screw-topped caps with rubber septa while inside the N_2-filled glove bag in order to minimize atmospheric CO_2

contamination. The vials were stored in the dark at 3°C for 48 hours prior to the initial measurement and also between analyses.

3.2.2 Headspace analysis

An initial headspace analysis prior to addition of the organic solution or CH_4 was performed to verify that no atmospheric contamination or sample outgassing had occurred. Analysis of CO_2 in the vial headspace was performed by gas chromatography (GC). A 1.0 cm^3 sample of the headspace was extracted using a gas-tight syringe and injected into an 8610C SRI Gas Chromatograph equipped with a PORAPAK Q 6' x 0.085" I.D. column. A thermal conductivity detector (TCD) was used to detect CO_2 and helium was used as the carrier gas. A four level CO_2 calibration was done using 1.0% and 5.0% CO_2 gas standards (Alltech). Analysis of CO_2 in the vial headspace was performed 24, 48, and 72 hours after the addition of the organic solution or CH_4. Two measurements were taken of each vial at each analysis and averaged, and error was calculated as the standard deviation of the two measurements. The data were corrected for the CO_2 removed from the vial during the previous headspace measurements. The same chromatography column and procedure was also used to monitor formaldehyde in select experiments.

3.2.3 Addition of organic compounds or CH_4

Immediately after the initial measurement at time (t) = 0 hr, either 1.0 cm^3 of 630 Torr 99.99% CH_4 (Alltech) or 0.5 mL of an equimolar solution of DL-alanine (Sigma, 99% purity), glycine (Sigma, >99% purity), formic acid (Sigma, >97%

purity), glycolic acid (Aldrich, 99% purity) and lactic acid (Sigma, 85-90% purity) was added to the vial with a gas-tight syringe. The total molarity of the organic solution was 0.25 M and the pH was adjusted to 8.0 with KOH before the solution was added to the appropriate vials. This aqueous solution of five organic species is similar to the solution used in the Viking LR experiment and will subsequently be referred to as the "organic solution".

3.2.4 Experimental controls

The contents of all vials including controls are listed in Table 1. One series of vials (A, E, J, M) contained both the oxidizing analog (TiO_2•H_2O_2, JSC-Mars-1 + H_2O_2 or perchlorate salt) and a carbon source (either organic solution or CH_4). A series of control vials (B, F, K, N) contained the oxidizing analog but no organic solution or CH_4. Instead, H_2O was added in place of the organic solution and N_2 gas was injected in place of CH_4. These controls were performed in order to determine if atmospheric CO_2 was contaminating the head space or if there was any organic contamination in the sample or vial. Another series of controls (C and G) contained a mineral (TiO_2 or JSC-Mars-1, respectively) and carbon source (organic compounds or CH_4) but no added oxidant (H_2O_2). Control H contained oxidant (H_2O_2) and a carbon source (organic solution or CH_4) but no mineral. These controls were performed in order to understand the relative importance of the mineral and the oxidant in the oxidation process. Lastly, a series of controls (D, I, L, O) contained only the carbon source (organic solution or CH_4). These were used to determine if any oxidation was

abbreviation	vial contents
A_{org}/A_{meth}	$TiO_2 \bullet H_2O_2$ + organic solution/CH_4
B_{org}/B_{meth}	$TiO_2 \bullet H_2O_2$ + H_2O/N_2
C_{org}/C_{meth}	TiO_2 + organic solution/CH_4
D_{org}/D_{meth}	organic solution/CH_4 only
E_{org}/E_{meth}	JSC-Mars-1 + H_2O_2 + organic solution/CH_4
F_{org}/F_{meth}	JSC-Mars-1 + H_2O_2 + H_2O/N_2
G_{org}/G_{meth}	JSC-Mars-1 + organic solution/CH_4
H_{org}/H_{meth}	H_2O_2 + organic solution/CH_4
I_{org}/I_{meth}	organic solution/CH_4 only
J_{org}/J_{meth}	$NaClO_4$ + organic solution/CH_4
K_{org}/K_{meth}	$NaClO_4$ + H_2O/N_2
L_{org}/L_{meth}	organic solution/CH_4 only
M_{org}/M_{meth}	$Mg(ClO_4)_2$ + organic solution/CH_4
N_{org}/N_{meth}	$Mg(ClO_4)_2$ + H_2O/N_2
O_{org}/O_{meth}	organic solution/CH_4 only

Table 3.1 Description of the contents of all vials used in the experiments. In the text, the subscript “org” or “meth” is used to denote if the vial series contained the organic solution (or corresponding control) or CH_4 (or corresponding control).

occurring which was unrelated to the either the mineral or oxidant; for example, due to chemical contamination, photolysis or microbial metabolization.

In the remainder of this paper, the subscript "org" will follow the vial letters given in Table 1 if the vial series being discussed contained organic solution (or corresponding controls) and the subscript "meth" will follow the letter if CH_4 was added (or corresponding control) (e.g.: A_{meth} represents a vial that contains $TiO_2 \bullet H_2O_2$ and CH_4, whereas O_{org} is a control containing organic solution only, etc.).

3.4 Results of methane and organic oxidation experiments

3.4.1 $TiO_2 \bullet H_2O_2$ experiments

At t = 0 hr, prior to the addition of the organic solution, there was very little CO_2 in all vials A_{org}, B_{org}, C_{org} or D_{org} (less than 50 nmol). When the organic solution was added to the 0.1 g $TiO_2 \bullet H_2O_2$ (vial A_{org}), CO_2 was produced at a rate of a few hundred nanomoles per day for the first few days, with the CO_2 production rate leveling off after 48 hours (Fig. 3.1a). None of the controls (B_{org}, C_{org} and D_{org}) contained appreciable amounts of CO_2 even after 72 hours, confirming that little chemical, biological or atmospheric contamination was occurring and also that the $TiO_2 \bullet H_2O_2$ complex, not just the TiO_2 mineral, was responsible for the observed oxidation.

The amount of CO_2 produced per gram of $TiO_2 \bullet H_2O_2$ sample upon addition of the organic solution is very similar to previous studies (Quinn and Zent, 1999). In our study, 4×10^2 nmol of CO_2 had been produced by oxidation of the organic molecules after 72 hours. Quinn and Zent measured 4.5×10^2 nmol CO_2 released

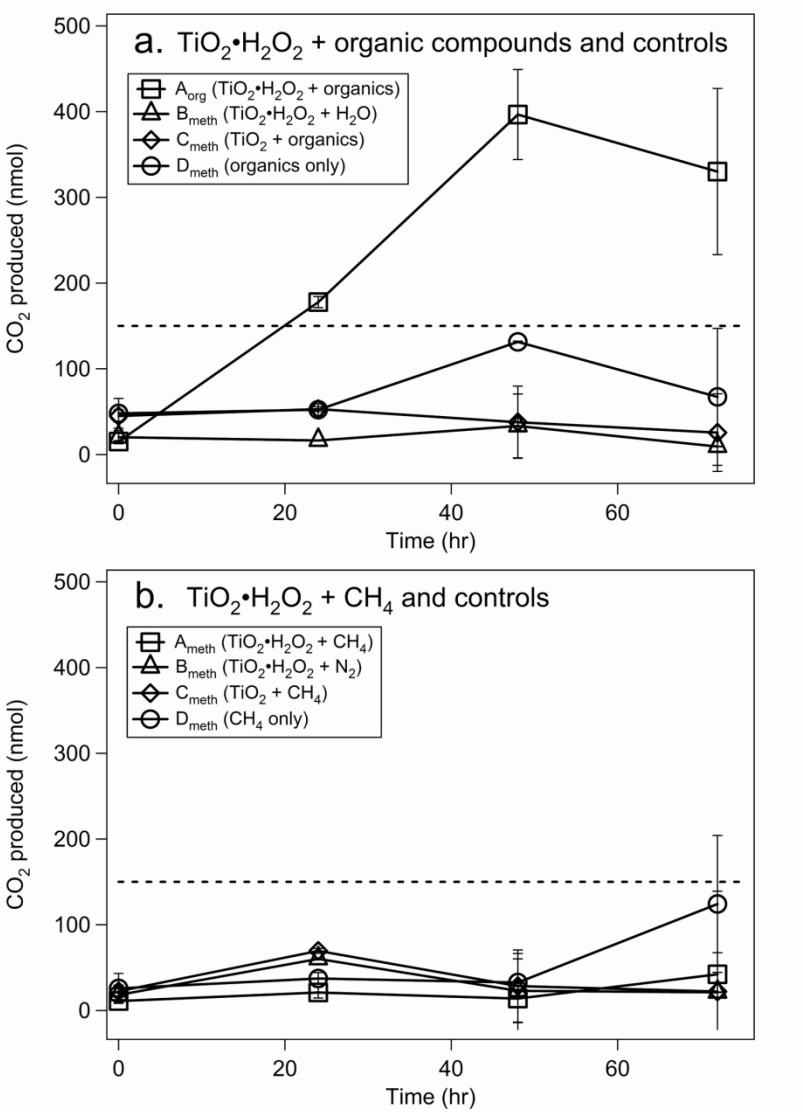

Figure 3.1 The amount of CO_2 produced when the organic solution (a.) or CH_4 (b.) was added to a vial containing TiO_2•H_2O_2 (Vial A, open squares). Other controls, described in Table 1, are also shown. The only vial in which any CO_2 was produced was that which contained TiO_2•H_2O_2 and organic solution. None of the vials to which CH_4 was added produced any CO_2 during the 72 hour experiment. The dashed line at 150 nmol CO_2 represents the current concentration of CO_2 in Earth's atmosphere.

from the same sample mass after 72 hrs, suggesting that our sample probably has similar BET surface area and peroxide coverage.

Before CH_4 was added to the second series of vials (A_{meth}, B_{meth}, C_{meth}, D_{meth}), there was less than 50 nmol of CO_2 present at $t = 0$. However, after CH_4 was added, no additional CO_2 was produced during the 72 hr experiment (Fig. 3.1b). The CO_2 present in vial A_{meth} (TiO_2•H_2O_2 and CH_4) after 72 hr was no greater than that in any of the control vials (B_{meth}, C_{meth} or D_{meth}), signifying that no CH_4 was oxidized to CO_2 within the detection limit of the TCD. The slight increase in control vial D_{meth} (CH_4 only) at $t = 72$ hr is likely due to a leak in the septum causing atmospheric CO_2 contamination and not due to oxidation of CH_4. In Figs. 3.1 through 3.3, the horizontal dashed line at 150 nmol CO_2 represents the current concentration of CO_2 in Earth's atmosphere, confirming that the CO_2 in some control vials is approaching ambient atmospheric mixing ratios due to slow leakage, but also that significantly more CO_2 is being produced by oxidation of the organic solution than could result from atmospheric contamination.

3.4.2 JSC-Mars-1 + H_2O_2 experiments

Unlike the vials containing TiO_2•H_2O_2, there was significant CO_2 in the headspace of the vials containing JSC-Mars-1 and H_2O_2 at $t = 0$ (even before the organic solution was added). Specifically, as seen in Fig. 3.2a, vials E_{org} and F_{org} contained 4.2×10^2 nmol of CO_2 at $t = 0$ hr. This is most likely due to the oxidation by H_2O_2 of organic compounds inherent to the JSC-Mars-1 sample. It is not surprising that this analog soil contains organic matter, as JSC-Mars-1 is an

environmental sample and was not chemically treated prior to these experiments. However, after the organic solution was added, there was much more additional CO_2 produced in vial E_{org} (JSC-Mars-1 + H_2O_2 + organic solution) than in control vial F_{org} (JSC-Mars-1 + H_2O_2 + H_2O). This suggests that the organic solution was being rapidly oxidized in addition to the organic compounds contained in JSC-Mars-1.

There was also a small amount of CO_2 produced in vial H_{org} (JSC-Mars-1 + organic solution) and I_{org} (H_2O_2 + organic solution). However, when both the mineral analog (JSC-Mars-1) and the oxidant (H_2O_2) were present, more oxidation of the organic solution occurred than when only one of these species was present, suggesting that there is an interaction between the surface and H_2O_2 which enhances oxidation of the organics. These results showing that H_2O_2 is a stronger oxidant in the presence of minerals are consistent with the results of Levin and Straat (1981). The only vial that did not contain any CO_2 even after 72 hours was control vial G_{org} (organic solution only), confirming that oxidation of the organic compounds due to chemical or biological contamination was not occurring.

As expected, there was also significant (3.7×10^2 nmol) CO_2 in both vials that contained JSC-Mars-1 and H_2O_2 (E_{meth} and F_{meth}) before CH_4 was injected (t = 0 hr) (see Fig. 3.2b.). However, the addition of CH_4 to the JSC-Mars-1 and H_2O_2 in vial E_{meth} did not result in the production of any CO_2 beyond that produced in control F_{meth} (to which no CH_4 was added). This indicates that that no CH_4 was oxidized to CO_2 within the detection limit of the TCD. The slight increase in CO_2 in several of the controls (G_{meth} and I_{meth}) is likely due to the slow leakage of atmospheric CO_2 into the vial which was discussed above.

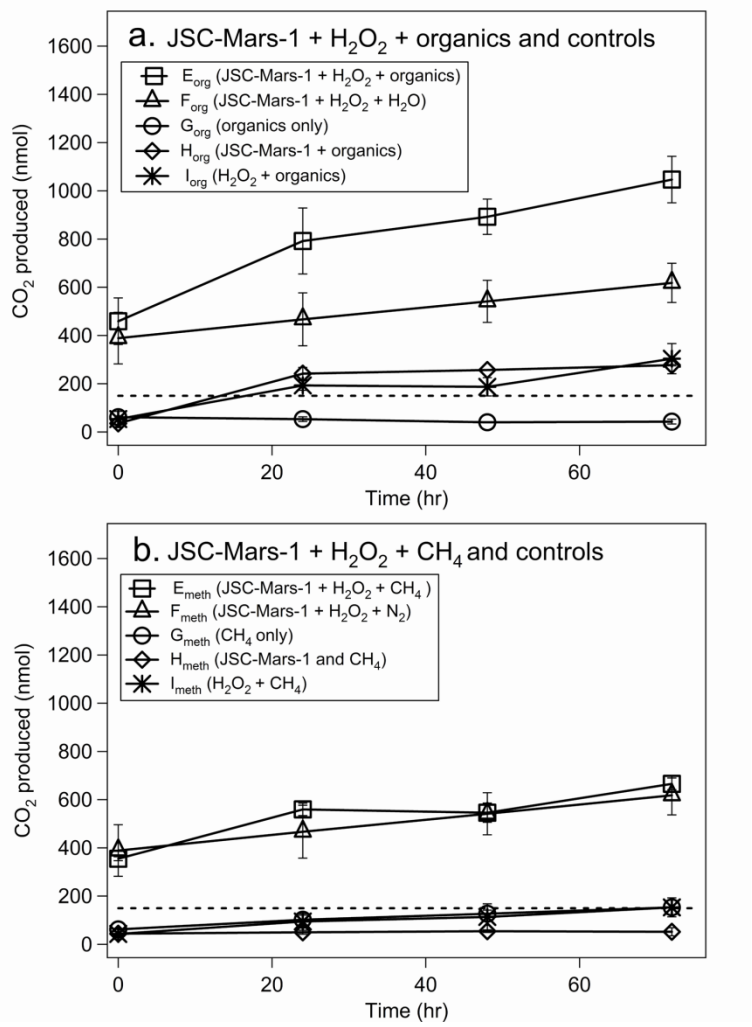

Figure 3.2 The amount of CO_2 produced when the organic solution (a.) or CH_4 (b.) was added to a vial containing JSC-Mars-1 and H_2O_2. Other controls, described in Table 1, are also shown. The large amounts of CO_2 present at $t = 0$ (before any organic solution or CH_4 was added) in vials E_{org} and F_{org} (as well as E_{meth} and F_{meth}) are due to oxidation by H_2O_2 of organic compounds contained in the JSC-Mars-1 sample. Although JSC-Mars-1 and H_2O_2 were able to oxidize the added organic solution, no CH_4 oxidation was observed. This statement is based on the fact that the E_{meth} vials (squares) contained no more evolved CO_2, within error, than the F_{meth} control vials (open triangles) to which only N_2 was added.

When the headspace of vial E_{meth} (JSC-Mars-1 + H_2O_2 + CH_4) was sampled, the observation time was extended past the elution of the CO_2 peak to allow for detection of formaldehyde (H_2CO). We chose to monitor for H_2CO in this particular experiment type as the most total CO_2 was produced during this experiment. However, no H_2CO was detected in the headspace within the limit of detection of the GC instrument. This suggests that there was no complete *or* incomplete oxidation of CH_4 occurring in the vial.

3.4.3 Perchlorate experiments

As seen in Figures 3.3a. and 3.3b., when either the organic solution or CH_4 were added to $Mg(ClO_4)_2$ no more CO_2 was produced in the vials than when only H_2O or N_2 were injected. Although some vials appeared to have a slight leak to the atmosphere, comparison with the control vials indicates that no CO_2 was produced within the detection limit of the TCD. $NaClO_4$ behaved similarly; no detectable CO_2 was observed after the addition of the organic solution or CH_4 (not shown). To the best of our knowledge, the oxidation of CH_4 by perchlorate salts has not been previously studied. The oxidation of a wide range of organic compounds by perchloric acid ($HClO_4$) was studied by Martinie and Schilt (1976). Even under elevated reaction temperatures (200°C), several organic molecules, including the amino acids glycine and alanine, were able to partially survive oxidation by $HClO_4$. It is therefore not surprising that the organic solution of amino acids and sugars was not directly oxidized by perchlorate salts in these low temperature studies. It is even less

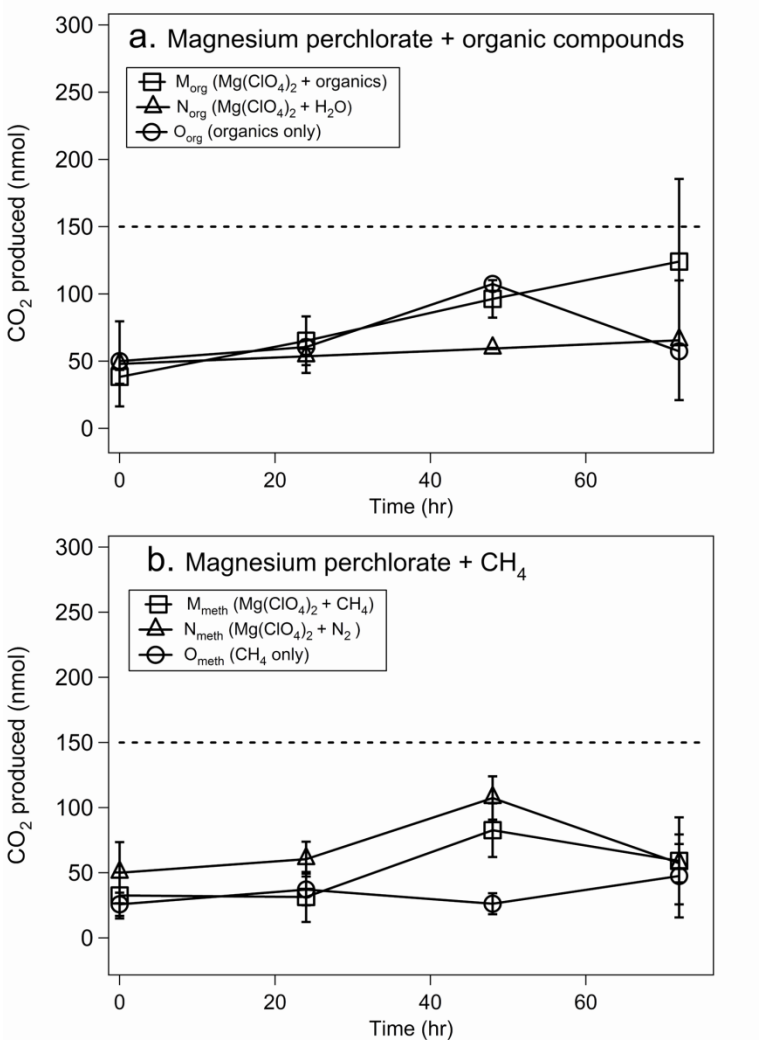

Figure 3.3 CO_2 produced when the organic solution (a.) or CH_4 (b.) was added to $Mg(ClO_4)_2$. Neither the organic solution or CH_4 were oxidized to CO_2 to any measurable extent (open squares).

surprising that CH_4, a low reactivity molecule, was not oxidized by perchlorate salts.

3.5 Discussion

To compare the reactivity of the samples used in this study to the reactivity of the Martian surface, we first normalize CO_2 production with respect to soil mass. As only $TiO_2 \bullet H_2O_2$ and JSC-Mars-1 + H_2O_2 oxidized the organic solution, only these two analogs are considered in this comparison. The Viking LR experiment utilized 0.5 cm^3 of soil, corresponding to a mass of 0.83 g assuming a soil density (ρ_{soil}) of 1650 kg m^{-3} (Feldman et al., 2004). In our experiments and presumably in the Viking LR experiments the oxidant (H_2O_2) was the stoichiometric limiting reagent (Levin and Straat, 1981), enabling a reasonable comparison. Additionally, the temperature of the mineral samples during the organic oxidation reaction in our study and in the Viking LR experiment are fairly similar: 3°C in this study vs. ~10°C inside the experimental cells of the Viking Landers (Levin and Straat, 1981).

In Fig. 3.4 we normalize the CO_2 produced from vials A_{org} ($TiO_2 \bullet H_2O_2$ + organic solution) and E_{org} (JSC-Mars-1 + H_2O_2 + organic solution) to a 0.83 g sample mass and compare our oxidation rates to the results of the LR experiment onboard Viking Landers 1 and 2 (VL1 and VL2). For each of the experimental analogs, we divide the nmol of CO_2 produced by organic oxidation by a constant to quantify the enhanced reactivity of the analogs relative to Martian soil. It can be seen in Fig. 3.4 that $TiO_2 \bullet H_2O_2$ is about 125 times more oxidizing than the Martian regolith, and JSC-Mars-1 combined with H_2O_2 is about 30 times more oxidizing. Quinn and Zent (1999) also found $TiO_2 \bullet H_2O_2$ to be about 100 times more reactive than the Martian surface

with respect to the organic solution, and suggested that this two order of magnitude difference could be due to the 1% abundance of TiO_2 in the Martian regolith (Clark et al., 1977). The 30 x greater reactivity of the JSC-Mars-1 + H_2O_2 sample could be due to mineralogical differences between this palagonitic material and the actual Martian soil, or due to the greater H_2O_2 content of our sample.

Despite the large difference in the magnitude of reactivity between the oxidative analogs studied (TiO_2•H_2O_2 and JSC-Mars-1 + H_2O_2) and the Martian regolith, the overall reactivity of the analogs appears to be similar to that observed by VL1 and VL2; namely, the oxidation of the organic solution proceeds via a rapid initial release of CO_2 followed by a slower, prolonged release. The diminished rate of production of CO_2 is perhaps due to the decrease in available organic reagent.

Although both of these systems (TiO_2•H_2O_2 and JSC-Mars-1 + H_2O_2) were able to oxidize the organic solution to CO_2, no CO_2 was observed to be produced as a result of CH_4 oxidation. As a result, only an upper-limit reaction coefficient for the oxidation of CH_4 by these mineral surfaces can be determined. This reaction coefficient (α) is defined as the fraction of collisions of CH_4 with the surface of the mineral that result in complete oxidation to CO_2. The perchlorate salts did not evolve any CO_2 from CH_4, nor did they oxidize the organic solution to any measureable extent. However, as we were not able to perform BET surface area analysis on the perchlorate salts, values of α could not be determined for CH_4

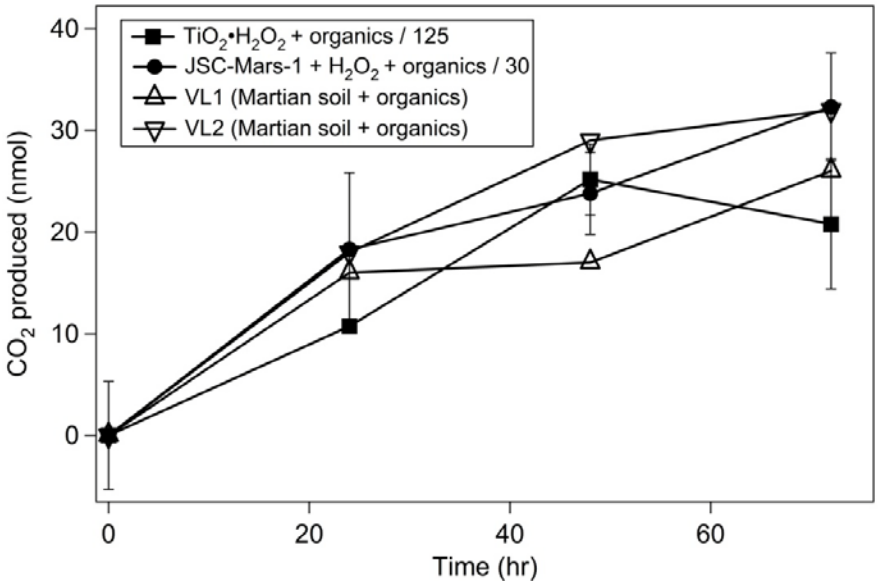

Figure 3.4 Comparison of the oxidation rates of the organic solution by the TiO_2•H_2O_2 and JSC-Mars-1 + H_2O_2 analogs (this work) and by the Martian surface during the Viking LR experiment (Quinn and Zent, 1999). All data is normalized to a 0.85 g sample mass. For the two lab analogs, the CO_2 produced by organic oxidation is divided by a constant to determine the enhanced reactivity of the analogs relative to the Martian surface. It can be seen that TiO_2•H_2O_2 is about 125 times more oxidizing than the Martian soil, and JSC-Mars-1 + H_2O_2 is about 30 times more oxidizing. Although both analogs used in this study are more reactive than the actual Martian regolith, the overall behavioral trend (rapid initial release followed by a slower, prolonged increase) is similar.

oxidation by these salts. Therefore, in the following section we only determine upper limit values of α for CH_4 on TiO_2•H_2O_2 and JSC-Mars-1 + H_2O_2.

Fuchs and Sutugin (1971) show α can be calculated by Eq. 3.1:

$$\frac{J_{net}}{J_{total}} = \frac{0.75\,\alpha(1 + Kn)}{Kn^2 + Kn + 0.283\,Kn\,\alpha + 0.75\alpha} \tag{3.1}$$

where J_{net} is the *net* flow of CH_4 to the entire mineral surface area (ie: the flow that either sticks or reacts) and J_{total} is the *total* flow to the mineral surface area assuming the system is in the continuum regime. In this regime, the Knudsen number (*Kn*), the ratio of the mean free path of a gas molecule (λ) to the particle radius (R_p), is small (< 1) and these conditions subsequently dictate the properties of molecular transport to the surface of a particle. As λ is 79 nm at atmospheric pressure and the mineral particle diameters range from 1-10 µm, $Kn << 1$ and the experimental system is in the continuum regime. Equation 3.2 was used to find J_{total}

$$J_{total} = \frac{D_{CH4}}{R_p}(c_\infty - c_s)\,SA \tag{3.2}$$

where J_{total} is the total flow (molec s^{-1}) toward the entire mineral surface area present in the vial assuming the system is in the continuum regime, D_{CH4} is the diffusion coefficient for CH_4 inside the vial, c_∞ and c_s are the concentrations of CH_4 far away from the particle and on the surface of the particle, respectively (Seinfeld and Pandis, 1998), and *SA* is the total surface area present in the vial. Based on SEM images of TiO_2•H_2O_2 and JSC-Mars-1, R_p is 2.5 (± 1) µm on average for both minerals. The approximate diffusion coefficient of CH_4 at room temperature is 0.2 cm^2 s^{-1} and was calculated using $D_{CH4} = 0.5\ \nu\lambda$, where ν is the mean molecular speed (m s^{-1}) of CH_4 at a temperature *T* given by the Maxwell-Boltzmann distribution of gas velocities, v =

$(8RT/\pi M_w)^{1/2}$ (Seinfeld and Pandis, 1998). Although no oxidation of CH_4 was observed, we assume we are simply measuring an upper limit of the heterogeneous reaction that is occurring; thus c_s is 0 and c_∞ is the bulk gas phase concentration of CH_4 in the vial (2.4×10^{18} molec cm^{-3}). The total surface area (*SA*) for each mineral was found by multiplying the mineral's BET specific surface area (SSA_{BET}) (m^2 kg^{-1}) by the sample mass (kg). Given the error in the estimation of R_p in the mineral sample, J_{total} is equal to 4×10^{26} ($\pm 2 \times 10^{26}$) molec s^{-1} for $TiO_2 \bullet H_2O_2$ and 1×10^{27} ($\pm 5 \times 10^{26}$) molec s^{-1} for JSC-Mars-1 + H_2O_2, with the difference due to the larger sample mass, and thus total surface area, of JSC-Mars-1.

Next, an upper limit of the net flow of CH_4 to all mineral particles in the vial, or the upper limit of total CH_4 that is oxidized to CO_2, J_{net}, can be derived from the detection limit of the experiment. The smallest amount of CO_2 that could be reasonably detected by the TCD is 7.7 nmol. As not even this small amount of CO_2 was present in the 1.0 cm^3 sample of vial headspace injected into the GC during the final measurement, less than 65.5 nmol of total CO_2 were present in the 8.5 cm^3 vial by the end of the 72 hr experiment (7.7 nmol cm^{-3} × 8.5 cm^3 = 65.5 nmol total). However, since there was leakage of atmospheric CO_2 in some vials, a more conservative upper limit is 150 nmol (150 nmol per 8.5 cm^3 corresponds to the mixing ratio of CO_2 in Earth's atmosphere). If more than this amount of CO_2 was formed in the vial headspace, we were certain to detect it. As less than 150 nmol CO_2 was produced after 72 hr, $J_{net} < 3.5 \times 10^{11}$ CH_4 molec s^{-1} assuming a 1:1 reaction stoichiometry between CH_4 and CO_2. From Eq. 3.1, α is less than ~3.7×10^{-17} for $TiO_2 \bullet H_2O_2$ and less than ~1.6×10^{-17} for JSC-Mars-1 + H_2O_2.

3.6 Martian Implications

The upper limit parameter α can be used to determine the kinetic importance of heterogeneous CH_4 oxidation on Mars. To quantify such CH_4 loss, first we approximate the CH_4 flux, Φ_{CH4} (molecules m^{-2} s^{-1}), to any surface on Mars. As the atmospheric pressure on Mars is low, heterogeneous processes are occurring in the kinetic/molecular regime and so Φ_{CH4} can be found using

$$\Phi_{CH4} = \frac{1}{4} \nu \, n_{CH4} \tag{3.3}$$

where n_{CH4} is the number density of CH_4 on Mars (molecules m^{-3}). On the surface of Mars, the average observed CH_4 mixing ratio of 10 ppbv corresponds to $n_{CH4} = 2.2 \times 10^{15}$ molecules m^{-3}, yielding an approximate value of Φ_{CH4} of 3×10^{17} molec m^{-2} s^{-1} at 210 K. We can then estimate a lower limit oxidation timescale, τ_{ox}, over which a column of CH_4 could be permanently removed from the atmosphere via oxidation by H_2O_2 complexed to mineral surfaces:

$$\tau_{ox} = \frac{N_{CH_4}}{\alpha \cdot \Phi_{CH4} \cdot SSA_{soil} \cdot \rho_{soil} \cdot d_{H2O2}} \tag{3.4}$$

where N_{CH4} is the CH_4 column abundance above 1 m^2 of regolith (molecules m^{-2}), SSA_{soil} and ρ_{soil} are the specific surface area (m^2 kg^{-1}) and density (kg m^{-3}) of the Martian soil, respectively, and d_{H2O2} is the depth (m) of the surface soil layer that contains adsorbed or complexed H_2O_2. A uniform mixing ratio of 10 ppbv at Martian surface gravity and pressure conditions corresponds to $N_{CH4} = 2.2 \times 10^{19}$ CH_4 molecules m^{-2}. We use a value for ρ_{soil} of 1650 kg m^{-3} (Feldman et al., 2004) and a value for SSA_{soil} of 1.7×10^4 m^2 kg^{-1} (Ballou et al., 1978). We assume that this entire

specific surface area is available to oxidize CH_4 and the H_2O_2 is homogeneously distributed from the surface down to d_{H2O2}.

The depth of Martian soil that contains H_2O_2 is a difficult parameter to constrain, as the H_2O_2 production mechanism(s), flux from the atmosphere to the surface, rates of adsorption and destruction upon interaction with the soil, and lifetime in the subsurface have only been estimated or theoretically calculated. However, as the gas chromatograph-mass spectrometer onboard Viking Lander 2 failed to detect any organic compounds in a sample collected at a depth of 10 cm (Biemann, 1979), it seems likely that the layer of strongly oxidizing soil extends at least 10 cm below the surface. Bullock et al. (1994) found that even if the lifetime of H_2O_2 in the soil is long (10^5 yrs), little H_2O_2 will penetrate below a depth of 3 m due to significant adsorption of H_2O_2 to soil grains. Impact gardening, aeolian activity or triboelectric processes could overturn the surface of the regolith and provide a mechanism for H_2O_2 to reach greater depths. However, it is highly unlikely that these processes could turn over meters of Martian soil every few years. It is therefore difficult to constrain a reasonable maximum value for d_{H2O2}, although at some depth the oxidation of CH_4 molecules will be limited by the timescale needed to diffuse to such depths. For example, it would take almost 3 years for CH_4 to reach depths of 100 m (Formisano et al., 2004; Gough et al., 2010), so values of d_{H2O2} greater than this are unrealistic. However, we do not specifically consider the diffusion time of CH_4 through the regolith during this calculation of τ_{ox}.

In Eq. 3.4, the reaction coefficient, α, is the upper limit value we have experimentally determined for either $TiO_2 \bullet H_2O_2$ ($\alpha < 3.7 \times 10^{-17}$) or JSC-Mars-1 +

H_2O_2 (α < ~1.6×10^{-17}). In Fig. 3.5 we plot the CH_4 lifetime (τ_{ox}) as a function of the depth of the soil layer that contains H_2O_2 (d_{H2O2}) using the two experimentally determined, upper limit values for α. It can be seen in Fig. 3.5 that τ_{ox} decreases with increasing d_{H2O2}. The horizontal dotted and dashed lines in Fig. 3.5 correspond to CH_4 lifetimes of 4 years and 200 days, respectively. These lines represent the two different CH_4 lifetimes which have been proposed: the ground-based observations of Mumma et al. (2009) are consistent with a CH_4 lifetime of 4 years or less, however Lefevre and Forget (2009) find these observations could actually suggest a lifetime of about 200 days.

In the case of both analogs, it can be seen in Fig. 3.5 that the CH_4 lifetime is very long for any reasonable oxidant depth. Even in the case of the more reactive analog (TiO_2•H_2O_2), more than 500 m of oxidized soil are required in order to remove CH_4 from the atmosphere in time scales of 4 years or less. At these depths, however, subsurface diffusion would limit the kinetics of CH_4 loss and therefore it is unlikely that H_2O_2 adsorbed to soil grains could be responsible for the rapid CH_4 loss which has been recently reported.

We have no way to accurately quantify the decreased reactivity of the Martian regolith toward CH_4 relative to the laboratory analog. However, the soil on Mars is likely to be less reactive than either of these analog materials as the analogs oxidized the organic solution much more rapidly than the actual Martian surface oxidized the organics during the LR experiment. Therefore, these upper limit α values are certainly an overestimation which will yield lower limit lifetimes. Additionally, the

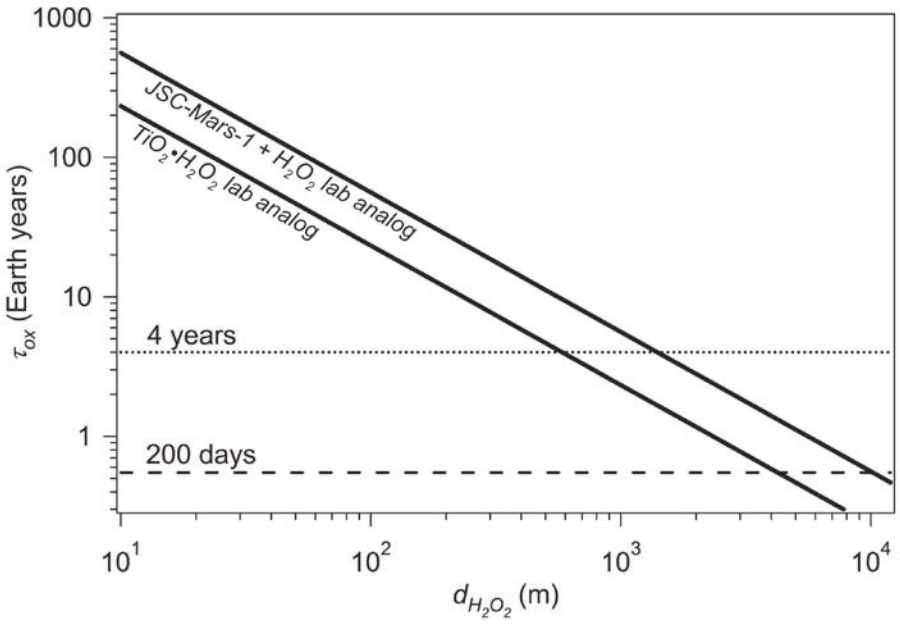

Figure 3.5 The lifetime of a CH_4 column in the Martian atmosphere due to heterogeneous oxidation by H_2O_2 adsorbed to soil (τ_{ox}) as a function of soil depth (d_{H2O2}). Results are shown for both experimentally-determined values of α: CH_4 on TiO_2•H_2O_2 (lower diagonal line) and CH_4 on JSC-Mars-1 + H_2O_2 (upper diagonal line). The horizontal dotted line represents τ_{ox} = 4 years, which is the upper limit lifetime consistent with the ground-based observations of Mumma et al. (2009). The horizontal dashed line corresponds to τ_{ox} = 200 days, which is the CH_4 lifetime needed to explain the observed atmospheric variability (Lefevre and Forget, 2009). Very large depths of oxidized soil (d_{H2O2} > 500 m) are needed for the CH_4 lifetime to be consistent with observations of the Martian atmosphere.

heterogeneous oxidation of CH_4 would most likely occur more slowly on Mars than in our study due to the lower temperatures present on the Martian surface. This correlation between reaction kinetics and temperature is predicted by both collision theory and transition state theory (Finlayson-Pitts and Pitts, 2000) and could increase the CH_4 lifetime even further beyond what could be relevant to the Martian CH_4 cycle.

It is important to point out that we assume CH_4 loss on Mars would be constant as a function of time over the entire calculated lower limit lifetime (τ_{ox}), which represents a different behavior than the decreased reactivity observed after a few days in our organic oxidation experiments. This plateauing, observed even more dramatically in similar experimental studies by Levin and Straat (1981) and Quinn and Zent (1999), is likely due to the large excess of organic molecules beginning to deplete the oxidant (H_2O_2). In the case of CH_4 oxidation on Mars, we do not believe the reaction would level off after a few days, as the oxidant (perhaps H_2O_2) would not be the limiting reagent. Estimates of soil H_2O_2 content on Mars vary from 1.4×10^{23} H_2O_2 molecules m^{-3} (Bullock et al., 1994) to 5.8×10^{26} H_2O_2 molecules m^{-3} (Levin and Straat, 1981), indicating there is enough oxidant in less than 200 µm depth of soil, at least stoichiometrically, to oxidize the 2.2×10^{19} molecules of CH_4 in a 1 m^2 atmospheric column above this regolith, assuming a 10 ppbv mixing ratio. Therefore, we do not believe that H_2O_2 would be depleted to any relevant extent during the reported 4 year (or shorter) CH_4 lifetime and thus the oxidation rate would not be expected to decrease.

We also consider the possibility that H_2O_2 adsorbed to mineral dust aerosol in the atmosphere could act as a CH_4 sink. However, even at the high optical depths (O.D.) present during dust storms, the surface area of mineral dust in the Martian atmosphere is relatively small. For example, Martin (1995) calculated that a localized dust storm monitored by the Viking orbiter (O.D. = 0.83) resulted in an atmospheric dust enhancement of 18,000 kg km^{-2}, corresponding to a 6 μm layer of dust if compacted. Even if this atmospheric mineral aerosol was coated with H_2O_2 to a greater extent than the regolith material due to condensation of electrostatically-produced oxidant (Atreya et al., 2006; Delory et al., 2006), it can be seen in Fig. 3.5 that this effective depth is many orders of magnitude too small to impact atmospheric CH_4 concentrations on a seasonal time scale.

It is therefore unlikely that H_2O_2 adsorbed to mineral grains in the Martian regolith or atmosphere is responsible for the rapid CH_4 destruction reported by Mumma et al. (2009) or the spatial and temporal variability observed by Geminale et al. (2008) and Fonti and Marzo (2010). As a CH_4 lifetime of less than 4 years is required to cause this reported variability (Mumma et al., 2009), some other loss process is likely occurring. It has been suggested that CH_4 is not being destroyed by H_2O_2, but rather by •OH formed during mineralogical processing of H_2O_2. Processes such as the Fenton reaction, which oxidizes Fe^{2+} to Fe^{3+} while reducing H_2O_2 to •OH, could be occurring on or in the iron-rich Martian regolith. Other proposed oxidants include superoxide (O_2^-) ions (Yen et al., 2000), iron (IV) salts (Tsapin et al., 2000) or peroxonitrite compounds (Plumb et al., 1989). Incident UV radiation could play a role in the destruction of CH_4 directly through a surface-enhanced destruction process or

indirectly through photochemical formation of oxidants on surfaces of minerals or ices. Perhaps chlorine species such as the reactive intermediate anionic chlorine oxides (ClO^-, ClO_2^- and ClO_3^-) exist in the regolith and could destroy organics or methane. It is also possible that the reactive components of the regolith or the mechanisms occurring have not yet been identified. Either way, more work must be done towards identifying chemical species or minerals that are reactive towards CH_4 over very short time scales (less than 4 years).

3.7 Conclusions

We have performed a series of experiments analyzing the reactivity of several oxidizing analogs toward CH_4. Perchlorate salts and H_2O_2 are thought to exist on Mars although their geographic distribution is not known. These species, especially peroxides, have been proposed to rapidly destroy CH_4, possibly resulting in a CH_4 lifetime short enough to explain the observations of Mumma et al. (2009) (less than 4 years) and the model results of Lefevre and Forget (2009) (200 days). However, we have shown that ClO_4^- salts are unreactive towards both CH_4 and the organic compounds used during the Viking LR experiment and are thus very unlikely to destroy CH_4 over these time scales on Mars. Hydrogen peroxide, complexed with TiO_2 and also added to JSC-Mars-1 soil analog, was able to oxidize the Viking organic solutions to CO_2 with even greater reactivity than the Martian surface. However, even the most reactive oxidative analog, TiO_2•H_2O_2, did not oxidize CH_4 to CO_2 during a 72 hour experiment within the detection limit of the GC instrument used. A calculated upper limit reaction coefficient, α, is less than ~3.7×10^{-17} for

$TiO_2 \bullet H_2O_2$ and less than ~1.6×10^{-17} for JSC-Mars-1 + H_2O_2. When these experimental results are extrapolated to Martian conditions, the CH_4 lifetimes calculated are too long to be relevant to the Martian CH_4 cycle. Depths of oxidized soil greater than 500 m are needed for the CH_4 lifetime to be consistent with observations of the Martian atmosphere. Moreover these reactions are likely temperature dependent and will be slower at Martian temperatures.

This study was not a comprehensive study of all possible mineral analogs and all possible H_2O_2 complexation or stabilization mechanisms. However, we have shown that neither ClO_4^- salts nor H_2O_2 alone are likely to be directly responsible for the recently observed rapid destruction and high temporal and spatial variability of atmospheric CH_4 on Mars.

Chapter IV

Experimental studies of perchlorate phase transitions relevant to Mars

4.1 Introduction

4.1.1 Perchlorate on Mars

Perchlorate salts were recently discovered on Mars at the Phoenix landing site at high northern latitudes (68°N, 234°E). The Wet Chemistry Laboratory (WCL) instrument onboard the Phoenix Mars Lander detected ~0.5% perchlorate (ClO_4^-) by mass in the soil nearby the lander (Hecht et al., 2009). A robotic arm was used to excavate samples from the surface as well as 5 cm below the surface. Both samples were found to contain approximately equal concentrations of ClO_4^- suggesting that, at least at this location, this salt is evenly distributed throughout the regolith. Independent evidence for perchlorate was provided by the Thermal and Evolved Gas Analyzer (TEGA), another instrument onboard the Phoenix Lander. When soil samples were heated, oxygen gas (O_2) was produced at the temperature expected for thermal decomposition of perchlorate.

This discovery has sparked interest due to the unique physical, chemical and potential biochemical properties of the salt. For example, perchlorate solutions have low eutectic temperatures (T_E). The eutectic temperature is the lowest temperature at which an aqueous salt solution can exist and occurs at some characteristic eutectic concentration. For many perchlorate salts, the freezing point of a salt solution can be depressed far below that of pure water. For example, it has been reported that the T_E

of $NaClO_4$ = -37°C and the T_E of $Mg(ClO_4)_2$ = -67°C (Chevrier et al., 2009). Therefore, aqueous perchlorate salt solutions on Mars could exist over a wider temperature range than could pure liquid water.

4.1.2 Phase transitions of inorganic salts

Perchlorate salts are highly deliquescent, in that the crystalline material is hygroscopic and readily absorbs H_2O vapor from the atmosphere to form an aqueous salt solution ($X_{(s)} \rightarrow X_{(aq)}$). This phase change occurs at the deliquescence relative humidity (DRH), a value which is typically below 100% RH. For example, at T = 293 K the DRH of NaCl is 75% (Cohen et al., 1987) and the DRH of Na_2SO_4 is 84% (Tang and Munkelwitz, 1994).

The reverse process, crystallization of a salt solution when the relative humidity of the system is lowered, is called efflorescence. The efflorescence relative humidity (ERH) is generally lower than the DRH. This hysteresis effect is widely known and exists for most inorganic salts (Martin, 2000). Figure 4.1 shows a schematic depicting the hysteresis curve that occurs for a typical inorganic salt during deliquescence and efflorescence. Specifically, liquid water content is graphed as a function of the RH with respect to the salt. As the RH is increased above a crystalline salt at constant T (arrow A), there is little uptake of water until some characteristic deliquescence relative humidity (DRH) is reached. When the RH with respect to the salt equals the DRH of the salt, the material absorbs H_2O from the atmosphere and becomes an aqueous solution (arrow B). As the RH is increased above the DRH, the

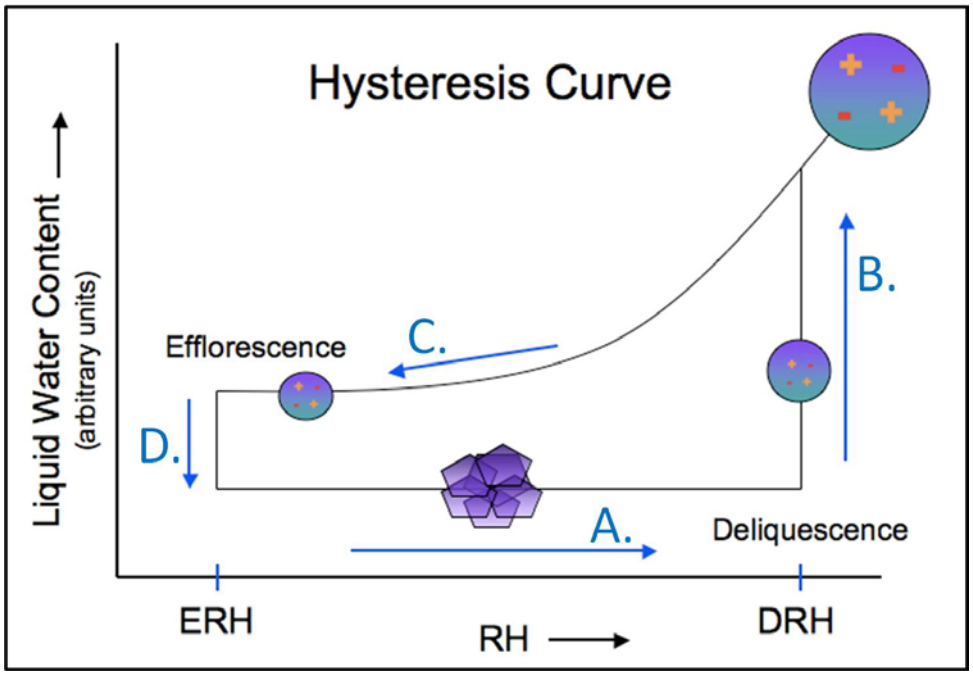

Figure 4.1 Plot of liquid water content as a function of relative humidity (RH) with respect to the sample. As a constant temperature, when the RH is increased above the DRH, the crystalline salt deliquesces into an aqueous salt solution. As RH is decreased, the salt does not recrystallize (effloresce) until the ERH is reached. This hysteresis effect occurs because efflorescence is controlled by nucleation kinetics whereas deliquescence is controlled by equilibrium thermodynamics.

salt solution becomes more dilute as the water content of the particle increases and the particle grows. Although deliquescence occurs as soon as the free energy of the crystalline phase and aqueous phase are equal (ie: as soon as the process is thermodynamically favorable), salt crystallization is a kinetically hindered process. As a result, a different path is taken as the RH above the system is lowered and the salt solution remains liquid even when RH < DRH. In this region (arrow C), the solution is supersaturated and metastable for potentially long periods of time. Finally, at some characteristic efflorescence relative humidity (ERH), the solution crystallizes and expels all liquid water (arrow D).

Efflorescence cannot be simply predicted from thermodynamic principles or phase diagrams, although free energy considerations are still a useful guide capable of providing constraints and predicting driving forces. Because metastable supersaturated salt solutions can exist for significant periods and at low RH values, laboratory experiments are needed to determine the ERH of salts.

4.1.3 Previous experimental studies of perchlorate deliquescence and efflorescence

Little laboratory work has been done to quantify the deliquescence of perchlorate salts. The few experimental studies of $NaClO_4$ have been conducted at 298 K and have measured DRH values of 43% RH (Zhao et al., 2005) and 46% RH (Zhang et al., 2005). Only one very approximate value exists for the deliquescence of $Mg(ClO_4)_2$ (DRH = ~50%) and this measurement was also performed at room temperature (295 K). However, as the DRH of many salts varies with temperature (Greenspan, 1977; Tang and Munkelwitz, 1994), it is important to study perchlorate

deliquescence at a range of temperatures more relevant to the system of interest. Recently, Zorzano et al. (2009) reported that under Mars-like conditions (225 K) $NaClO_4$ deliquesced at ~37% RH, suggesting that the temperature-dependence of deliquescence is small and perhaps the correlation is negative. However, this study reported a single data point with unknown error bars and so further low temperature studies are needed.

Neither the deliquescence of $Mg(ClO_4)_2$ nor its hydrates has been studied at low temperatures. However, as results from the WCL instrument onboard the Phoenix Lander suggest the Mg^{2+}/Na^{+} ratio at the Phoenix landing site is ~3/1 (Hecht et al., 2009), it is particularly important to understand the low temperature deliquescence of $Mg(ClO_4)_2$.

Similarly, there have been few experimental studies of the efflorescence of aqueous perchlorate solutions and they have all been performed at 25°C. ERH values of 11% (Zhang and Chan, 2003) and 20% (Zhang et al., 2005) have been reported for $NaClO_4$, as well as one upper limit value of 19% (Zhao et al., 2005). There has only been one study of the efflorescence of aqueous $Mg(ClO_4)_2$ solutions: Zhang and Chan (2003) report that the ERH can range from 10-18%. No experimental work has been done to determine the ERH of any perchlorate salt at lower temperatures. There is a scarcity of experimental data regarding the temperature dependence of efflorescence of salts in general, and the few studies that do exist often disagree (Xu et al., 1998; Onasch et al., 1999). Given the discrepancy between the previous literature values for the ERH of both $NaClO_4$ and $Mg(ClO_4)_2$ and the unknown temperature dependence

of this phase transition, experimental studies of the efflorescence of low temperature perchlorate solutions are needed.

4.1.4 Previous theoretical studies of perchlorate phase transitions on Mars

Previous studies of perchlorate phase transitions on Mars and the stability of potential perchlorate salt solutions at the Phoenix landing sites have considered only thermodynamics in their analyses (Chevrier et al., 2009; Marion et al., 2010). This is likely to be problematic for two reasons: first, at a given temperature, deliquescence and efflorescence are predicted to occur at the same RH. When only equilibrium thermodynamics is considered, both transitions are predicted to occur under the RH and temperature conditions at which the phase change first becomes energetically favorable. Deliquescence may be predicted correctly using such theory; however, as discussed above, the kinetic inhibition of crystallization will often allow supersaturated, metastable aqueous perchlorate solutions to persist at RH values below what is predicted by thermodynamics. This hysteresis would certainly affect the stability and duration of aqueous salt solutions on Mars and therefore is important to explore in the laboratory.

Secondly, previous papers assume that all intermediate hydration states are reached during phase transitions. For example, thermodynamic models predict when the RH above an anhydrous $NaClO_4$ sample is increased, the monohydrated salt ($NaClO_4 \cdot H_2O$) and then, depending on T, the dihydrated salt ($NaClO_4 \cdot 2H_2O$) will form prior to deliquescence. In reality, however, the hydration of salts is a slow, process requiring the diffusion of water into a solid and often takes several days

(Espinosa et al., 2008). Therefore, salt hydration may not occur during the diurnal H_2O cycle on Mars. As both the DRH and T_E of salts can decrease with decreasing hydration state (Cohen et al., 1987), it is essential to understand how the number of waters of hydration of a salt can affect the deliquescence of perchlorate salts. It would also be useful to constrain the kinetics of perchlorate salt hydration.

4.1.5 Perchlorate salts studied in this work

Under Martian surface conditions, the magnesium perchlorate hexahydrate ($Mg(ClO_4)_2 \bullet 6H_2O$) is predicted to be the dominant $Mg(ClO_4)_2$ phase (Chevrier et al., 2009; Robertson and Bish, 2010) as temperatures higher than 400 K are needed for dehydration of $Mg(ClO_4)_2 \bullet 6H_2O$ to occur (Dobrynina et al., 1980). Therefore, the hexahydrate was the only $Mg(ClO_4)_2$ salt studied in this work. Thermodynamic calculations by Chevrier et al., (2009) suggest the mono- and dihydrated sodium perchlorate salts are the $NaClO_4$ phases most relevant to Mars (Chevrier et al., 2009). However, as the dihydrate ($NaClO_4 \bullet 2H_2O$) is not commercially available and synthesis presents an experimental challenge, we chose to study the monohydrated ($NaClO_4 \bullet H_2O$) and anhydrous $NaClO_4$ salts.

In this study, we use a Raman microscope to experimentally determine the DRH and ERH of these three perchlorate salts ($NaClO_4$, $NaClO_4 \bullet H_2O$ and $Mg(ClO_4)_2 \bullet 6H_2O$) under a range of low temperatures relevant to Mars (223 - 273 K). We then apply our results to the Martian surface, estimating the stability of aqueous perchlorate solutions at the Phoenix landing site.

4.2 Experimental methods: Raman microscope

4.2.1 General description of microscope system

The experimental system used to detect perchlorate deliquescence and efflorescence has been previously described in detail by Baustian et al. (2010) and is shown schematically in Fig. 4.2. Briefly, a Nicolet Almega XR Dispersive Raman spectrometer was outfitted with a Linkam THMS600 environmental cell, a Buck Research chilled-mirror hygrometer and a Linkam automated temperature controller. Phase changes can be monitored visually (with the optical microscope) or spectrally (using Raman scattering spectroscopy).

4.2.2 Environmental cell: Temperature and humidity control

The environmental sample cell is mounted on a high precision motorized microscope stage that sits within the microscope. Samples are deposited onto a hydrophobic quartz disc and placed on a silver sample block attached to the microscope stage which is cooled with a continuous flow of liquid nitrogen (LN_2). A platinum resistance sensor mounted within the silver block monitors cell temperature accurately to ±0.1°C. The cell is operated in a continuous flow manner with a background of highly purified N_2 that may be humidified as desired. Humidified air is generated by running a separate stream of N_2 through a glass frit submerged in deionized H_2O. Variable RH values inside the cell are created by changing the humidified flow relative to the dry N_2 flow (held constant).

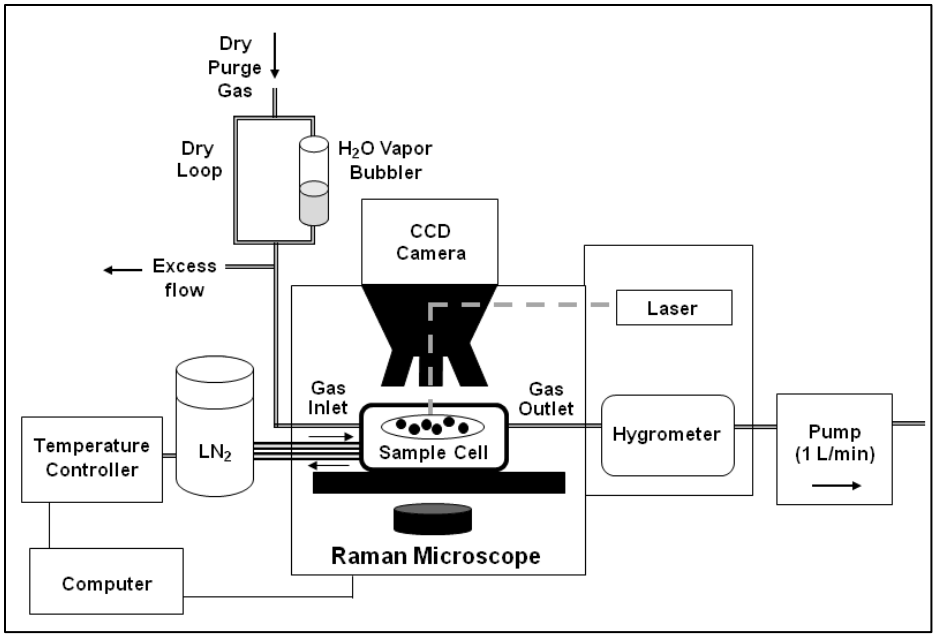

Figure 4.2 A schematic of the Raman microscope used in the perchlorate phase transition studies.

The RH environment of the sample is monitored using a CR-1A chilled-mirror hygrometer (Buck Research Instruments) attached to the gas outlet of the cell. The hygrometer measures frost points as low as −120°C with an accuracy of ±0.15°C. Frost point measurements from the hygrometer and sample temperature from the platinum resistor sensor allow for real-time monitoring of the RH with respect to the sample. The liquid N_2 lines have been insulated and the cell walls are at room temperature, ensuring that the sample is the coldest point within the cell and thus the RH will always be highest with respect to the sample. This minimizes the adsorption of H_2O on other surfaces. A diaphragm pump pulling at a rate of 1 L/min is attached to the outlet of the hygrometer. The pump ensures the airflow through the cell will always be 1 L/min, regardless of any variability due to changing the flow rate through the H_2O vapor bubbler.

4.2.3 Raman spectrometer and microscope

The Raman spectrometer has two lasers (532 nm and 780 nm) that can be used to probe particles as small as 1 μm in diameter. For all experiments performed in this study, the 532 nm laser was used to gather spectral information. The resolution of the spectrometer in all spectra shown is 2 cm^{-1}. The Raman vibrational spectra obtained are chemically specific and allow for molecular identification on a particle by particle basis. Specifically, in this study, Raman spectra were used to detect perchlorate phase changes (deliquescence and crystallization) and also to determine the hydration state of the crystalline perchlorate salt. An optical microscope (Olympus BX51) with 10X, 20X, 50X and 100X magnification capabilities could also used to observe phase

transitions of perchlorate particles. In this study, Raman spectral changes were used to quantitatively determine the DRH and ERH of perchlorate salts, although spectral and optical/visual methods provide very similar results.

4.3 Spectral determination of deliquescence and efflorescence

4.3.1 Anhydrous $NaClO_4$ phase transitions

Shown in Fig. 4.3 are Raman spectra taken during the deliquescence and efflorescence of $NaClO_4$. All spectra are offset slightly for clarity. Figure 4.3A depicts the deliquescence of a single $NaClO_4$ particle at 243 K. There are no spectral changes until the RH with respect to the salt reaches 44.0% and above. At this point, there are changes to the Raman spectrum indicative of the transition from crystalline salt to aqueous salt solution. These spectral changes primarily occur in two regions which are boxed and expanded in Fig. 4.3B and 4.3C.

The broad peak seen in Fig. 4.3B between 3100 and 3700 cm^{-1} is the O-H stretch of condensed-phase H_2O. The broad shape of this peak is due to hydrogen bonding between H_2O molecules and confirms the H_2O is in the liquid phase. The spectra of the anhydrous salt under “dry” conditions (2.1% RH) and at 40.2% RH both show no feature in this region. As the RH is increased to 44.0% and above, this peak appears and grows, signifying that condensed-phase H_2O is dissolving the salt particle.

Figure 4.3C depicts the peak at 952 cm^{-1} decreasing and a nearby peak at 936 cm^{-1} appearing when H_2O vapor is added to the environmental cell. Previous spectral studies of perchlorate deliquescence have reported a similar shift in this region of the

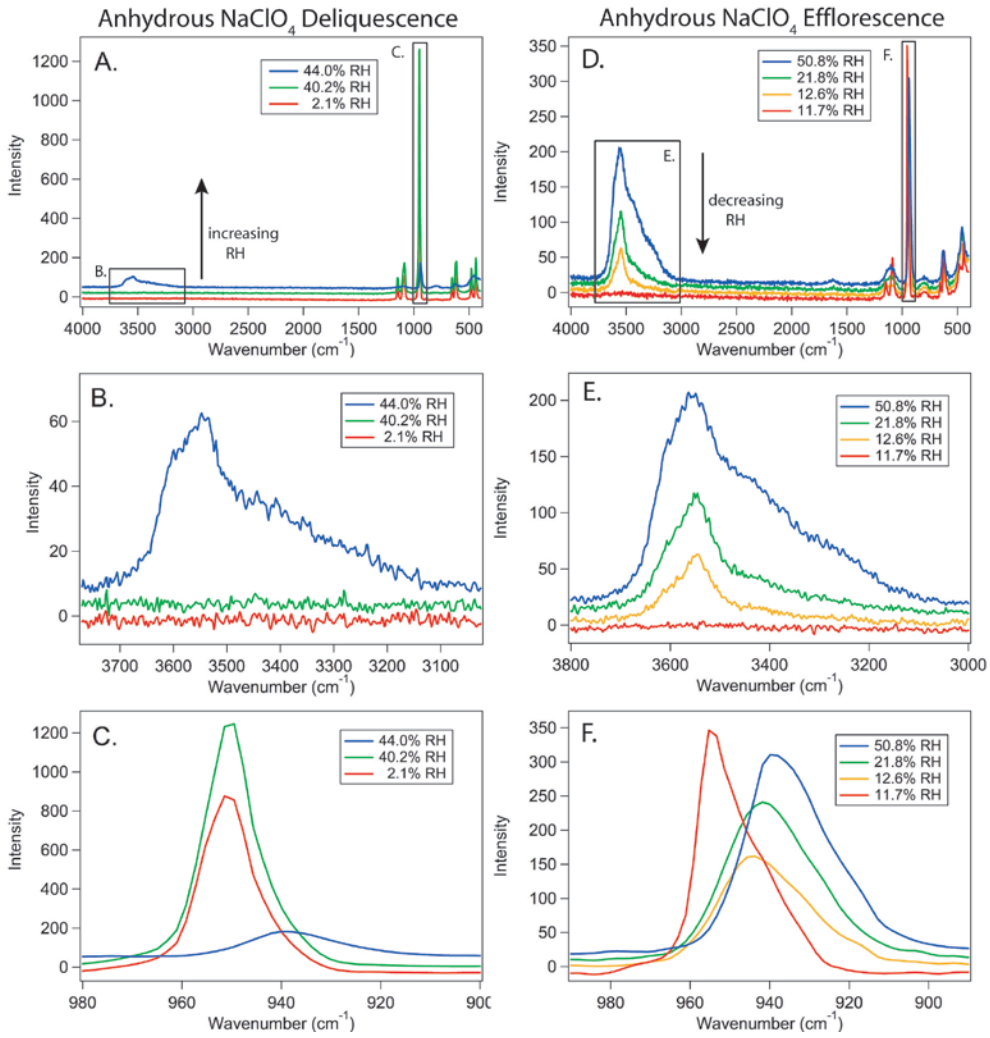

Figure 4.3 Raman spectra illustrating the deliquescence (A, B, C) and efflorescence (D, E, F) of anhydrous $NaClO_4$ (T = 243 K). The boxed regions in (A) and (D) are labeled and expanded below. As the relative humidity in the environmental cell is increased, two main regions in (A) show spectral changes. These boxed regions are expanded below and depict the spectral regions of the O-H stretching vibration (B) and the ClO_4^- symmetric vibration (C). As the RH is increased, the broad O-H stretching vibration increases and the ClO_4^- symmetric vibration shifts to smaller wavenumbers, both indicative of the formation of an aqueous solution. In this particular experiment, the DRH is recorded as 44.0%. (D) Entire spectral region monitored during the reverse process (efflorescence). As RH in the environmental cell is decreased, the same two regions show spectral changes: the region of the O-H stretching vibration (E) and the ClO_4^- symmetric vibration (F). When efflorescence occurs, the broad O-H stretching vibration suddenly disappears and the ClO_4^- symmetric vibration suddenly shifts to smaller wavenumbers, both indicative of the crystallization of the aqueous solution. In this particular experiment, the ERH is recorded as 11.7%.

Raman spectrum which corresponds to the υ_1 ClO_4^- symmetric stretch, and have concluded this spectral change is due to the transformation of crystalline $NaClO_4$ (952 cm^{-1}) to free ClO_4^- ions in aqueous solution (936 cm^{-1}) (Miller and Macklin, 1985). This spectral shift was used to quantitatively determine the DRH of $NaClO_4$ in this study; specifically, the RH at which the crystalline perchlorate peak at 952 cm^{-1} fully disappears was taken to be the DRH. By this point, all ClO_4^- exists as free, solvated ions in the aqueous phase and deliquescence is complete. In this experiment, the crystalline ClO_4^- peak at 952 cm^{-1} is not gone until 44.0% RH. Therefore, for the deliquescence experiment shown in Fig. 4.3, the DRH was recorded to be 44.0%.

These same regions were used to monitor the reverse process: efflorescence of the aqueous solution into crystalline $NaClO_4$. The entire spectral region monitored by the Raman microscope (Fig. 4.3D), the O-H stretch of condensed-phase H_2O (Fig. 4.3E), and the ClO_4^- symmetric stretch (Fig. 4.3F) are shown for a typical $NaClO_4$ efflorescence experiment (T = 253 K). As the RH inside the cell is lowered, the intensity of the O-H stretch decreases as H_2O is lost from the particle but the peak does not completely disappear until 11.7% RH (Fig. 4.3E). The disappearance of H_2O is sudden and occurs over a very small RH range (between 12.6 and 11.7% RH in this particular experiment). As seen in Fig. 4.3F, the shift in the υ_1 ClO_4^- symmetric stretch corresponding to the crystallization of the salt from aqueous solution also occurs very suddenly, and at an RH consistent with the disappearance of the O-H stretch of liquid H_2O. For all experiments performed on $NaClO_4$ in this study, the RH value at which the ClO_4^- band had completely shifted back to 952 cm^{-1} is defined as

the efflorescence relative humidity (ERH). For the particular efflorescence experiment shown here, the ERH was recorded to be 11.7% RH.

Prior to the sudden shift of the υ_1 ClO_4^- symmetric stretch back to 952 cm^{-1} (crystalline ClO_4^-) at 11.7% RH, there is a gradual increase in the location of the peak maxima from 936 to 946 cm^{-1} as RH is lowered below the DRH and the salt solution becomes supersaturated. This shift of the υ_1 ClO_4^- symmetric stretch has been observed in other studies of increasingly supersaturated $NaClO_4$ solutions (Miller and Macklin, 1985; Zhao et al., 2005) and occurs because higher salt concentrations result in enhanced ion interactions which affect the energy of vibrational transitions.

4.3.2 $NaClO_4 \bullet H_2O$ phase transitions

Spectra collected during the deliquescence and efflorescence of the monohydrated sodium perchlorate salt ($NaClO_4 \bullet H_2O$) are shown in Fig. 4.4. The entire spectral region is not shown for this salt. However, as spectral changes occur in the same regions as during phase transitions of anhydrous $NaClO_4$, these regions are expanded in A (O-H stretch during deliquescence), B (ClO_4^- symmetric stretch during deliquescence), C (O-H stretch during efflorescence) and D (ClO_4^- symmetric stretch during efflorescence).

As seen Figure 4.4A, the spectrum of the solid monohydrated $NaClO_4$ salts prior to deliquescence contains a sharp peak at 3500 cm^{-1} due to the presence of crystalline H_2O molecules in the lattice of the hydrated salt. When the RH in the environmental cell increases to the DRH (55.0% RH), the intensity of this sharp peak at 3500 cm^{-1} decreases as the crystalline, hydrated solid dissolves into aqueous ions.

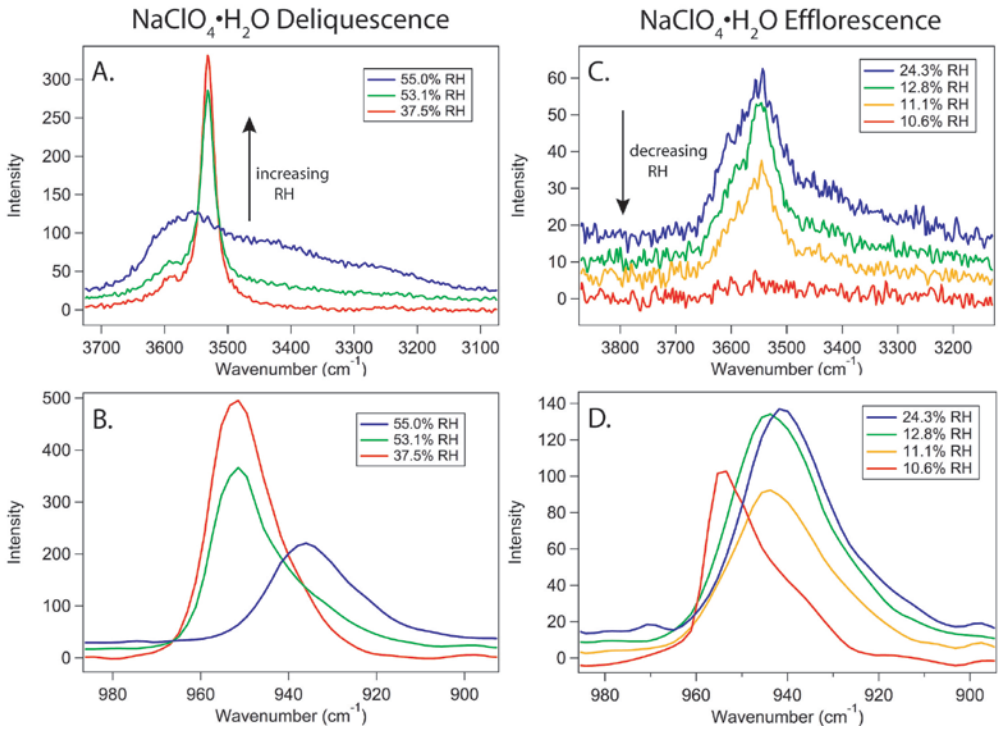

Figure 4.4 Spectra depicting the deliquescence of monohydrated $NaClO_4$ ($NaClO_4 \bullet H_2O$) (A, B) and the efflorescence of the resulting aqueous $NaClO_4$ solution (C, D). The spectral changes which occur during the $NaClO_4 \bullet H_2O$ phase transitions are similar to those of the anhydrous salt. However, the spectrum of the $NaClO_4 \bullet H_2O$ contains a sharp Raman feature at 3530 cm^{-1} due to the crystalline H_2O present in the crystal lattice. When the RH reaches the DRH (44.0% RH), the sharp O-H stretch of crystalline water disappears and the broad O-H stretch of liquid H_2O appears (A). Simultaneously, the ClO_4^- symmetric stretch shifts to shorter wavenumbers (B). When the RH above this solution is lowered to the ERH (10.6% RH), the broad O-H stretching vibration suddenly disappears (C) and the ClO_4^- symmetric vibration simultaneously shifts to higher wavenumbers (D), both indicative of the crystallization of the aqueous solution into solid anhydrous salt.

Simultaneously, the broad O-H stretch indicative of liquid H_2O (3100 - 3700 cm^{-1}) grows, confirming the occurrence of deliquescence. As with anhydrous $NaClO_4$, the shift between crystalline (952 cm^{-1}) and aqueous (936 cm^{-1}) ClO_4^- vibrational frequencies was used to determine the DRH for the salt. As seen in Fig. 4.4B, the υ_1 ClO_4^- symmetric stretch suddenly shifts to lower wavenumbers at 55.0% RH, indicating the solvation of the solid salt crystals. In the deliquescence experiment shown in Fig. 4.4A-C, the DRH was recorded to be 55.0% RH.

Shown in Fig. 4.4C and D are spectra depicting the efflorescence of the solution that results from the deliquescence of $NaClO_4 \bullet H_2O$. Figure 4.3C shows the disappearance of the broad O-H stretch of liquid H_2O at 10.6% RH. At this same RH, the ClO_4^- stretch shifts to higher wavenumbers (Fig. 4.4D). Therefore in this particular efflorescence experiment the ERH is 10.6% RH. Although this aqueous solution was produced by deliquescing $NaClO_4 \bullet H_2O$, the solution clearly effloresces into the *anhydrous* crystalline salt. There is no crystalline H_2O present in the solid salt as there is no sharp peak at 3500 cm^{-1} due to the crystalline H_2O molecules that would be present if the salt was hydrated (compare red spectrum in Fig. 4.4A to the red spectrum in 4.4C). This result was found for all $NaClO_4 \bullet H_2O$ efflorescence experiments.

4.3.3 $Mg(ClO_4)_2 \bullet 6H_2O$ phase transitions

Like crystalline $NaClO_4 \bullet H_2O$, the spectrum of $Mg(ClO_4)_2 \bullet 6H_2O$ contains a sharp peak at 3500 cm^{-1} due to the crystalline H_2O molecules in the lattice of this hydrated salt (Fig. 4.5A). When deliquescence occurs, the intensity of this peak

decreases and the broad O-H stretch indicative of liquid H_2O (3100 - 3700 cm^{-1}) grows. In this study, $Mg(ClO_4)_2 \cdot 6H_2O$ was considered to be deliquesced when the crystalline O-H stretch had fully disappeared and only the broad vibrational feature of liquid H_2O remained. For the experiment shown in Fig. 4.5A, the DRH is 51.8% RH.

This O-H stretch region was also used to quantify the ERH of $Mg(ClO_4)_2$ solutions. A particle of aqueous $Mg(ClO_4)_2$ was considered to be effloresced when the broad O-H stretch of liquid H_2O had disappeared and only the O-H stretch of crystalline water remained. As with the salts previously discussed, this transition was sudden and obvious. In the efflorescence experiment shown in Fig. 4.5B, the ERH is 20.6% RH. Efflorescence of $Mg(ClO_4)_2$ solutions always resulted in a *hydrated* crystalline solid.

4.4 Results

4.4.1 Results of sodium perchlorate deliquescence and efflorescence

The results of the $NaClO_4$ deliquescence and efflorescence experiments are plotted on a stability diagram (T vs. RH) of the $NaClO_4/H_2O$ system (Fig. 4.6). Experimental DRH data for the two salts studied is represented by solid symbols and ERH data by open symbols. The error bars for each DRH and ERH data point in this study are the standard deviation of multiple (>3) measurements performed at that temperature. Also plotted in Fig. 4.6 are several lines representing calculated theoretical stable and metastable phase transitions derived from Chevrier et al. (2009). In this figure, all red lines and symbols correspond to the deliquescence of anhydrous $NaClO_4$, all green lines and symbols correspond to the deliquescence of

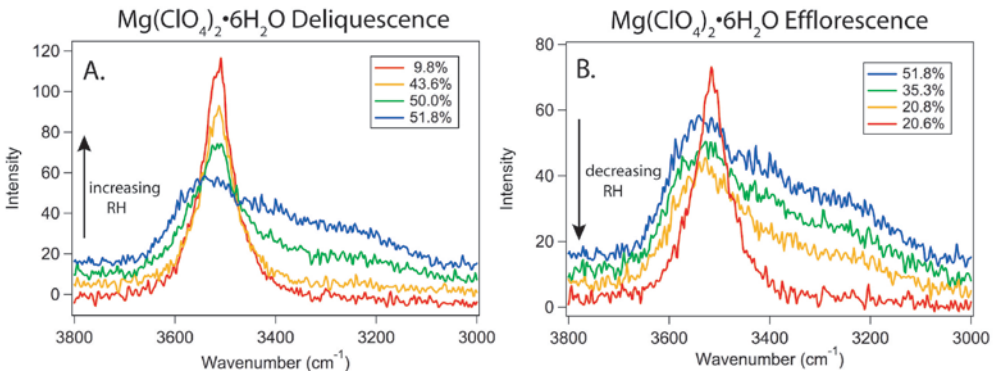

Figure 4.5 Spectra depicting (A) the deliquescence of hexahydrated magnesium perchlorate ($Mg(ClO_4)_2$•$6H_2O$) and (B) the efflorescence of the resulting aqueous $Mg(ClO_4)_2$ solution. The spectral region shown is the of the O-H stretch of water. When the salt deliquesces, the intensity of the sharp crystalline H_2O peak decreases and the broad O-H stretch indicative of liquid water (3100 - 3700 cm^{-1}) grows. In this study, $Mg(ClO_4)_2$•$6H_2O$ was considered to be deliquesced when the crystalline O-H stretch had fully disappeared and only the broad vibrational feature of liquid H_2O remained (51.8% in this experiment). The salt was considered to be effloresced when the broad O-H stretch of liquid water had disappeared and only the O-H stretch of crystalline water remained (20.6% in this experiment).

$NaClO_4 \bullet H_2O$, and the blue line corresponds to the calculated deliquescence of $NaClO_4 \bullet 2H_2O$. Solid lines represent thermodynamically stable transitions and dashed lines represent metastable transitions.

It can be seen from Fig. 4.6 that the experimental DRH values of anhydrous $NaClO_4$ (red symbols) depend only slightly on temperature. The DRH of anhydrous $NaClO_4$ was measured to be 35.4($\pm$2.3)% RH at 273 K and appears to increase only slightly with decreasing T, although the data point at 223 K does not appear to follow this trend. There are experimental difficulties associated with measuring RH at low temperatures, hence the increase in the size of error bars as T decreases. The DRH of $NaClO_4 \bullet H_2O$ (green symbols) had a greater dependence on T, increasing from 50.9% at 273 K to 64.1% RH at 228 K. Attempts to deliquesce $NaClO_4 \bullet H_2O$ at 223 K resulted in the formation of ice. This is predicted by the stability diagram, as 223 K is below the metastable eutectic temperature for the monohydrated salt and deliquescence into an aqueous solution is not expected to occur. Rather, increasing the RH above a 223 K $NaClO_4 \bullet H_2O$ particle is predicted to nucleate ice.

The DRH values of both $NaClO_4$ salts can be predicted by the phase diagram shown in Fig. 4.6: deliquescence of anhydrous $NaClO_4$ (red points) occurred on the dashed red line and deliquescence of $NaClO_4 \bullet H_2O$ (green points) occurred on the dashed green line. If the system had been strictly controlled by thermodynamics, the following sequence of events should have occurred when the RH was increased from 0% RH above an anhydrous $NaClO_4$ particle at T = 243 K (for example): First, the monohydrate should form when the RH > 14.8%. Then, the dihydrate should form when the RH > 54.0%. Finally, deliquescence should occur when RH > 66% (on the

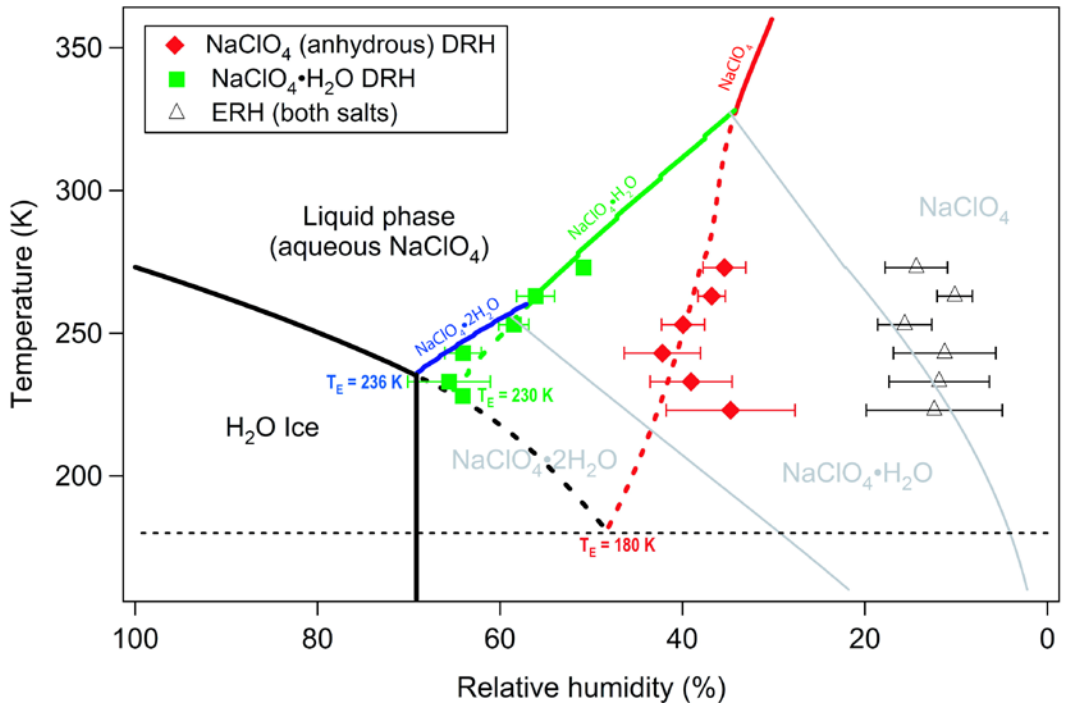

Figure 4.6 Experimentally determined deliquescence relative humidity (DRH) and efflorescence relative humidity (ERH) for $NaClO_4$ and $NaClO_4•H_2O$ (symbols) overlaid on a phase diagram of the $NaClO_4/H_2O$ system. The thermodynamically predicted stable phase transitions between solid and liquid are depicted with solid colored lines (blue = $NaClO_4•2H_2O$, green = $NaClO_4•H_2O$, red = anhydrous $NaClO_4$). The dashed colored lines represent the predicted metastable phase transitions of these salts. The gray lines represent transitions between different hydration states of $NaClO_4$.The eutectic point and eutectic temperature (T_E) of each hydrate are labeled. Anhydrous and monohydrated $NaClO_4$ samples both deliquesced close to the thermodynamically predicted RH values at each temperature studied. Aqueous solutions of each salt, however, effloresced at 13(±4)% RH, exhibiting the hysteresis effect commonly observed during salt efflorescence.

solid blue line). Clearly, this sequence of events does not occur, and the reason is that salt hydration kinetics are slow. Over the time scale of our experiments (~ 1 hr), the RH with respect to anhydrous $NaClO_4$ reaches the dashed red line before the anhydrous salt has started to hydrate. As the salt hydration processes predicted by thermodynamics are bypassed, metastable deliquescence occurs at a much lower RH (~42% RH at 243 K).

In the case of $NaClO_4 \bullet H_2O$, deliquescence at $T \leq 253$ K was also a metastable transition. Further hydration of the monohydrate to $NaClO_4 \bullet 2H_2O$ is predicted to occur at these temperatures when RH is increased; however, because hydration was slow, direct deliquescence into an aqueous solution occurred.

As mentioned previously, the efflorescence of $NaClO_4$ solutions always occurred at 12.6(±2.0)% RH (open triangles in Fig. 4.6) regardless of if the solution was formed by deliquescence of anhydrous $NaClO_4$ or by deliquescence of $NaClO_4 \bullet H_2O$. As expected the behavior was hysteretic and the ERH was significantly lower than the DRH at every temperature studied. Our experimentally determined ERH value is similar to the results of Zhang and Chan (2003) who found ERH = 11% and is consistent with the upper limit value of ERH <19% (Zhao et al., 2005). This hysteresis effect suggests that a supersaturated salt solution is metastable for all RH values between the DRH for a given hydration state and 12.6% RH.

The $NaClO_4$ solution always crystallized into the anhydrous salt. This was confirmed by Raman spectroscopy (no crystalline H_2O peak was present in the solid salt after efflorescence) and also by subsequent deliquescence experiments (in which the sample still deliquesced on the red anhydrous metastable transition line (red

dashed line). This is consistent with the $NaClO_4$ stability diagram (Fig. 4.6), as the measured ERH data points are primarily in the stability region of the anhydrous salt. Efflorescence of $NaClO_4$ solutions into anhydrous $NaClO_4$ has also been observed by previous studies (Zhang and Chan, 2003; Zhao et al., 2005).

4.4.2 Magnesium perchlorate deliquescence and efflorescence

The results of $Mg(ClO_4)_2 \cdot 6H_2O$ deliquescence and efflorescence experiments are plotted on a stability diagram (T vs. RH) of the $Mg(ClO_4)_2/H_2O$ system (Fig. 4.7). This is a simpler stability diagram, as there are no metastable transitions that occur in the T and RH ranges studied and only one hydration state is involved (the hexahydrate). Deliquescence of the crystalline $Mg(ClO_4)_2 \cdot 6H_2O$ salt (blue symbols) occurred where predicted and was the DRH was found to depend on T, increasing from 42.0% RH at 273 K to 55.1% RH at 223 K. Efflorescence of the $Mg(ClO_4)_2$ solutions (orange symbols) was found to be less dependent on T and occurred at ERH = 19.3($\pm$2.9)% RH. This ERH is near the upper end of the range of 10-18% RH found by Zhang and Chan (2003) at 298 K, the single literature value that exists. As the ERH was much lower than the DRH at every temperature studied, it seems that supersaturated solutions are common. Specifically, the data show that a supersaturated salt solution is metastable at RH values lower than the DRH but above 19.3% RH.

Raman spectroscopy allows us to differentiate between an anhydrous salt, a hydrated salt, and an aqueous salt solution. We are not able to constrain the exact hydration state of a crystalline salt (e.g.: $Mg(ClO_4)_2 \cdot 6H_2O$ vs. $Mg(ClO_4)_2 \cdot 5H_2O$).

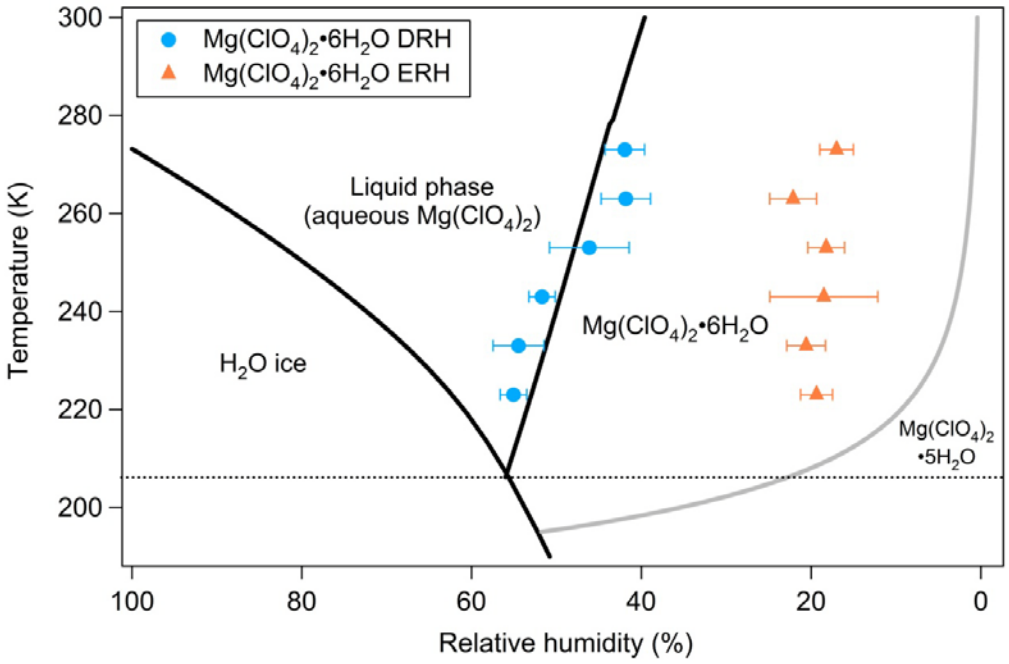

Figure 4.7 Experimentally determined deliquescence relative humidity (DRH) and efflorescence relative humidity (ERH) values for $Mg(ClO_4)_2 \bullet 6H_2O$ (symbols) overlaid on a phase diagram of the $Mg(ClO_4)_2/H_2O$ system. The thermodynamically predicted phase transitions are depicted with solid black lines. The gray line represents the thermodynamic transition between the hexahydrate and pentahydrate of $Mg(ClO_4)_2$. In our experiments, $Mg(ClO_4)_2 \bullet 6H_2O$ deliquesced very close to the thermodynamically predicted RH values for all temperatures studied (blue symbols). However, when the RH in the cell was lowered the aqueous salts effloresced at 19(±3)% RH (orange symbols), exhibiting the hysteresis effect commonly observed during salt efflorescence.

However, as efflorescence occurs in the hexahydrate stability region (see Fig. 4.7), crystallization of this $Mg(ClO_4)_2$ solution should result in the hexahydrate salt. To confirm this, a crystalline salt particle that had already experienced a complete deliquescence/efflorescence cycle was deliquesced again. The DRH of this sample occurred on the hexahydrate solid/aqueous solution transition line, confirming the efflorescence product is indeed $Mg(ClO_4)_2 \bullet 6H_2O$.

4.4.3 Long time scale experiments

The experiments discussed thus far were performed over time scales of 30 minutes to 1 hour. During these deliquescence and efflorescence experiments, H_2O vapor was increased or decreased slowly and held at a given value for several minutes until the H_2O vapor flow through the environmental cell was constant and the spectra were not changing. However, two types of longer time scale experiments were performed in order to place upper limits on the rates of efflorescence and salt hydration, both of which are kinetically hindered processes.

First, experiments were performed to constrain the time needed to hydrate anhydrous $NaClO_4$. It is critical to understand hydration kinetics as hydration state affects both DRH and T_E. An anhydrous $NaClO_4$ sample was kept at RH = 25% and T = 263 K for 5 hours. Under these T and RH conditions, the monohydrated salt is predicted to form (see Fig. 4.6). However, during and after this 5 hour time period, Raman spectroscopy was used to confirm that there was no crystalline water present in the sample (i.e.: there was no sharp feature at 3550 cm^{-1}). Also, subsequent deliquescence of this sample occurred on the red dashed line representing the

metastable deliquescence of anhydrous $NaClO_4$, verifying that the salt had not been hydrated. As the efflorescence of $NaClO_4$ always results in the formation of the anhydrous salt, these slow hydration kinetics have important implications. For example, anhydrous $NaClO_4$ could deliquesce at low DRH values (~40% RH) when humidity increases, efflorescence into the anhydrous salt once RH drops below 13%, and then deliquescence again at low DRH values (~40% RH) when humidity increases again. In such a cycle, hydrated forms of $NaClO_4$ might rarely or never exist and the stable transitions predicted by thermodynamics may never occur.

Also, in order to constrain the length of time over which a metastable, supersaturated salt solution could remain aqueous, we performed a modified efflorescence experiment. Instead of slowly lowering the RH in the environmental cell constantly until efflorescence occurred, the RH was held constant at 25% RH while the temperature of the $NaClO_4$ solution was held at 263 K. As seen in Fig. 4.6, under these conditions the RH is below the DRH of $NaClO_4$ (36.8% RH) but above the ERH (12.6% RH). Therefore the solution is supersaturated and thermodynamics predicts crystallization should be spontaneous. These conditions were maintained for 5 hours, during which no crystallization occurred. This experiment suggests metastable, supersaturated salt solutions can exist for significant portions of a day.

4.5 Discussion

The eutectic temperature (T_E) of 236 K previously reported for $NaClO_4$ considered only stable transitions (Chevrier et al., 2009). If metastable transitions (such as deliquescence of anhydrous $NaClO_4$ or $NaClO_4 \cdot H_2O$) occur, then the T_E

values are actually 230 and 180 K, respectively. Although we were not able to probe the very low eutectic point of anhydrous $NaClO_4$ due to experimental constraints, we were able to deliquesce anhydrous $NaClO_4$ as low as 223 K, a temperature below T_E for either $NaClO_4 \cdot H_2O$ or $NaClO_4 \cdot 2H_2O$. This low theoretical metastable eutectic temperature for anhydrous $NaClO_4$ (T_E = 180 K) effectively represents a significant decrease of 56 K from the previously published minimum freezing point of sodium perchlorate solutions. Also, as shown in Fig. 4.6, the anhydrous salt deliquesces at lower RH than the monohydrate at all temperatures studied. Consideration of the properties of this anhydrous salt significantly broadens the range of conditions (both T and RH) for which aqueous sodium perchlorate solutions can exist.

For both salts, we have shown that supersaturated salt solutions are common due to the hysteretic nature of phase transitions. At all temperatures studied (223 – 273 K), perchlorate salt solutions effloresced at much lower RH values than the crystalline solid deliquesced. Consideration of this hysteresis effect of the crystallization of salt solutions at all temperatures studied is critical for predicting which phase will be present under a given set of environmental conditions. Doing so will certainly expand the range of RH conditions for which aqueous sodium perchlorate solutions can exist. Next, we apply these experimental results to the perchlorate/water system likely to be found in the shallow Martian subsurface.

4.6 Implications for aqueous solutions on Mars

The Phoenix landing site is the only location on Mars where perchlorate salts have been detected in the soil. However, it is also the only place where the detection

or quantification of ClO_4^- has been attempted, so it is not known if the distribution is local or global, homogenous or spatially variable. The source has been proposed to be atmospheric (Catling et al., 2010) which suggests ClO_4^- is likely to exist in the regolith at all latitudes. However, here we only discuss the likely phase transitions of perchlorate salts at the Phoenix landing site (68°N, 234°E) where the presence of ClO_4^- is confirmed.

The relative humidity at the Phoenix landing site was measured by the Thermal and Electrical and Conductivity Probe (TECP) instrument which was located on the robotic arm of the lander. Humidity was measured by a GE Panametrics MiniCap 2 polymer relative humidity sensor (Zent et al., 2010). Due to power dissipation on the TECP electronics board, the temperature of the RH sensor was typically slightly higher than the ambient air temperature during operation and a correction of the raw data was required. Conversion to true atmospheric RH was accomplished by first calculating the vapor pressure of H_2O at a given time and then using atmospheric temperature data measured by the MET temperature sensors to calculate true atmospheric RH (Hudson et al., 2009). The RH sensor was about 5 cm above the surface and the MET mast was about 1 m in height. Therefore, the reported RH is the humidity with respect to the air temperature, as well as any material that has the same temperature as the air. Here, we assume that perchlorate in the top soil layers is experiencing the same RH as the air just above the surface (lowest 1 m).

Shown in Fig. 4.8A and B are diurnal RH data measured by the TECP instrument onboard the Phoenix lander (Hudson et al., 2009). Several different sols (Martian days) are shown in different colors. The x-axis is local mean solar time

(LMST). All of the measurements occur during the northern summer on Mars, as this is the only season during which the instruments onboard Phoenix actively took measurements. We use our experimentally determined DRH and ERH data to determine the time periods in a typical day during which aqueous sodium perchlorate solutions are either stable or metastable. We assume that the kinetics of ice nucleation and ice melting and sublimation are rapid. Specifically, we assume ice is present whenever the phase diagram would predict ice to form based on RH and T conditions.

The blue shaded areas in Fig. 4.8A represent conditions during which aqueous $NaClO_4$ solutions could potentially exist. It can be seen that there are two periods of time during a typical summer day during which liquid water may be present: mid morning and late evening. In total, it is possible that aqueous $NaClO_4$ solutions would exist for almost 8 hours/day. During the other times of day, the $NaClO_4$ salt will either be in the crystalline form or frozen, as ice. During the day, the RH is low and the temperature is high and so the salt will be a crystalline solid (most likely anhydrous $NaClO_4$). As the temperature drops in the evening, RH increases and the anhydrous $NaClO_4$ salt will deliquescence around 21:00. As the RH continues to increase and T continues to decrease, ice will form. Around 06:00 in the morning, the temperature warms and the RH decreases and the frozen solution will melt into salty liquid. The solution is stable until the RH drops below about 40% RH. At this point, the solution becomes supersaturated but can still exist for several more hours (according to the results of our long time scale experiments). This metastable solution exists throughout the morning as RH decreases until the ERH is reached (~13% RH) at 10:30, then efflorescence occurs and the supersaturated solution crystallizes into

the anhydrous solid. It is not likely that hydrated forms of $NaClO_4$ will exist on Mars at any point during a diurnal cycle.

Shown in Fig. 4.8B are periods of time during a typical summer day during which aqueous $Mg(ClO_4)_2$ solutions are either stable or metastable (shaded blue regions). Compared to $NaClO_4$, there are fewer hours during a typical Martian day during which aqueous $Mg(ClO_4)_2$ solutions can exist. This is expected, as magnesium perchlorate has higher DRH values, especially at the low temperatures more relevant to Mars. Additionally, the ERH is higher than that of $NaClO_4$ (19% instead of 13%) so a supersaturated solution of the magnesium salt will precipitate first when the RH is lowered over a system that contains aqueous solutions of both $NaClO_4$ and $Mg(ClO_4)_2$.

From 06:00 to 10:00 in the morning, stable or metastable $Mg(ClO_4)_2$ solutions are likely to exist (blue shaded region). In the evening, it is unclear if aqueous solutions are possible, as the humidity and temperature trajectory at the Phoenix landing site passes right through, or just above, the triple point located at the intersection of the ice phase, the aqueous phase, and the solid $Mg(ClO_4)_2 \cdot 6H_2O$ phase (see Fig. 4.7). It is possible that during some sols, especially during warmer times of the year, aqueous solutions could exist briefly in the late evening when the RH is increasing and the temperature is dropping. As we are not certain of the phases that could exist, this time period is depicted with hatched blue shading. In summary, our studies suggest $Mg(ClO_4)_2$ solutions could exist for between 4 and 6 hours/day.

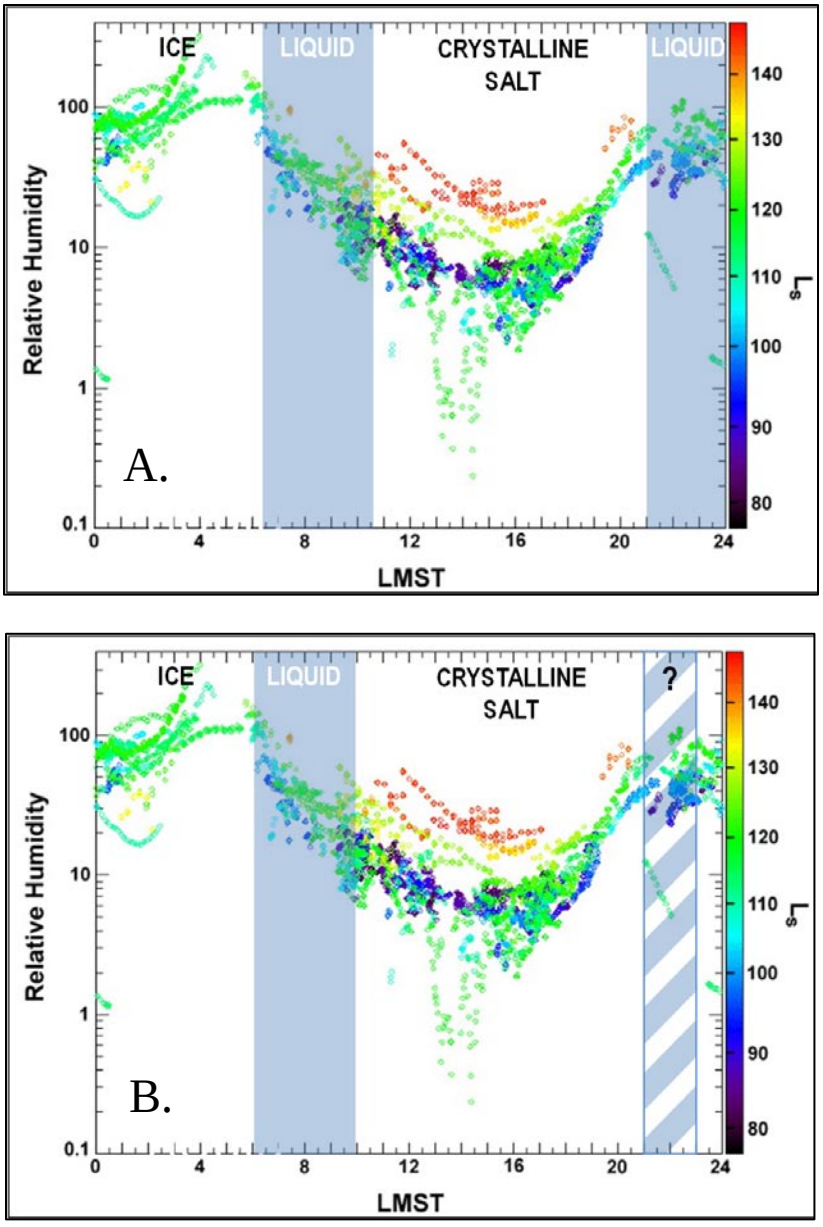

Figure 4.8 Diurnal RH cycle at the Phoenix landing site (Hudson et al., 2009) with blue shaded areas representing times of day during which (A) aqueous $NaClO_4$ solutions or (B) aqueous $Mg(ClO_4)_2$ solutions could be stable or metastable based on our phase transition experiments. We find aqueous $NaClO_4$ solutions could exist for almost 8 hrs/day and aqueous $Mg(ClO_4)_2$ solutions could exist for 4 hrs/day and possibly longer. During the other times of day, the salt will either be in frozen water ice or in the anhydrous crystalline form.

Our calculations oversimplify several processes and make some assumptions. First, we assume that water transport is not limiting. This may not be true, as H_2O does not instantly diffuse through 5 cm of fine grained regolith and H_2O also does not immediately travel vertically through the atmosphere to reach the surface. Additionally, the subsurface temperature is variable, with thermal waves affecting the temperature of soil layers (and the perchlorate salts therein) on diurnal and seasonal time scales. In order to accurately determine the phase of perchlorate salts at each point in time, a model is needed which involves the changing temperature profiles of the regolith, the kinetics of water vapor diffusion (both upwards from the ice table and downwards from the atmosphere), and also the adsorption of water to the surfaces of mineral grains. Involving these processes will help more accurately predict the times of day and the months/seasons of a Martian year during which aqueous solutions can exist. This more sophisticated approach may result in different results than those shown in Figs. 4.8 and 4.9. However, it is the general consensus that the RH on Mars cycles between a few percent and 100% RH daily, and therefore it seems likely there some periods of time when perchlorate salts in the soil at the Phoenix landing site are deliquesced and small pockets of salty liquid could exist among the soil grains.

More detailed theoretical work could also investigate the likelihood of salt solutions existing at other latitudes. As the DRH values of perchlorate salts were observed to decrease as temperature increased, it seems probable that liquid water could be stable for longer time periods equatorward of the Phoenix landing site. Additionally, once deliquesced, the region of aqueous solution stability is larger at

higher temperatures because ice does not form as readily at high RH. For example (as seen in Fig. 4.7), ice will form at 61% RH at T = 220 K but not until 80% RH at T = 250 K.

4.7 Conclusions

Deliquescence relative humidity (DRH) values for $NaClO_4$ (anhydrous and monohydrate) and $Mg(ClO_4)_2$ (hexahydrate) salts were experimentally determined from 223-273 K using a Raman microscope equipped with an environmental cell. DRH values for all salts were consistent with thermodynamic calculations if both stable and metastable solid to liquid transitions are involved. DRH values were typically found to increase with decreasing temperature. DRH values for anhydrous $NaClO_4$ were the lowest, with deliquescence occurring between 35-42% RH with very little temperature dependence.

As predicted by thermodynamics, salts with higher hydration states were found to deliquesce at higher RH values and have higher eutectic temperatures (T_E). Anhydrous $NaClO_4$ was found to deliquesce at RH values 15-27% RH lower than the monohydrated $NaClO_4$ salt, and has a T_E value 56 K lower than $NaClO_4 \bullet H_2O$.

Efflorescence relative humidity (ERH) values found for aqueous $NaClO_4$ and $Mg(ClO_4)_2$ solutions are far below the measured DRH values. The ERH was found to be 12.6(±2.0)% RH for $NaClO_4$ and 19.3(±2.9)% RH for $Mg(ClO_4)_2$. This hysteresis effect commonly occurs during the crystallization of salts from aqueous solutions as a result of the slow nucleation kinetics, and results in large ranges of RH values for which supersaturated salt solutions can exist in a metastable state.

We also show hydration is slow (takes longer than 5 hours), implying that the anhydrous efflorescence product would not become hydrated for at least several hours on Mars. Also, we found that supersaturated solutions can exist for at least 5 hours at RH values below the DRH.

Past studies of perchlorate solutions on Mars have ignored hysteresis effect, as well as the slow kinetics of salt hydration. When these details are considered, the range of temperature and relative humidity values for which liquid solutions can exist is wider. We show it is possible that aqueous perchlorate solutions may exist for longer periods than previously believed: up to 8 hours a day in the case of $NaClO_4$ solutions or between 4 and 6 hours a day in the case of $Mg(ClO_4)_2$ solutions.

Chapter V

Summary, Conclusions and Future Directions

5.1 Heterogeneous chemistry of CH_4 on Mars

The first part of this thesis has focused on understanding the recently observed Martian CH_4 variability. The short lived CH_4 plumes and potential seasonal and spatial variability require a large, present-day source as well as a rapid CH_4 sink. These unknown production and loss mechanisms have inspired many hypotheses, perhaps the most exciting of which is potential microbiological life. Perhaps elaborate subsurface colonies of methanogenic (CH_4 producing) and methanotrophic (CH_4 metabolizing) bacteria could result in the observed spatial and seasonal variability. However, it is important to explore abiotic mechanisms which can produce and/or rapidly destroy CH_4 on Mars. Here, we have experimentally studied two possible pathways via which CH_4 could be removed from the Martian atmosphere. Both mechanisms involved interaction with the mineral dust that is ubiquitous both on the surface and in the atmosphere of Mars.

First, in Chapter 2, we studied the reversible, temperature-dependent adsorption of CH_4 to JSC-Mars-1, a common Martian surface analog. Our low temperature experiments were performed in a high-vacuum Knudsen cell which uses mass spectrometry to quantify the temperature-dependent adsorption of CH_4 to the mineral surface. Uptake coefficient (γ) values were measured for CH_4 on JSC-Mars-1 between 115 and 145 K and, as expected for physisorption, the value of γ increases

with decreasing T. These values were then used to estimate the kinetics of adsorptive loss for CH_4 on Martian minerals.

We find that colder surface temperatures, deeper diffusion depths, and high surface area soil would increase the rate of atmospheric CH_4 loss. Under certain conditions, significant CH_4 depletion could occur during the winter months. Although shallow ice table depths would prevent significant CH_4 loss in the coldest areas of Mars (the polar regions), the mid latitudes (±50-60°) experience similarly cold temperatures (150 K) during the winter and have at least 1 meter of dry, ice-free regolith above the ice table. At these latitudes, CH_4 adsorption could be contributing to the observed atmospheric CH_4 variability in two ways. First, the regolith could act as a CH_4 sink in the winter when the surface is cold and absorption is occurring, and then as a CH_4 "source" in the summer months when warmer soil temperatures would cause net CH_4 desorption. This process is likely to be fully reversible on an annual time scale, and is only recycling the Martian CH_4. There is no net destruction of CH_4, and thus no required increase in the magnitude of a potential CH_4 source to account for the observed mixing ratio. Although biogenic production and/or metabolization of CH_4 is still a possibility which could explain the recent observations, perhaps this abiotic process could explain the variability of CH_4 as well.

Next, in Chapter 3 we explored a more permanent CH_4 sink: oxidation of CH_4 by reactive species thought to exist in the Martian surface. The life detection experiments onboard the Viking landers most likely failed to detect life, but they did determine that the surface of Mars is oxidizing. Previous laboratory studies and photochemical models suggest the oxidant is photochemically-produced H_2O_2,

although recently discovered ClO_4^- salts are potential oxidants as well. It was not previously known if such oxidants, or possibly the soil itself, could oxidize CH_4. If so, this heterogeneous CH_4 oxidation could contribute to the recently observed variability and would also have implications for the size of the required CH_4 source. Therefore, we performed experiments examining the kinetics of CH_4 oxidation by TiO_2•H_2O_2, JSC-Mars-1 treated with H_2O_2, as well as sodium and magnesium perchlorate salts.

We used gas chromatography for quantitative analysis of any CO_2 evolved from the sample after addition of either CH_4 or the "Viking organics". Perchlorate salts did not oxidize either the organic solution or CH_4, an expected result. Although the TiO_2•H_2O_2 and JSC-Mars-1 + H_2O_2 were able to oxidize the organics, no CH_4 was oxidized within the detection limit of the experiment.

Although only negative results were found, an upper limit reaction coefficient (α) can be found by calculating the total collisions of gaseous CH_4 molecules with the surface and using detection limits to determine the maximum number of oxidation reactions that could have occurred in the system. These α values are small: 4×10^{17} for CH_4 loss on TiO_2•H_2O_2 and 2×10^{17} for CH_4 loss on JSC-Mars-1 with H_2O_2. The lifetime of CH_4 with respect to heterogeneous oxidation will depend on the depth of soil which contains oxidant, a value that is not known for Mars. However, we show that even unfeasibly large (> 500 m) depths of oxidized soil are not sufficient to oxidize an atmospheric column of CH_4 in a few years. Therefore it is not likely that H_2O_2 bound to soil grains is responsible for the CH_4 variability observed in the atmosphere of Mars.

5.2 Phase transitions of perchlorate salts

In Chapter 4, we study a different gas-surface process important to Mars: the interaction of water vapor with salts that exist in the Martian soil. Perchlorate salts, found at a 0.5% concentration in the regolith at the Phoenix landing site, are known to be hygroscopic and deliquescent, but the uptake of water had not been quantified at any temperatures below 298 K. In this chapter, we described experiments designed to determine the deliquescence relative humidity (DRH) and the efflorescence relative humidity (ERH) of both sodium and magnesium perchlorate salts at a range of temperatures from 223 to 273 K.

We performed these studies using a Raman microscope, an instrument which allowed us to monitor the phase transitions with optical microscopy as well as Raman spectroscopy. We find that the deliquescence of anhydrous $NaClO_4$ is only slightly dependent on temperature and occurs at 38(±3)% RH. The DRH of $NaClO_4 \cdot H_2O$, however, increases with decreasing temperature from 51% at 273 K to 64% at 228 K. The DRH of $Mg(ClO_4)_2 \cdot 6H_2O$, probably the perchlorate salt most relevant to Mars due to the ~3/1 Mg^{2+}/Na^{+} ratio at the Phoenix landing site (Hecht et al., 2009), also increases with decreasing temperature from 42% at 273 K to 64% at 223 K.

We also find a hysteresis between deliquescence and efflorescence. In the case of perchlorate salts, efflorescence of the salt solutions occurred at a significantly lower RH than deliquescence due to the kinetic inhibition of crystallization. This hysteretic behavior was observed at all temperatures and for all salts studied. Sodium perchlorate solutions effloresced at 13(±2)% RH and $Mg(ClO_4)_2$ solutions effloresced

at 19(±3)% RH. Prior to efflorescence, the solutions are supersaturated and metastable, yet can exist for at least several (> 5) hours.

Another important finding was that supersaturated $NaClO_4$ solutions always effloresce into the anhydrous salt. Additionally, longer time scale studies show that salt hydration is slow (also > 5 hrs). In combination, these findings suggest anhydrous $NaClO_4$ is likely to be the most relevant sodium perchlorate salt over the course of a diurnal cycle on Mars. Anhydrous $NaClO_4$ deliquesces at very low humidity values (DRH = 38(±3)%) and has a very low eutectic temperature (T_E = 180 K). Therefore, it can exist in the aqueous phase under a much wider range of temperature and humidity conditions than can the hydrated forms of $NaClO_4$.

Using versions of the perchlorate stability diagrams which show metastable phase transitions, account for the hysteresis effect and consider the slow kinetics of hydration, we estimated which times of day perchlorate salts at the Phoenix landing site exist in the aqueous phase. We find that sodium perchlorate solutions are likely to be stable or metastable for as many as 8 hours/day during the northern summer months. The higher DRH and lower T_E values of $Mg(ClO_4)_2 \cdot 6H_2O$ limit the windows of aqueous solution stability/metastability of this salt to 4-6 hrs/sol.

Of all the salts known to exist on Mars, perchlorates are arguably the most hygroscopic and the most likely to contribute to the potential formation of aqueous solutions. Our experimental work described here has shown that even at low temperatures, deliquescence can occur and supersaturation readily occurs. We have shown that the absorption of H_2O by perchlorate salts is a mechanism by which small

amounts of liquid water could exist on the surface or in the shallow subsurface of Mars.

5.3 Future Directions

Here are some future steps that could be taken to continue the experimental work that has been described here and improve the relevance and accuracy of the implications to Mars. These projects include laboratory studies and also complimentary theoretical work. Of course, any work should also reflect and incorporate any new information or results from future Mars landers (Mars Science Laboratory (2011)), orbiters (MAVEN (2013), Trace Gas Orbiter (2016)), and earth-based observations, as well as any new results of the ever-improving GCMs of the Mars surface/atmosphere system.

5.3.1 Methane projects

In this thesis, we only reported the adsorption of CH_4 onto JSC-Mars-1. It would be interesting to study the interaction of CH_4 with other minerals, especially high surface area materials such as clays and zeolites. Also, it would be interesting to study the co-adsorption of other species such as CO_2 or H_2O to analog surfaces. Although we suspect that competing physisorption processes would not significantly interfere with CH_4 adsorption due to the very low fraction of sites filled by CH_4, it is possible that monolayer (or more) coverage of H_2O or CO_2 would prevent CH_4 from sticking to soil grains. However, perhaps layers of ice formed atop adsorbed CH_4 would serve to trap the CH_4, preventing desorption.

Also, further work should be done towards finding an oxidant that is reactive towards CH_4 over short time scales and is likely to be found on the surface, in the subsurface, or in the atmosphere of Mars. Potential oxidants such as reactive chlorine species with oxidation states between chloride (Cl^-, chlorine oxidation state = -1) and perchlorate (ClO_4^-, chlorine oxidation state = +7) could be studied. Additionally, several reactive oxygen species such as OH radical and superoxide ions (O_2^-) should be experimentally studied to determine their reactivity towards CH_4 and constrain the kinetics of these reactions.

To help determine the relevance and implications of these experiments, theoretical studies are needed. For example, a GCM that involves subsurface diffusion, absorption and reaction would be important for quantifying the strength of a temporary or permanent CH_4 sink and determining its seasonality. Although the surface area of mineral dust suspended in the atmosphere is small (relative to the regolith) even during heavy dust activity, it is possible that an extremely reactive species could exist on these aerosols and act as a CH_4 sink. Perhaps the oxidizing component would be formed by photochemical processes unique to the upper atmosphere or produced by electrostatic mechanisms which can only occur during dust storms. Regardless, any atmospheric heterogeneous CH_4 loss pathway studied in the laboratory should also be analyzed with a GCM that involves dust activity.

5.3.2 Perchlorate project

Thus far, we have only studied the phase transitions of pure perchlorate salts and aqueous salt solutions. There are several steps that need to be taken before the

role of perchlorate salts on Mars can be fully understood. First, the kinetics of other relevant phase transitions should be experimentally studied. Specifically, in Chapter 5 we assume that the freezing of perchlorate solutions, as well as the melting or sublimating of the solid states that would result, are instant. As we show in Chapter 4, some phase transitions are kinetically hindered and stability diagrams cannot always predict what phases will be present under a given set of environmental conditions. It is important to perform these experiments rather than just predict the results from thermodynamic calculations. Typically, the less ordered to more ordered phase transitions (such as crystallization and nucleation) are kinetically hindered (Martin, 2000). Therefore, it is especially important to study the freezing of salt solutions. This process could proceed slowly and require supersaturations, as did the nucleation of solid salt crystals from solutions. (In the case of ice nucleation, the supersaturation required would a supersaturation of H_2O vapor with respect to ice as opposed to a supersaturation of salt in the aqueous phase.)

Another step towards understanding the phase transitions of perchlorate salts on Mars would be to study deliquescence and efflorescence in an environment more similar to the Martian regolith. For example, the effects of other salts as well as mineral grains should be experimentally investigated. It has been reported that mixtures of salts can deliquesce at RH values below the DRH of either pure salt. Therefore, it would be interesting to determine the DRH and ERH of internal mixtures of $Mg(ClO_4)_2$ and $NaClO_4$ salts. Additionally, the soil at the Phoenix landing site was found to contain chloride anions and may contain sulfate salts (Hecht et al., 2009). Phase transition experiments should be performed on mixtures of these

salts as well. Obviously perchlorate is only a minor component of the regolith (~0.5% by mass), and therefore future studies should investigate the deliquescent behavior of salts mixed into Martian soil analog minerals. Would adsorption of H_2O by mineral surfaces compete with absorption of water by hygroscopic salts or would the processes occur independently? Also, would supersaturated salt solutions still occur as readily if sub-micron mineral particles were present to act as crystallization nuclei?

Lastly, as suggested with respect to heterogeneous CH_4 reactions, theoretical work will be critical to understanding the behavior of these (and other) salts on Mars. Our experiments intentionally left out complications such as the diffusion of H_2O through layers of soil and the possible control of H_2O vapor and humidity by other salts or adsorption of H_2O to soils. Additionally, mass transport of H_2O through the atmosphere (ie: vertical mixing), latent heat of phase transitions, and the variation of temperature due to both diurnal and seasonal thermal waves would be important to both experimentally and theoretically investigate in the future. The results of such a study would help to determine if there are periods of time on Mars during which aqueous phases could exist and, if so, the soil depths and regions on Mars where they could occur.

References

Adamson, A. W., 1973. Textbook of Physical Chemistry. Academic Press, New York, NY.

Allen, C. C., Jager, K. M., Morris, R. V., Lindstrom, D. J., Lindstrom, M. M. and Lockwood, J. P., 1998. Martian soil simulant available for scientific, educational study. EOS 79: 405-412.

Atreya, S. K., Mahaffy, P. R. and Wong, A. S. (2007). Methane and related trace species on Mars: Origin, loss, implications for life, and habitability, Pergamon-Elsevier Science Ltd.

Atreya, S. K., Mahaffy, P. R. and Wong, A. S., 2007. Methane and related trace species on Mars: Origin, loss, implications for life, and habitability. Planet. Space Sci. 55(3): 358-369.

Atreya, S. K., Wong, A. S., Renno, N. O., Farrell, W. M., Delory, G. T., Sentman, D. D., Cummer, S. A., Marshall, J. R., Rafkin, S. C. R. and Catling, D. C., 2006. Oxidant enhancement in Martian dust devils and storms: Implications for life and habitability. Astrobiology 6(3): 439-450.

Ballou, E. V., Wood, P. C., Wydeven, T., Lehwalt, M. E. and Mack, R. E., 1978. Chemical interpretation of Viking Lander 1 life detection. Nature 271(5646): 644-645.

Bandfield, J. L., Hamilton, V. E. and Christensen, P. R., 2000. A global view of Martian surface compositions from MGS-TES. Science 287(5458): 1626-1630.

Baustian, K. J., Wise, M. E. and Tolbert, M. A., 2010. Depositional ice nucleation on solid ammonium sulfate and glutaric acid particles. Atmos. Chem. Phys. 10(5): 2307-2317.

Bell, J. F., McSween, H. Y., Crisp, J. A., Morris, R. V., Murchie, S. L., Bridges, N. T., Johnson, J. R., Britt, D. T., Golombek, M. P., Moore, H. J., et al., 2000. Mineralogic and compositional properties of Martian soil and dust: Results from Mars Pathfinder. J. Geophys. Res.-Planets 105(E1): 1721-1755.

Biemann, K., 1979. Implications and limitations of the findings of the Viking organic-analysis experiment. J. Mol. Evol. 14(1-3): 65-70.

Boston, P. J., Ivanov, M. V. and McKay, C. P., 1992. On the possibility of chemosynthetic ecosystems in subsurface habitats on Mars. Icarus 95(2): 300-308.

Boudart, M. and Djega-Mariadassou, G., 1984. Kinetics of Heterogeneous Catalytic Reactions. Princeton University Press, Princeton, NJ.

Bullock, M. A., Stoker, C. R., McKay, C. P. and Zent, A. P., 1994. A coupled soil atmosphere model of H_2O_2 on Mars. Icarus 107(1): 142-154.

Carlos-Cuellar, S., Li, P., Christensen, A. P., Krueger, B. J., Burrichter, C. and Grassian, V. H., 2003. Heterogeneous uptake kinetics of volatile organic compounds on oxide surfaces using a Knudsen cell reactor: Adsorption of acetic acid, formaldehyde, and methanol on α-Fe_2O_3, α-Al_2O_3, and SiO_2. J. Phys. Chem. B 107(21): 4250-4261.

Catling, D. C., Claire, M. W., Zahnle, K. J., Quinn, R. C., Clark, B. C., Hecht, M. H. and Kounaves, S., 2010. Atmospheric origins of perchlorate on Mars and in the Atacama. J. Geophys. Res.-Planets 115(E00E11).

Chaix, L. and Domine, F., 1997. Effect of the thermal history of ice crushed at 77 K on its surface structure as determined by adsorption of CH_4 at low surface coverage. J. Phys. Chem. B 101(32): 6105-6108.

Chassefiere, E., Drossart, P. and Korablev, O., 1995. Post-Phobos model for the altitude and size distribution of dust in the lower Martian atmosphere. J. Geophys. Res. 100(E3): 5525-5539.

Chastain, B. K. and Chevrier, V., 2007. Methane clathrate hydrates as a potential source for Martian atmospheric methane. Planet. Space Sci. 55(10): 1246-1256.

Chevrier, V., Hanley, J. and Altheide, T., 2009. Stability of perchlorate hydrates and their liquid solutions at the Phoenix landing site, Mars. Geophys. Res. Lett. 36(L10202).

Christensen, P. R., Wyatt, M. B., Glotch, T. D., Rogers, A. D., Anwar, S., Arvidson, R. E., Bandfield, J. L., Blaney, D. L., Budney, C., Calvin, W. M., et al., 2004. Mineralogy at Meridiani Planum from the Mini-TES experiment on the Opportunity Rover. Science 306(5702): 1733-1739.

Clark, B. C., Baird, A. K., Rose, H. J., Toulmin, P., Christian, R. P., Kelliher, W. C., Castro, A. J., Rowe, C. D., Keil, K. and Huss, G. R., 1977. Viking x-ray-fluorescence experiment - Analytical methods and early results. Transactions-American Geophysical Union 58(8): 829-829.

Clifford, S. M. and Hillel, D., 1983. The stability of ground ice in the equatorial region of Mars J. Geophys. Res. 88(NB3): 2456-2474.

Cohen, M. D., Flagan, R. C. and Seinfeld, J. H., 1987. Studies of Concentrated Electrolyte-Solutions Using the Electrodynamic Balance .1. Water Activities for Single-Electrolyte Solutions. J. Phys. Chem. 91(17): 4563-4574.

Colburn, D. S., Pollack, J. B. and Haberle, R. M., 1989. Diurnal-Variations in Optical Depth at Mars. Icarus 79(1): 159-189.

Cooper, C. D. and Mustard, J. F., 1999. Effects of very fine particle size on reflectance spectra of smectite and palagonitic soil. Icarus 142(2): 557-570.

Davila, A. F., Fairen, A. G., Gago-Duport, L., Stoker, C., Amils, R., Bonaccorsi, R., Zavaleta, J., Lim, D., Schulze-Makuch, D. and McKay, C. P., 2008. Subsurface formation of oxidants on Mars and implications for the preservation of organic biosignatures. Earth Planet. Sci. Lett. 272(1-2): 456-463.

Delory, G. T., Farrell, W. M., Atreya, S. K., Renno, N. O., Wong, A. S., Cummer, S. A., Sentman, D. D., Marshall, J. R., Rafkin, S. C. R. and Catling, D. C., 2006. Oxidant enhancement in martian dust devils and storms: Storm electric fields and electron dissociative attachment. Astrobiology 6(3): 451-462.

Dobrynina, T. A., Chernyshova, A. M., Akhapkina, N. A. and Rosolovskii, V. Y., 1980. Fusion diagram of the magnesium perchlorate-water system. Russ. J. Inorg. Chem. 25: 2233–2236.

Espinosa, R. M., Franke, L. and Deckelmann, G., 2008. Phase changes of salts in porous materials: Crystallization, hydration and deliquescence. Construction and Building Materials 22(8): 1758-1773.

Fanale, F. P., Salvail, J. R., Zent, A. P. and Postawko, S. E., 1986. Global distribution and migration of subsurface ice on Mars Icarus 67(1): 1-18.

Farrell, W. M., Delory, G. T. and Atreya, S. K., 2006. Martian dust storms as a possible sink of atmospheric methane. Geophys. Res. Lett. 33(21).

Feldman, W. C., Prettyman, T. H., Maurice, S., Plaut, J. J., Bish, D. L., Vaniman, D. T., Mellon, M. T., Metzger, A. E., Squyres, S. W., Karunatillake, S., et al., 2004. Global distribution of near-surface hydrogen on Mars. J. Geophys. Res. 109(E9): 13.

Finlayson-Pitts, B. and Pitts, J., 2000. Chemistry of the Upper and Lower Atmosphere. Academic Press, San Diego, CA.

Formisano, V., Atreya, S., Encrenaz, T. r. s., Ignatiev, N. and Giuranna, M., 2004. Detection of methane in the atmosphere of Mars. Science 306(5702): 1758-1761.

Frinak, E. K., Mashburn, C. D., Tolbert, M. A. and Toon, O. B., 2005. Infrared characterization of water uptake by low-temperature Na-montmorillonite: Implications for Earth and Mars. J. Geophys. Res. 110(D9).

Frinak, E. K., Wermeille, S. J., Mashburn, C. D., Tolbert, M. A. and Pursell, C. J., 2004. Heterogeneous reaction of gaseous nitric acid on gamma-phase iron(III) oxide. J. Phys. Chem. B 108(9): 1560-1566.

Fuchs, N. and Sutugin, A. (1971). High dispersed aerosols. Topics in Current Aerosol Research (Part 2). G. Hidy and J. Brock. New York, NY, Pergamon**:** 1-200.

Geminale, A., Formisano, V. and Giuranna, M., 2008. Methane in Martian atmosphere: Average spatial, diurnal, and seasonal behaviour. Planet. Space Sci. 56(9): 1194-1203.

Golden, T. C. and Sircar, S., 1994. Gas adsorption on silicalite. J. Colloid Interface Sci. 162(1): 182-188.

Gough, R. V., Tolbert, M. A., McKay, C. P. and Toon, O. B., 2010. Methane adsorption on a Martian soil analog: An abiogenic explanation for methane variability in the Martian atmosphere. Icarus 207(1): 165-174.

Greenspan, L., 1977. Humidity Fixed-Points of Binary Saturated Aqueous-Solutions. Journal of Research of the National Bureau of Standards - A 81(1): 89-96.

Hamilton, V. E., McSween, H. Y. and Hapke, B., 2005. Mineralogy of Martian atmospheric dust inferred from thermal infrared spectra of aerosols. J. Geophys. Res. 110(E12).

Hatch, C. D., Gough, R. V. and Tolbert, M. A., 2007. Heterogeneous uptake of the C-1 to C-4 organic acids on a swelling clay mineral. Atmos. Chem. Phys. 7(16): 4445-4458.

Haynes, D. R., Tro, N. J. and George, S. M., 1992. Condensation and evaporation of H_2O on ice surfaces J. Phys. Chem. 96(21): 8502-8509.

Hecht, M. H., Kounaves, S. P., Quinn, R. C., West, S. J., Young, S. M. M., Ming, D. W., Catling, D. C., Clark, B. C., Boynton, W. V., Hoffman, J., et al., 2009. Detection of perchlorate and the soluble chemistry of Martian soil at the Phoenix Lander site. Science 325(5936): 64-67.

Himeno, S., Tomita, T., Suzuki, K. and Yoshida, S., 2007. Characterization and selectivity for methane and carbon dioxide adsorption on the all-silica DD3R zeolite. Microporous Mesoporous Mat. 98(1-3): 62-69.

Hirschfelder, J. O., 1954. Molecular theory of gases and liquids. Wiley, New York, NY.

Hudson, P. K., Shilling, J. E., Tolbert, M. A. and Toon, O. B., 2002. Uptake of nitric acid on ice at tropospheric temperatures: Implications for cirrus clouds. J. Phys. Chem. B 106(42): 9874-9882.

Hudson, T. L., Aharonson, O., Schorghofer, N., Farmer, C. B., Hecht, M. H. and Bridges, N. T., 2007. Water vapor diffusion in Mars subsurface environments. J. Geophys. Res. 112(E5): 27.

Hudson, T. L., Zent, A., Hecht, M. H., Wood, S. and Cobos, D. (2009). Near-Surface Humidity at the Phoenix Landing Site as Measured by the Thermal and Electrical Conductivity Probe (TECP). LPSC, The Woodlands, TX.

Huguenin, R. L., Miller, K. J. and Harwood, W. S., 1979. Frost-weathering on Mars-Experimental evidence for peroxide formation. J. Mol. Evol. 14(1-3): 103-132.

Hunten, D. M., 1979. Possible oxidant sources in the atmosphere and surface of Mars. J. Mol. Evol. 14(1-3): 71-78.

Hurowitz, J. A., Tosca, N. J., McLennan, S. M. and Schoonen, M. A. A., 2007. Production of hydrogen peroxide in Martian and lunar soils. Earth Planet. Sci. Lett. 255(1-2): 41-52.

Jakosky, B. M., 1983. The role of seasonal reservoirs in the Mars water cycle. 1. Seasonal exchange of water with the regolith. Icarus 55(1): 1-18.

Jakosky, B. M., Nealson, K. H., Bakermans, C., Ley, R. E. and Mellon, M. T., 2003. Subfreezing activity of microorganisms and the potential habitability of Mars' polar regions. Astrobiology 3(2): 343-350.

Jayne, J. T., Duan, S. X., Davidovits, P., Worsnop, D. R., Zahniser, M. S. and Kolb, C. E., 1991. Uptake of gas-phase alcohol and organic-acid molecules by water surfaces. J. Phys. Chem. 95(16): 6329-6336.

Kiyosu, Y. and Imaizumi, S., 1996. Carbon and hydrogen isotope fractionation during oxidation of methane by metal oxides at temperatures from 400° to 530°C. Chem. Geol. 133(1-4): 279-287

Kiyosu, Y. and Krouse, H. R., 1989. Carbon isotope effect during abiogenic oxidation of methane. Earth Planet. Sci. Lett. 95(3-4): 302-306.

Kok, J. F. and Renno, N. O., 2009. Electrification of wind-blown sand on Mars and its implications for atmospheric chemistry. Geophys. Res. Lett. 36: L05202.

Krasnopolsky, V. A., 1993. Photochemistry of the Martian atmosphere (Mean conditions). Icarus 101(2): 313-332.

Krasnopolsky, V. A., 2006. Some problems related to the origin of methane on Mars. Icarus 180(2): 359-367.

Krasnopolsky, V. A., Maillard, J. P. and Owen, T. C., 2004. Detection of methane in the Martian atmosphere: evidence for life? Icarus 172(2): 537-547.

Lefevre, F. and Forget, F., 2009. Observed variations of methane on Mars unexplained by known atmospheric chemistry and physics. Nature 460(7256): 720-723.

Lemmon, M. T., Wolff, M. J., Smith, M. D., Clancy, R. T., Banfield, D., Landis, G. A., Ghosh, A., Smith, P. H., Spanovich, N., Whitney, B., et al., 2004. Atmospheric imaging results from the Mars exploration rovers: Spirit and Opportunity. Science 306(5702): 1753-1756.

Levin, G. V. and Straat, P. A., 1976. Viking Labeled Release Biology Experiment - Interim results Science 194(4271): 1322-1329.

Levin, G. V. and Straat, P. A., 1981. A search for a non-biological explanation of the Viking Labeled Release life detection experiment. Icarus 45(2): 494-516.

Lyons, J. R., Manning, C. and Nimmo, F., 2005. Formation of methane on Mars by fluid-rock interaction in the crust. Geophys. Res. Lett. 32(13): 4.

Madden, M. E. E., Ulrich, S. M., Onstott, T. C. and Phelps, T. J., 2007. Salinity-induced hydrate dissociation: A mechanism for recent CH_4 release on Mars. Geophys. Res. Lett. 34(11): 5.

Marion, G. M., Catling, D. C., Zahnle, K. J. and Claire, M. W., 2010. Modeling aqueous perchlorate chemistries with applications to Mars. Icarus in press.

Martin, S. T., 2000. Phase Transitions of Aqueous Atmospheric Particles. Chem. Rev. 100(9): 3403-3454.

Martin, T. Z., 1995. Mass of dust in the martian atmosphere. J. Geophys. Res. 100(E4): 7509-7512.

Martinie, G. D. and Schilt, A. A., 1976. Investigation of wet oxidation efficiencies of perchloric-acid mixtures for various organic-substances and identities of residual matter. Anal. Chem. 48(1): 70-74.

Max, M. D. and Clifford, S. M., 2000. The state, potential distribution, and biological implications of methane in the Martian crust. J. Geophys. Res. 105(E2): 4165-4171.

McSween, H. Y. and Keil, K., 2000. Mixing relationships in the Martian regolith and the composition of globally homogeneous dust. Geochim. Cosmochim. Acta 64(12): 2155-2166.

Mellon, M. T., Feldman, W. C. and Prettyman, T. H., 2004. The presence and stability of ground ice in the southern hemisphere of Mars. Icarus 169(2): 324-340.

Mellon, M. T. and Jakosky, B. M., 1993. Geographic variations in the thermal and diffusive stability of ground ice on Mars. J. Geophys. Res. 98(E2): 3345-3364.

Miller, A. G. and Macklin, J. W., 1985. Vibrational Spectroscopic Studies of Sodium-Perchlorate Contact Ion-Pair Formation in Aqueous-Solution. J. Phys. Chem. 89(7): 1193-1201.

Mohlmann, D. (2003). Liquid-like sorption water in the upper Martian surface - Physical, chemical and possible biological consequences. Proceedings of the Third European Workshop on Exo-Astrobiology. Madrid, Spain**:** 11-14.

Mohlmann, D. T. F., 2004. Water in the upper martian surface at mid- and low-latitudes: presence, state, and consequences. Icarus 168(2): 318-323.

Moore, H. J., Bickler, D. B., Crisp, J. A., Eisen, H. J., Gensler, J. A., Haldemann, A. F. C., Matijevic, J. R., Reid, L. K. and Pavlics, F., 1999. Soil-like deposits observed by Sojourner, the Pathfinder rover. J. Geophys. Res. 104(E4): 8729-8746.

Morris, R. V., Graff, T. G., Ming, D. W., Mertzman, S. A. and Bell III, J. F. (2003). Hydrothermal alteration on basaltic Mauna Kea volcano as a template for identification of hydrothermal alteration on basaltic Mars. Lunar and Planetary Science XXXIV.

Mumma, M., Novak, R., DiSanti, M., Bonev, B. and Dello Russo, N., 2004. Detection and mapping of methane and water on Mars. Bull. Amer. Astron. 36(4): 1127.

Mumma, M., Villanueva, G, Novak, RE, Hewagama, T, Bonev, BP, DiSanti, MA and Smith, MD (2008). Absolute Measurements of Methane on Mars: the current status. Mars Atmosphere: Modeling and Observations. Williamsburg, VA.

Mumma, M. J., Villanueva, G. L., Novak, R. E., Hewagama, T., Bonev, B. P., DiSanti, M. A., Mandell, A. M. and Smith, M. D., 2009. Strong release of methane on Mars in northern summer 2003. Science 323(5917): 1041-1045.

Munuera, G., Gonzalezelipe, A. R., Soria, J. and Sanz, J., 1980. Photo-Adsorption and Photo-Desorption of Oxygen on Highly Hydroxylated TiO_2 Surfaces .3. Role of H_2O_2 in Photo-Desorption of O_2. Journal of the Chemical Society - Faraday Transactions I 76: 1535-1546.

Murakami, T., Banba, T., Jercinovic, M. J. and Ewing, R. C., 1989. Formation and evolution of alteration layers on borosilicate and basalt glasses: Initial stage. Mat. Res. Soc. Symp. Proc. 127: 65-72.

Onasch, T. B., Siefert, R. L., Brooks, S. D., Prenni, A. J., Murray, B., Wilson, M. A. and Tolbert, M. A., 1999. Infrared spectroscopic study of the deliquescence and efflorescence of ammonium sulfate aerosol as a function of temperature. J. Geophys. Res. 104(D17): 21317-21326.

Orenberg, J. and Handy, J., 1992. Reflectance spectroscopy of palagonite and iron-rich montmorillonite clay mixtures - Implications for the surface composition of Mars. Icarus 96(2): 219-225.

Oze, C. and Sharma, M., 2005. Have olivine, will gas: Serpentinization and the abiogenic production of methane on Mars. Geophys. Res. Lett. 32(10): 4.

Pereira, P. R., Pires, J. and de Carvalho, M. B., 2001. Adsorption of methane and ethane in zirconium oxide pillared clays. Sep. Purif. Technol. 21(3): 237-246.

Pick, M. A., 1981. Kinetics of hydrogen absorption-desorption by niobium. Phys. Rev. B 24(8): 4287-4294.

Plumb, R. C., Tantayanon, R., Libby, M. and Xu, W. W., 1989. Chemical-model for Viking biology experiments - Implications for the composition of the Martian regolith. Nature 338(6217): 633-635.

Prasetyo, I. and Do, D. D., 1999. Adsorption kinetics of light paraffins in AC by a constant molar flow-rate method. Aiche J. 45(9): 1892-1900.

Prieto-Ballesteros, O., Kargel, J. S., Fairen, A. G., Fernandez-Remolar, D. C., Dohm, J. M. and Amils, R., 2006. Interglacial clathrate destabilization on Mars: Possible contributing source of its atmospheric methane. Geology 34(3): 149-152.

Putzig, N. E., Mellon, M. T., Kretke, K. A. and Arvidson, R. E., 2005. Global thermal inertia and surface properties of Mars from the MGS mapping mission. ICARUS 173(2): 325-341.

Quinn, R. and Orenberg, J., 1993. Simulations of the Viking Gas-Exchange experiment using palagonite and Fe-rich montmorillonite as terrestrial analogs - Implications for the surface composition of Mars. Geochim. Cosmochim. Acta 57(19): 4611-4618.

Quinn, R. C. and Zent, A. P., 1999. Peroxide-modified titanium dioxide: A chemical analog of putative Martian soil oxidants. Origins Life Evol. Biosphere 29(1): 59-72.

Robertson, K. and Bish, D. (2010). Thermal behavior of the magnisium perchlorate-H_2O system 41st LPSC. Houston, TX.

Satterfield, C. N., 1970. Mass transfer in heterogeneous catalysis M.I.T. Press, Cambridge, Mass.

Seinfeld, J. H. and Pandis, S. N., 1998. Atmospheric Chemistry and Physics. John Wiley & Sons, New York, NY.

Shilling, J. E., Connelly, B. M. and Tolbert, M. A., 2006. Uptake of small oxygenated organic molecules onto ammonium nitrate under upper tropospheric conditions. J. Phys. Chem. B 110(21): 6687-6695.

Singer, R. B., 1982. Spectral evidence for the mineralogy of high albedo soils and dust on Mars. J. Geophys. Res. 87(NB12): 159-168.

Skorov, Y. V., Markiewicz, W. J., Basilevsky, A. T. and Keller, H. U., 2001. Stability of water ice under a porous nonvolatile layer: implications to the south polar layered deposits of Mars. Planet. Space Sci. 49(1): 59-63.

Tang, I. N. and Munkelwitz, H. R., 1994. Water Activities, Densities, and Refractive-Indexes of Aqueous Sulfates and Sodium-Nitrate Droplets of Atmospheric Importance. J. Geophys. Res.-Atmos. 99(D9): 18801-18808.

Tokano, T., 2003. Precession-driven migration of water in the surficial layers of Mars. Int. J. Astrobiol. 2(3): 155-170.

Tokano, T., 2003. Spatial inhomogeneity of the martian subsurface water distribution: implication from a global water cycle model. Icarus 164(1): 50-78.

Tomoko, I.-F., Shinichiro, H., Takeo, H. and Katsuyuki, K., 2002. Molecular dynamics studies of molecular diffusion in ice Ih. J. Chem. Phys. 117(8): 3886-3896.

Trainer, M., Tolbert, M., McKay, C. and Toon, O., 2009. Limits on the Trapping of Atmospheric CH_4 in Martian Polar Ice Analogs. Icarus submitted.

Tsapin, A. I., Goldfeld, M. G., McDonald, G. D., Nealson, K. H., Moskovitz, B., Solheid, P., Kemner, K. M., Kelly, S. D. and Orlandini, K. A., 2000. Iron(VI): Hypothetical candidate for the martian oxidant. Icarus 147(1): 68-78.

Varnes, E. S., Jakosky, B. M. and McCollom, T. M., 2003. Biological potential of martian hydrothermal systems. Astrobiology 3(2): 407-414.

Weiss, B. P. and Ingersoll, A. P. (2000). Cold spots in the Martian polar regions: Evidence of carbon dioxide depletion?, Academic Press Inc.

Weiss, B. P., Yung, Y. L. and Nealson, K. H., 2000. Atmospheric energy for subsurface life on Mars? Proc. Nat. Acad. Sci. U.S.A. 97(4): 1395-1399.

Wong, A. S., Atreya, S. K. and Encrenaz, T., 2003. Chemical markers of possible hot spots on Mars. J. Geophys. Res. 108(E4): 11.

Worsnop, D. R., Zahniser, M. S., Kolb, C. E., Gardner, J. A., Watson, L. R., Vandoren, J. M., Jayne, J. T. and Davidovits, P., 1989. Temperature-dependence of mass accommodation of SO_2 and H_2O_2 on aqueous surfaces. J. Phys. Chem. 93(3): 1159-1172.

Xu, J., Imre, D., McGraw, R. and Tang, I., 1998. Ammonium sulfate: Equilibrium and metastability phase diagrams from 40 to -50 degrees C. J. Phys. Chem. B 102(38): 7462-7469.

Yen, A. S., Kim, S. S., Hecht, M. H., Frant, M. S. and Murray, B., 2000. Evidence that the reactivity of the Martian soil is due to superoxide ions. Science 289(5486): 1909-1912.

Zahnle, K., Freedman, R. and Catling, D. (2010). Is there methane on Mars? 41st Lunar and Planetary Science Conference The Woodlands, TX.

Zent, A. P., Hecht, M. H., Cobos, D. R., Wood, S. E., Hudson, T. L., Milkovich, S. M., DeFlores, L. P. and Mellon, M. T., 2010. Initial results from the thermal and electrical conductivity probe (TECP) on Phoenix. J. Geophys. Res. 115.

Zent, A. P., Howard, D. J. and Quinn, R. C., 2001. H_2O adsorption on smectites: Application to the diurnal variation of H_2O in the Martian atmosphere. J. Geophys. Res. 106(E7): 14667-14674.

Zent, A. P. and McKay, C. P., 1994. The chemical reactivity of the Martian soil and implications for future missions. Icarus 108(1): 146-157.

Zhang, S. Y., Talu, O. and Hayhurst, D. T., 1991. High pressure adsorption of methane in NaX, MgX, CaX, SrX and BaX J. Phys. Chem. 95(4): 1722-1726.

Zhang, Y. H. and Chan, C. K., 2003. Observations of water monomers in supersaturated NaClO4, LiClO4, and Mg(ClO4)(2) droplets using Raman spectroscopy. J. Phys. Chem. B 107(31): 5956-5962.

Zhang, Y. H., Hu, Y. A., Ding, F. and Zhao, L. J., 2005. FTIR-ATR chamber for observation of efflorescence and deliquescence processes of NaClO4 aerosol particles on ZnSe substrate. Chin. Sci. Bull. 50(19): 2149-2152.

Zhao, L. J., Zhang, Y. H., Wang, L. Y., Hu, Y. A. and Ding, F., 2005. FTIR spectroscopic investigations of supersaturated NaClO4 aerosols. Physical Chemistry Chemical Physics 7(14): 2723-2730.

Zorzano, M. P., Mateo-Marti, E., Prieto-Ballesteros, O., Osuna, S. and Renno, N., 2009. Stability of liquid saline water on present day Mars. Geophys. Res. Lett. 36.

Appendix A: Glossary of uncommon terms

Anhydrous Containing no water in the crystal structure.

Autoclave A device which sterilizes equipment and supplies by subjecting them to high pressure steam.

BET surface area Initially proposed by Brunauer, Emmett, and Teller in 1938, a surface science measurement which considers the total surface available for physisorption by gaseous molecules. BET theory is often used to determine the specific surface area of a material (m^2/kg).

Calcination Heating a material to a high temperature so that volatile matter is driven off.

Chemisorption A process in which a substance is adsorbed onto the surface of a substrate by means of chemical rather than physical bonding. The interaction typically has binding energies greater than -20 kJ/mol.

Clathrate A substance consisting of a lattice of one type of molecule (“host molecule”) trapping a second type of molecule (“guest molecule”) by intermolecular interaction. Sometimes called a hydrate.

Deliquescence The process of a solid material (typically an inorganic salt) absorbing water vapor from the atmosphere to produce a saturated aqueous solution.

Dose In this work, dose is the product of pressure and time and therefore has units of Torr·s. Dose is a quantity normalized to the total number of molecules that a surface has been exposed to during an experiment.

Efflorescence Crystallization of an aqueous salt solution into a solid particle. This process typically requires supersaturation of the solute and therefore occurs at lower humidities than deliquescence.

Eutectic point The lowest freezing point that can be achieved for a given solution of water and a salt. This is the bottom of the "V"-shaped curve on a phase diagram and occurs at some characteristic eutectic concentration.

GC Gas chromotograpy; a technique that provides non-destructive separation based on the ability of the analyte species to adsorb to the solid phase. Common detectors are the thermal conductivity detector (TCD), flame ionization detector (FID) or photoionization detector (PID).

Hydration state The number of crystalline H_2O molecules associated with a given molecule or formula unit. Waters of hydration are incorporated into a crystal lattice and are different from the H_2O found in a deliquesced particle.

Hygrometer Instrument for measuring the relative humidity of a system. The hygrometer used in this study contained a chilled mirror and optoelectronic mechanism to detect condensation on the mirror surface and determine the dewpoint temperature.

Hysteresis effect When a system demonstrates path dependence, it can be said to exhibit a hysteresis effect. For example, the phase transitions of salts involve hysteretic transitions when efflorescence occurs at lower relative humidity values than deliquescence.

Ice table A sharp boundary between dry soil and hard, subsurface ice that exists in the subsurface of Mars. This shallowly buried ice is found at a depth of a few cm in the polar regions and increases in depth with decreasing latitude.

JSC-Mars-1 A common terrestrial analog for the regolith of Mars. The material is a type of palagonite (glassy volcanic ash) and is cited as a good spectral analog to certain regions of Mars (Morris et al., 2003).

Metastable A thermodynamically unstable but potentially long-lived state. Supersaturated solutions and supercooled liquids are examples of metastable phases of matter.

Reaction coefficient In this work, defined as the fraction of collisions of CH_4 with a mineral surface that result in complete oxidation to CO_2.

Phoenix Lander A robotic spacecraft which landed near the north pole of Mars on May 25th, 2008. The lander contained several instruments designed to look for habitable environments.

Physisorption The physical condensation of a gas on the surface of a solid. In constrast to chemisorptions, the electronic structure of the atom or molecule is barely perturbed when phyisisorption occurs.

QMS Quadrupole mass spectrometer.

Raman spectroscopy Spectroscopic technique used to study vibrational modes of a system. Relies on inelastic (or Raman) scattering, of monochromatic light such as from a laser. Yields similar, although complementary, information to infrared spectroscopy.

Regolith A term used to describe a layer of loose, heterogeneous material covering solid rock, especially with respect to Mars or the Moon. Often preferred to “soil” as soil is defined as having organic content.

Sol	The duration of a solar day on Mars. In Earth time, a sol is 24 hours, 39 minutes, and 35.244 seconds.
TCD	Thermal conductivity detector. The type of detector used in this work to monitor the elution of molecules from a chromatography column. The detector senses changes in the thermal conductivity of the column effluent due to the presence of molecular species.
TECP	Thermal and Electrical Conductivity Probe onboard the Phoenix Lander. The instrument was on the robotic arm of the lander and measured the relative humidity as well as the thermal conductivity, electrical conductivity and dielectric permittivity of the regolith.
TPD	Temperature programmed desorption. An experimental technique in which molecules are desorbed from a surface by increasing the temperature of the surface at a constant rate. The desorbed molecules are typically quantified using mass spectrometry.
Uptake coefficient	In this study, defined as the net fraction of collisions of a gas with a surface that result in adsorptive uptake.
Viking	NASA's Viking program sent an orbiter and two landers to Mars in the 1970's. The landers had cameras, an x-ray fluorescence spectrometer, pressure, temperature and wind velocity sensors, a seismometer and a suite of life-detection experiments.

Appendix B: List of symbols and variables

A	Arrhenius pre-exponential factor	unitless
α	reaction coefficient	unitless
A_{eff}	effective area of escape orifice	cm^2
c_∞	gas concentration far away from particle	molec cm^{-3}
c_s	gas concentration at particle surface	molec cm^{-3}
D_{CH4}	diffusion coefficient of CH_4	$m^2\ s^{-1}$
d_{H2O2}	depth of soil layer containing H_2O_2	m
DRH	deliquescence relative humidity	%
d_{soil}	diffusion depth	cm
ERH	efflorescence relative humidity	%
Φ_{ads}	flux to a surface that is adsorbed	molec $m^{-2}\ s^{-1}$
Φ_{CH4}	total CH_4 flux	molec $m^{-2}\ s^{-1}$
F_{CH4}	flow of CH_4	molec s^{-1}
γ	uptake coefficient	unitless
ΔH	change in enthalpy of a process	J mol^{-1}
I	thermal inertia	J $m^{-2}\ K^{-1}\ s^{-½}$
J_{net}	net flow of gas to a surface	molec s^{-1}
J_{total}	total flow of gas to a surface	molec s^{-1}
k_B	Boltzmann constant = 1.38×10^{-23}	$m^2\ kg\ s^{-2}\ K^{-1}$
K_{eq}	equilibrium constant	unitless
Kn	Knudsen number	unitless
LMST	local mean solar time	hr
ML_{CH4}	monolayer coverage of $CH_4 = 5.21 \times 10^{14}$	molec cm^{-2}
m_{sample}	sample mass	g
M_w	molecular weight	kg mol^{-1}
n	mean molecular speed of a gas	m s^{-1}
N_{ads}	number of molecules adsorbed to sample	molecules
N_{CH4}	methane column abundance	molec m^{-2}
n_{CH4}	number density of CH_4	molec m^{-3}
N_{des}	number of molecules desorbed from sample	molecules

P_{CH4}	partial pressure of CH_4	Torr
R	gas constant = 8.314	J mol^{-1} K^{-1}
RH	relative humidity	%
R_p	particle radius	µm
r_{pore}	pore radius	cm
SA	total mineral surface area	m^2
SSA_{BET}	BET specific surface area	m^2 kg^{-1}
SSA_{soil}	specific surface area of soil	m^2 kg^{-1}
T	temperature	K
t	time	s
t_{ads}	lifetime of CH_4 due to adsorption by the regolith	s
t_{diff}	diffusion time	s
T_E	eutectic temperature	K
t_{exp}	exposure time of experiment	s
T_{mean}	annual mean surface temperature	K
T_{min}	annual minimum surface temperature	K
t_{ox}	lifetime of CH_4 due to heterogeneous oxidation	s
ω	mass accommodation coefficient	unitless
η	evaporation coefficient	unitless
Θ	fractional monolayer coverage	unitless
Θ_{eq}	equilibrium surface coverage	unitless
λ	mean free path of a gas molecule	µm
ρ_{soil}	soil density	kg m^{-3}